MINISTÉRIO DA CIÊNCIA, TECNOLOGIA E INOVAÇÕES
INSTITUTO NACIONAL DE PESQUISAS ESPACIAIS

sid.inpe.br/mtc-m12e/2025/10.02.14.06-TDI

ECOLOGICAL DRIVERS OF BIOMASS IN FOREST ECOSYSTEMS: A LIDAR-BASED APPROACH ACROSS SUCCESSIONAL AND DISTURBANCE GRADIENTS

Gabriel Máximo da Silva

Doctorate Thesis of the Graduate Course in Remote Sensing, guided by Drs. Carlos Alberto Silva, and Yosio Shimabukuro (in memoriam), approved in August 13, 2025.

URL of the original document:
<http://urlib.net/8JMKD2USNRW34T/4EBLLM2>

INPE
São José dos Campos
2025

PUBLISHED BY:

Instituto Nacional de Pesquisas Espaciais - INPE
Coordenação de Ensino, Pesquisa e Extensão (COEPE)
Divisão de Biblioteca (DIBIB)
CEP 12.227-010
São José dos Campos - SP - Brasil
Tel.:(012) 3208-6923/7348
E-mail: pubtc@inpe.br

BOARD OF PUBLISHING AND PRESERVATION OF INPE INTELLECTUAL PRODUCTION - CEPPII (PORTARIA Nº 176/2018/SEI-INPE):
Chairperson:
Dr. Thales Sehn Korting - Coordenação-Geral de Ciências da Terra (CGCT)
Members:
Dr. Antonio Fernando Bertachini de Almeida Prado - Conselho de Pós-Graduação (CPG)
Dr. Evandro Marconi Rocco - Coordenação-Geral de Engenharia, Tecnologia e Ciência Espaciais (CGCE)
Dr. Heyder Hey - Coordenação-Geral de Infraestrutura e Pesquisas Aplicadas (CGIP)
Simone Angélica Del Ducca Barbedo - Divisão de Biblioteca (DIBIB)
DIGITAL LIBRARY:
Dr. Gerald Jean Francis Banon
Clayton Martins Pereira - Divisão de Biblioteca (DIBIB)
DOCUMENT REVIEW:
Simone Angélica Del Ducca Barbedo - Divisão de Biblioteca (DIBIB)
André Luis Dias Fernandes - Divisão de Biblioteca (DIBIB)
ELECTRONIC EDITING:
Ivone Martins - Divisão de Biblioteca (DIBIB)
André Luis Dias Fernandes - Divisão de Biblioteca (DIBIB)

MINISTÉRIO DA CIÊNCIA, TECNOLOGIA E INOVAÇÕES
INSTITUTO NACIONAL DE PESQUISAS ESPACIAIS

sid.inpe.br/mtc-m12e/2025/10.02.14.06-TDI

ECOLOGICAL DRIVERS OF BIOMASS IN FOREST ECOSYSTEMS: A LIDAR-BASED APPROACH ACROSS SUCCESSIONAL AND DISTURBANCE GRADIENTS

Gabriel Máximo da Silva

Doctorate Thesis of the Graduate Course in Remote Sensing, guided by Drs. Carlos Alberto Silva, and Yosio Shimabukuro (in memoriam), approved in August 13, 2025.

URL of the original document:
<http://urlib.net/8JMKD2USNRW34T/4EBLLM2>

INPE
São José dos Campos
2025

Cataloging in Publication Data

Silva, Gabriel Máximo da.

Si38e Ecological drivers of biomass in forest ecosystems: A LiDAR-based approach across successional and disturbance gradients / Gabriel Máximo da Silva. – São José dos Campos : INPE, 2025.

xxiv + 88 p. ; (sid.inpe.br/mtc-m12e/2025/10.02.14.06-TDI)

Thesis (Doctorate in Remote Sensing) – Instituto Nacional de Pesquisas Espaciais, São José dos Campos, 2025.

Guiding : Drs. Carlos Alberto Silva, and Yosio Shimabukuro (in memoriam).

1. LiDAR. 2. Aboveground biomass. 3. ALS. 4. TLS. I.Title.

CDU 528.835:631.614



Esta obra foi licenciada sob uma Licença Creative Commons Atribuição-NãoComercial 3.0 Não Adaptada.

This work is licensed under a Creative Commons Attribution-NonCommercial 3.0 Unported License.

MINISTÉRIO DA CIÊNCIA, TECNOLOGIA E INOVAÇÃO

INSTITUTO NACIONAL DE PESQUISAS ESPACIAIS

Serviço de Pós-Graduação - SEPGR

FOLHA DE APROVAÇÃO

Aluno (a): Gabriel Máximo da Silva

Título: Ecological drivers of Biomass in Forest Ecosystems: A LiDAR-based Approach Across Successional and Disturbance Gradients

Aprovado (a) pela Banca Examinadora em cumprimento ao requisito exigido para obtenção do Título de Doutor (a) em Sensoriamento Remoto.

(assinado eletronicamente)
Dr. Marcos Adami – Presidente – INPE
(X) Aprovado ( ) Reprovado

(assinado eletronicamente)
Dr. Carlos Alberto Silva – Orientador – University of Florida
(X) Aprovado ( ) Reprovado

(assinado eletronicamente)
Dr. Thales Sehn Körting – Membro Interno – INPE
(X) Aprovado ( ) Reprovado

(assinado eletronicamente)
Dr. Rodrigo Vieira Leite – Membro Externo – NASA / University of Maryland
(X) Aprovado ( ) Reprovado

(assinado eletronicamente)
Dr. Inacio Thomaz Bueno – Membro Externo – University of Florida
(X) Aprovado ( ) Reprovado

Este trabalho foi aprovado por:

( ) maioria simples
(X) unanimidade

São José dos Campos, 13 de agosto de 2025.

Documento assinado eletronicamente por **Marcos Adami**, **Pesquisador**, em 27/08/2025, às 12:53 (horário oficial de Brasília), com fundamento no § 3º do art. 4º do Decreto nº 10.543, de 13 de novembro de 2020.

Documento assinado eletronicamente por **Thales Sehn Korting**, **Pesquisador**, em 27/08/2025, às 12:54 (horário oficial de Brasília), com fundamento no § 3º do art. 4º do Decreto nº 10.543, de 13 de novembro de 2020.

Documento assinado eletronicamente por **Rodrigo Vieira Leite**, **Usuário Externo**, em 26/09/2025, às 11:24 (horário oficial de Brasília), com fundamento no § 3º do art. 4º do Decreto nº 10.543, de 13 de novembro de 2020.

Documento assinado eletronicamente por **Carlos Alberto Silva**, **Usuário Externo**, em 26/09/2025, às 11:50 (horário oficial de Brasília), com fundamento no § 3º do art. 4º do Decreto nº 10.543, de 13 de novembro de 2020.

Documento assinado eletronicamente por **Inacio Thomaz Bueno**, **Usuário Externo**, em 29/09/2025, às 17:29 (horário oficial de Brasília), com fundamento no § 3º do art. 4º do Decreto nº 10.543, de 13 de novembro de 2020.

A autenticidade deste documento pode ser conferida no site https://sei.mcti.gov.br/verifica.html, informando o código verificador **13040319** e o código CRC **3083F669**.

Referência: Processo nº 01340.005920/2025-92 SEI nº 13040319

“The tree that offers shade does not decide who may rest beneath it”.

Yanomami proverb

ACKNOWLEDGMENTS

The conclusion of this thesis represents not only the end of an academic cycle but also the materialization of a journey filled with challenges, learning, and both personal and professional growth. There were scholarship cuts, a pandemic, boycotts, severe physical and mental health problems, exhausting fieldwork — a journey that was arduous and, at times, cruel. For this reason, it is with profound gratitude that I record here my most sincere acknowledgments.

I am deeply grateful to my family for their unconditional love, constant encouragement, and support in every moment. To my mother, Mrs. Enilva, and my father, Mr. Arlindo, for the solid foundation they gave me, for their example of strength and dedication, and for never sparing efforts so that I could pursue my dreams — even though they did not have the opportunity to complete elementary and high school. To my sister Gabriela and my niece Alice, for their unwavering emotional support throughout this journey.

To my advisor, Dr. Yosio Edemir Shimabukuro (in memoriam), for his generous and inspiring guidance at all stages of this work. His trust in my potential was essential for me to move forward, even in the face of the greatest challenges. He was an example of humility, wisdom, and dedication, and his legacy will continue to inspire my personal and professional path. I am grateful for the opportunities he opened, the reflections he encouraged, and the autonomy he always nurtured. His absence is deeply felt, but his legacy remains alive in every page of this thesis and in all those who had the privilege of learning by his side.

To my co-advisor, Dr. Carlos Silva, my deepest gratitude for welcoming me at the University of Florida, for the valuable learning opportunities, and for the high-quality academic discussions. During my exchange, I was able to explore methods, equipment, and ecosystems that once seemed distant from my reality — and all of this was only possible thanks to his support.

I also thank Dr. Marcos Adami, for introducing me to scientific research during my undergraduate studies. His guidance during my scientific initiation was

fundamental in sparking my interest in remote sensing and consolidating my academic journey from its very first steps. I am immensely grateful not only for his technical guidance but also for the emotional support and kindness with which he always accompanied my growth. His generosity, friendship, and encouragement played a decisive role in shaping the path that led me here.

I gratefully acknowledge the support of the Coordination for the Improvement of Higher Education Personnel for the scholarship granted during part of this work, without which this research would not have been possible. This thesis was carried out with the support of the Coordination for the Improvement of Higher Education Personnel – Brazil (CAPES) – Funding Code 001.

To my lifetime best friends, Diego Rocha, Jinyi Xia, and Monique Schlickmann, I could not be more grateful that our paths crossed in this life. During my time in Florida, you were not only my daily support, but also my source of strength, laughter, and inspiration. Three people so different, yet each so extraordinary in your own uniqueness, you brought light to the hardest days and joy to the simplest moments. If it were not for your friendship, kindness, and unwavering presence, I would not have made it this far. This achievement is as much yours as it is mine.

To Carlos Albertini, for the unconditional emotional support, the attentive listening, and the constant presence during the most challenging moments of this journey. Your presence and generosity were essential for me to move forward with courage and balance.

To Dr. Inacio Bueno, Dr. Caio Hammamura, and Dr. Ana Paula Dalla Corte, my sincere thanks for so many enriching exchanges and valuable lessons that I will carry with me.

To my friends Andresson and Renan, and their children Thiago and Matheus, who warmly welcomed me back to São José dos Campos.

To the SilvaLab team, for the productive debates, technical support, and companionship. To INPE and the University of Florida, for providing a stimulating research environment and the infrastructure that made this work possible.

To my coauthors and research colleagues — Carine Klauberg, Eva Louise Loudermilk, Christie Stegall Hawley, Scott Pokswinski, Nuria Sánchez-López, and Andrew T. Hudak — thank you for the scientific partnership, valuable contributions, and every dialogue that expanded my vision of science and international collaboration.

I would like to express my deepest gratitude to all my colleagues and professors at INPE for their invaluable support throughout my graduate journey.

To my professors, thank you for your guidance, patience, and inspiration, your commitment to excellence in research and education has profoundly shaped my scientific path.

To my fellow graduate colleagues and friends, I am deeply thankful for the partnership, shared experiences, and countless hours spent in discussions, fieldwork, and laughter. You made this journey lighter, more collaborative, and truly meaningful.

The time spent at INPE will always be remembered not only for the knowledge I gained but also for the genuine friendships and mentorship that have enriched both my academic and personal life.

To my friends who stood by me, even from a distance, with words of encouragement and comfort, especially Lorena and Talita, my heartfelt thanks.

To my colleagues from the PPA, thank you for your partnership over the past years, for your daily companionship, and for your constant support, even during the most challenging moments. Living and working alongside you was essential to maintain balance between professional commitments and research.

To the institutions that directly or indirectly funded and supported this work, I extend my gratitude for enabling scientific research with commitment and seriousness.

To the members of the examining committee, I am profoundly grateful for your availability, your valuable contributions, and the time you dedicated to reading and evaluating this thesis. Your constructive critiques, suggestions, and reflections significantly enhanced the quality of this work, enriching it with diverse

perspectives and experiences. It is an honor to have the participation of researchers I deeply admire, who have contributed in different ways to my academic and scientific formation.

Finally, I thank the forest, the main reason for this work, for inspiring me at every step and for always reminding me of the importance of fighting for its conservation with science, ethics, and respect.

ABSTRACT

This thesis investigates the variation of AGB in forest ecosystems across two contrasting ecological pathways: forest regeneration and fire disturbance. It integrates multiscale remote sensing data, including airborne and terrestrial LiDAR, with land use history and fire recurrence records to improve the accuracy and ecological relevance of AGB estimation. The study is structured in two core chapters. The first examines how biomass accumulates across successional stages in secondary forests in the Brazilian Amazon. Using multitemporal LULC data from the TerraClass project and airborne LiDAR-derived biomass estimates, the analysis reveals that the spatial distribution of secondary forests is non-random, with a higher concentration in regions historically impacted by deforestation and agricultural expansion. Even mature secondary forests defined operationally here as forests ≥10 years old store only 23–33% of the biomass found in old-growth forests, emphasizing the long-term legacy of land-use change. The second chapter evaluates how fire recurrence affects AGB and fuel components in a prescribed burn experiment using high-resolution TLS. Structural metrics derived from TLS were used in Random Forest regression models to estimate surface biomass and fuel consumption with high accuracy (R^2 up to 0.82). The models captured fine-scale heterogeneity in forest structure, particularly in the understory, which is often overlooked by airborne or satellite sensors. By combining ecological history and 3D structural information, this thesis advances a hybrid modeling framework that links TLS-based measurements at the plot scale with landscape-scale applicability. The findings contribute to a deeper understanding of AGB dynamics in regenerating and degraded forests, offering valuable insights for monitoring systems, forest restoration strategies, and climate policy mechanisms such as REDD+.

Keywords: LiDAR. Aboveground Biomass. ALS. TLS.

DETERMINANTES ECOLÓGICOS DA BIOMASSA EM ECOSSISTEMAS FLORESTAIS: UMA ABORDAGEM BASEADA EM LIDAR AO LONGO DE GRADIENTES DE SUCESSÃO E DISTÚRBIO

RESUMO

Esta tese investiga a variação da biomassa acima do solo (BAS) em ecossistemas florestais a partir de dois caminhos ecológicos contrastantes: a regeneração florestal e a perturbação por fogo. Integra dados de sensoriamento remoto em múltiplas escalas, incluindo LiDAR aerotransportado e terrestre, com o histórico de uso da terra e registros de recorrência de fogo, a fim de aprimorar a acurácia e a relevância ecológica da estimativa de BAS. O estudo está estruturado em dois capítulos principais. O primeiro examina como a biomassa se acumula ao longo dos estágios sucessionais em florestas secundárias na Amazônia brasileira. Utilizando dados multitemporais de uso e cobertura da terra do projeto TerraClass e estimativas de biomassa derivadas de LiDAR aerotransportado, a análise revelou que a distribuição espacial das florestas secundárias é não aleatória e fortemente associada a regiões historicamente impactadas pelo desmatamento. Mesmo florestas secundárias maduras (≥10 anos) armazenam apenas 23–33% da biomassa observada em florestas primárias, evidenciando o legado de longo prazo do uso da terra. O segundo capítulo avalia como a recorrência de fogo afeta a BAS e os componentes de combustível em um experimento de queima prescrita, utilizando varredura a laser terrestre (TLS) de alta resolução. Métricas estruturais derivadas do TLS foram empregadas em modelos de regressão Random Forest para estimar a biomassa superficial e o consumo de combustível com alta acurácia (R^2 de até 0,82). Os modelos capturaram heterogeneidades estruturais em escala fina, especialmente no sub-bosque, frequentemente não detectadas por sensores orbitais ou aerotransportados. Ao combinar o histórico ecológico com informações tridimensionais da estrutura florestal, esta tese propõe um modelo híbrido que conecta a precisão de escala de parcela com a aplicabilidade em escala de paisagem. Os resultados contribuem para uma compreensão mais aprofundada da dinâmica do carbono em florestas regenerantes e degradadas, além de fornecer subsídios valiosos para sistemas de monitoramento, estratégias de restauração florestal e instrumentos de política climática, como o REDD+.

Palavras-chave: LiDAR. Biomassa Acima do Solo. ALS. TLS.

LIST OF FIGURES

Pag.

Figure 2.1 - Representation of TLS scanning positions and combined point cloud results. 17
Figure 3.1 - Land use and land cover map of Pará state according to TerraClass for 2014. 21
Figure 3.2 - Pilot study areas in Pará State. 22
Figure 3.3 - Flowchart of the methodological approach. 23
Figure 3.4 - Hot spot analysis of SF incidence in Pará State by age class. 28
Figure 3.5 - Hot spot analysis of SF deforestation on a time series. 29
Figure 3.6 - Deforestation of SF in Pará State (2014). 29
Figure 3.7. SF balance in Pará. 30
Figure 3.8 - Distribution of aboveground biomass carbon density by SF age class group. 31
Figure 4.1 - Study area and sampling distribution of TLS scans and vegetation and fuel biomass samples (n = 139). 44
Figure 4.2 - Representation of the 3D fuel clip plot. 45
Figure 4.3 - Tree extraction representation on the point cloud. 47
Figure 4.4 - Workflow of biomass and fuel load modeling using TLS-derived metrics and Random Forest regression. 57
Figure 4.5 - Predicted vs observed surface fuel at the clip plot scale. 60
Figure 4.6 - Variable importance for eight Random Forest models predicting different biomass and fuel components. 61
Figure 4.7 - Boxplots of pre-fire, post-fire, and consumed biomass and fuel components across three fire return intervals (1-year, 2-year, and 4-year). 64
Figure 4.8 - Spatial distribution of predicted biomass (g/m²) for eight fuel components under pre-fire (.1) and post-fire (.2) conditions using Random Forest models. 66
Figure 4.9 - Spatial distribution of predicted fuel consumption (g/m²) for eight biomass components, calculated as the difference between pre-fire and post-fire Random Forest model predictions. 68

LIST OF TABLES

Pag.

Table 2.1 - Application of radar according to the frequency band. 12
Table 2.2 - Sentinel 1A main characteristics. 13
Table 3.1 - Classification of SF age in age interval. 24
Table 3.2 - Descriptive statistics of aboveground biomass carbon density (MgC.ha-1). 31
Table 3.3 - Analysis of variance test (ANOVA). 32
Table 3.4 - Tukey multiple comparisons of mean test at 95% family-wise confidence level. 32
Table 4.1- TLS-Derived Predictor metrics used in the Random Forest model (n=46). 47
Table 4.2- Table of fuel categories collected in the field and their descriptions. 49
Table 4.3 - Selected metrics used in the Random Forest model. 52
Table 4.4 - Model Performance Metrics (bootstrap). 58

LIST OF ACRONYMS AND ABBREVIATIONS

AGBCD	Aboveground Biomass Carbon Density
AGB	Aboveground Biomass
ALS	Airborne Laser Scanning
ANOVA	Analysis of Variance
ATLAS	Advanced Topographic Laser Altimeter System
BLA	Brazilian Legal Amazon
CRS	Complete Spatial Randomness
DBH	Diameter at Breast Height
DF	Degrees of Freedom
EVI	Enhanced Vegetation Index
ESA	European Space Agency
GEE	Google Earth Engine
GEDI	Global Ecosystem Dynamics Investigation
IBGE	Instituto Brasileiro de Geografia e Estatística
INPE	Instituto Nacional de Pesquisas Espaciais
LULC	Land Use and Land Cover
MODIS	Moderate Resolution Imaging Spectroradiometer
NDVI	Normalized Difference Vegetation Index
OLS	Ordinary Least Squares
OLI	Operational Land Imager
REDD+	Reducing Emissions from Deforestation and Forest Degradation
RMSE	Root Mean Square Error
SAR	Synthetic Aperture Radar
SAVI	Soil-Adjusted Vegetation Index
SF	Secondary Forest
TSAGB	Total Surface Available Biomass
TLS	Terrestrial Laser Scanning

LISTA DE SYMBOLS

$MgC.ha^{-1}$	Megagrams of Carbon per Hectare
g/m^2	Grams per Square Meter
R^2	Coefficient of Determination
$\bar{X}$	Mean
σ	Standard Deviation
σ^2	Variance

SUMMARY

Pag.

1 INTRODUCTION 1
1.1 Objective 4
1.1.1 Specific objectives 4
2 LITERATURE REVIEW 5
2.1 Aboveground biomass 5
2.2 Aboveground biomass estimation using remote sensing 6
2.3 Remote sensors 9
2.3.1 Optical sensors 9
2.3.2 Synthetic Aperture Radar 11
2.3.3 Light Detection and Ranging (LiDAR) 14
3 BIOMASS ACCUMULATION IN SECONDARY FORESTS: SPATIAL PATTERNS AND SUCCESSIONAL AGE EFFECTS IN THE BRAZILIAN AMAZON 18
3.1 Materials and methods 20
3.1.1 Study area 20
3.1.2 Methodological approach 22
3.1.3 Land use change and secondary forest 23
3.1.4 Secondary forest age 24
3.1.5 Aboveground biomass estimation data 25
3.1.6 Data analysis 25
3.2 Results 27
3.2.1 SF spatial distribution patterns 27
3.2.2 Aboveground biomass estimation for different SF age classes 30
3.3 Discussion 35
3.4 Conclusion 38
3.5 Framing the analysis of biomass in fire-affected forests 38

4 BIOMASS LOSS IN FIRE-PRONE LANDSCAPES: TLS-BASED ANALYSIS OF FUEL LOAD AND CONSUMPTION ACROSS FIRE REGIMES IN PINE ECOSYSTEMS 40
4.1 Materials and methods 43
4.1.1 Study site 43
4.1.2 Sampling design and in situ fuel load collection 44
4.1.3 Terrestrial laser scan collection and processing 46
4.1.4 Reference fuel classes 49
4.1.5 Fuel load modeling and assessment 50
4.2 Results 57
4.3 Discussion 68
4.3.1 Structural predictors of biomass and fuels 69
4.3.2 Fire regime effects and ecological interpretation 71
4.3.3 Advances, applications and limitations 71
4.4 Conclusions 72
5 GENERAL CONCLUSION: INTEGRATING BIOMASS DYNAMICS FROM REGENERATION TO DISTURBANCE 74
REFERENCES 76

1 INTRODUCTION

Environmental monitoring of natural vegetation cover has become crucial over the years, especially with the increase in human-driven land use expansion combined with the exploitation of natural resources. Such expansion has led to forest fragmentation, habitat and biodiversity loss, deforestation and greenhouse gas emissions (RIBEIRO et al., 2009; RODRIGUES et al., 2011; ELMQVIST et al., 2013). Understanding LULC dynamics, along with appropriate methods and technologies, is essential to assess the effects of anthropogenic pressure on ecosystem functioning.

Aboveground biomass (AGB) is widely used as a key indicator in restoration ecology, forest management, and climate policy (PAN et al., 2011; CHAVE et al., 2014; IPCC 2019, 2019a). Traditionally, AGB has been estimated through destructive sampling or field inventories calibrated with allometric equations. While these methods are accurate at the plot level, they are labor-intensive, limited in spatial coverage, and challenging to scale up. As a result, remote sensing has emerged as an essential tool for extending biomass estimates to larger areas, typically using statistical or machine learning models calibrated with field data. It is important to emphasize, however, that remote sensing does not replace fieldwork, but rather complements it by enabling spatially explicit extrapolation and continuous monitoring across broad geographic scales. These techniques significantly support the monitoring and assessment of natural and regenerating forests (ALMEIDA et al., 2016a; WANG et al., 2019a, 2020a). Accurate AGB estimation is essential not only for understanding ecological processes but also for supporting strategies to reduce carbon emissions from deforestation and forest degradation (SULLIVAN et al., 2018).

Airborne and spaceborne remote sensing technologies have demonstrated strong potential for biomass estimation across different forest types and geographic regions (SAATCHI et al., 2011b; ASNER et al., 2012; BACCINI et al., 2012a). Airborne LiDAR (ALS) provides highly detailed three-dimensional structural information but is limited in spatial coverage and cost. Spaceborne sensors, including optical and SAR satellites, enable large-scale and repeated

observations; however, optical sensors are constrained by cloud cover, spectral resolution, and signal saturation in dense forests, whereas SAR systems, although less affected by atmospheric conditions and capable of partial canopy penetration, also suffer from signal saturation at high biomass levels (IMHOFF, 1995; KELLNDORFER et al., 2010; MITCHARD et al., 2011; YU; SAATCHI, 2016). Despite these advantages, both airborne and spaceborne sensors often fail to capture fine-scale structural variation and understory complexity, which are critical components of many forest ecosystems (ALMEIDA et al., 2019; CALDERS et al., 2020).

To overcome these limitations, TLS has emerged as a highly promising technique for detailed three-dimensional forest characterization. TLS provides ground-based, high-resolution point clouds that allow for direct measurements of forest structure, including canopy height, density, surface roughness, and vertical heterogeneity (CALDERS et al., 2015; WILKES et al., 2017). Its ability to capture fine-scale variability makes TLS especially valuable in complex or disturbed environments, such as areas affected by succession, degradation, or fire (ROWELL et al., 2016; WILKES et al., 2017; WALLACE et al., 2022).

Despite its limited spatial coverage compared to orbital sensors, TLS offers key advantages for forest ecology and carbon estimation (XU et al., 2020). It can be used to calibrate or validate broader-scale models and to analyze ecological gradients such as succession, degradation, or fire impacts (ROWELL et al., 2016; KROFCHECK et al., 2019; LOUDERMILK et al., 2023). TLS also enhances the precision of biomass modeling by providing direct, high-resolution measurements of forest structural attributes (e.g., canopy height, stem density, and vertical heterogeneity). When combined with machine learning algorithms and extensive field inventories, TLS-derived metrics reduce uncertainties associated with allometric models and improve the accuracy of biomass predictions at fine spatial scales (WALLACE et al., 2022; TANEJA et al., 2023).

While LiDAR-derived metrics provide detailed information on forest structure at local scales, linking these attributes to broader disturbance and recovery patterns requires integration with LULC studies. LULC change detection using remote

sensing has been instrumental in advancing our understanding of ecosystem dynamics, including the identification of burned areas and forest degradation trajectories (SHIMABUKURO et al., 2009, 2017, 2025). In the Brazilian Amazon, analyzing the temporal patterns of LULC is critical for quantifying AGB and understanding the spatial distribution of forest regrowth, degradation, and resilience (DA SILVA et al., 2023).

Fire plays a central role in shaping forest biomass and structure, acting both as a driver of loss and a catalyst for ecological transformation. In tropical ecosystems, recurrent fire events can cause significant reductions in aboveground biomass, alter successional trajectories, and compromise forest resilience (COCHRANE; SCHULZE, 1999; BARLOW; LAGAN; PERES, 2003; BRANDO et al., 2014). In the Amazon, fire is closely linked to human activity and land-use change, with recurring disturbances amplifying forest degradation and carbon emissions (ARAGÃO et al., 2018; PEREIRA et al., 2024). These dynamics highlight the need to integrate fire occurrence data with structural information to assess both biomass loss and the potential for regrowth under different disturbance regimes. Understanding how fire recurrence influences biomass accumulation and structural heterogeneity is therefore critical for improving AGB estimation and anticipating ecosystem responses under different disturbance regimes.

This thesis aims to advance AGB and fuels estimation by integrating TLS-derived structural metrics with field data and machine learning techniques. The central scientific question is: How can the integration of LiDAR-derived forest structural metrics with land-use history and fire occurrence data improve the ability of remote sensing to identify ecological patterns and processes, such as AGB accumulation and fuel dynamics, across different successional and disturbance contexts?

To address this overarching question, the first research article investigates how the spatial and temporal patterns of LULC influence AGB accumulation in SF of the Brazilian Amazon. The second article evaluates the impacts of recurrent fires

on AGB and fuel components, using TLS-derived metrics and machine learning to capture fine-scale structural heterogeneity.

Although methodologically independent, these studies are conceptually integrated. Together, they contribute to a comprehensive understanding of biomass dynamics in forested landscapes and support scalable, high-accuracy AGB estimation for restoration, management, and climate policy applications.

1.1 Objective

This thesis aims to improve the accuracy of AGB estimation across different stages of vegetation development by integrating LiDAR-derived structural metrics with historical land use and fire occurrence data, using field measurements and machine learning techniques.

1.1.1 Specific objectives

a) To evaluate the influence of historical LULC trajectories on AGB distribution and accumulation in SF in the Brazilian Amazon.

b) To assess the impact of fire recurrence on AGB across different disturbance regimes and successional stages.

c) To develop and compare biomass prediction models using machine learning algorithms, calibrated with field inventory data and LiDAR-derived metrics.

d) To extract and analyze three-dimensional structural metrics from TLS point clouds to characterize forest architecture and identify features most predictive of AGB.

2 LITERATURE REVIEW

2.1 Aboveground biomass

AGB is defined as the amount of standing dry mass of live or dead matter above the soil from trees or shrub vegetation expressed as a mass (DUNCANSON et al., 2021). During photosynthesis, the vegetation captures CO_2 and H_2O from the atmosphere and soil to form organic compounds and convert light energy into chemical energy. When photosynthesis exceeds respiration, carbon becomes stored in ecosystems and its concentration in the atmosphere decreases. However, the storage capacity of forest ecosystems varies according to the vegetation characteristics (age and composition of species) and environment (climate and soil) (BROWN; LUGO, 1990; PAN et al., 2013; POORTER et al., 2016a; SULLIVAN et al., 2020). Some studies indicate that pioneer species have a lower carbon storage capacity than the species of other ecological groups (LAURANCE, 1997; AGUIAR; GAMA; BELDINI, 2017). The patterns and capacity of aboveground biomass storage is also determined by successional stages, ranging from early pioneer-dominated phases to late-mature forests and forest disturbances (e.g., fire, selective logging, windthrow) that alter forest structure and function.

In tropical forests, AGB is commonly used as a proxy to estimate carbon stocks, since roughly 50% of dry biomass is carbon (IPCC 2019, 2019a). However, the estimation of carbon stock may still be very uncertain depending on the scale of analysis, due to the great environmental heterogeneity and because most studies use only data from woody vegetation with diameter at breast height (DBH) >10 cm (SRINIVAS; SUNDARAPANDIAN, 2019). It is important to highlight, though, that individuals with DBH <10 cm grow faster and represent a significant portion of aboveground biomass (CHATURVEDI; RAGHUBANSHI; SINGH, 2012). Furthermore, some studies point out problems in estimating AGB in tropical forests due to the saturation of remote sensors in areas with high biomass volume (IMHOFF, 1995; MITCHARD et al., 2012a; YU; SAATCHI, 2016).

The amount of carbon aboveground can reach above 200 t C/ha in tropical forests, almost four times greater than that found in temperate forests (DALAL;

ALLEN, 2008; PAN et al., 2013; POORTER et al., 2016a; SULLIVAN et al., 2020). The dynamics of AGB are closely linked to forest successional stages, influenced by growth, recruitment, and mortality processes, as well as by climatic effects (ROZENDAAL et al., 2017a). In this context, carbon dynamics in degraded old-growth forests also play a critical role in the regional carbon balance(ARAGÃO et al., 2014a).

There are several approaches to estimate AGB or carbon in forests. Some methods, such as destructive sampling, provide precise measurements but are not feasible at scale. Allometric models, widely used in forest inventories, estimate biomass based on dendrometric variables such as DBH, total tree height, and wood density (NELSON et al., 1999; JUCKER et al., 2017). These field-based methods remain the foundation for biomass estimation, but their spatial coverage is limited. To overcome this, remote sensing and geoprocessing techniques, when combined with field data, provide an effective way to upscale estimates and extend measurements across broader spatial and temporal scales (SANTOS et al., 2019). In particular, models based on spectral and structural responses derived from remote sensing have been increasingly integrated with field inventories to optimize AGB prediction (LONGO et al., 2016a; FENG et al., 2017; SILVA et al., 2017b, 2017a).

2.2 Aboveground biomass estimation using remote sensing

The estimation of AGB using remote sensing relies on sensors capable of capturing the vertical structure of forests, such as LiDAR and interferometric radar, often combined with optical data. These technologies use indirect measurements or backscattered signals, which are then related to AGB through empirical models and statistical functions (SANTORO; CARTUS, 2018). In general, LiDAR-based AGB estimation is conducted by developing regression models using structural metrics—particularly canopy height—calibrated with forest inventory plots and then extrapolated to broader areas (ASNER; MASCARO, 2014).

In the Atlantic Forest biome, a study applied a hybrid modeling approach that integrated optical remote sensing, environmental, and terrain variables. The

study demonstrated a significant reduction in the RMSE (from 40.78 to 33.43 Mg/ha) and an increase in the coefficient of determination (R^2, from 0.28 to 0.57), underscoring the benefits of incorporating multiple data sources for site-specific biomass modeling (SILVEIRA et al., 2021). These findings reinforce the importance of selecting predictor variables that help explaining the variability of the biophysical characteristics of the vegetation in each region to optimize AGB model performance (SILVEIRA et al., 2021).

Selecting appropriate predictor variables is essential for improving model performance, and these should capture vegetation properties that directly reflect canopy structure, understory density, and height variability (SILVEIRA et al., 2021). Among the different remote sensing platforms, LiDAR has become one of the most widely used sensors for AGB modeling. Most parametric models for LiDAR-based biomass estimation rely on statistical descriptors of return height distributions, including mean and maximum canopy height, height percentiles (e.g., P25, P50, P95), and canopy cover fractions (LONGO et al., 2016a). These models require calibration with field inventory data to ensure robust training and validation, providing the ground-truth information necessary to improve remote sensing–based biomass models

Another prominent class of sensors for biomass estimation is radar. Synthetic Aperture Radar (SAR) is an active remote sensing system that transmits microwave signals and records the backscattered energy, enabling data acquisition regardless of cloud cover or solar illumination (SINHA et al., 2015). The interest in using radar systems to estimate forest biomass dates back to the 1980s, but more consistent exploration began in the 1990s with missions such as ERS-1/2, JERS-1, SIR-C/X-SAR, AIRSAR, and CARABAS (SANTORO; CARTUS, 2018). Unlike optical systems, SAR enables the analysis of backscatter intensity, polarimetric parameters, and interferometric coherence, all of which provide useful information for estimating aboveground biomass. Studies applying SAR data to discriminate forest successional stages have demonstrated its potential to capture structural variability across different forest types (WIEDERKEHR et al., 2020). In Brazil, SAR applications for AGB estimation are particularly common in the Amazon, making use of P-, L-, C-, and X-band

systems. These studies typically rely on backscatter intensity, polarimetry, texture measures, and interferometric methods to characterize vegetation structure and improve biomass predictions (BOURGOIN et al., 2018; BISPO et al., 2019; DEBASTIANI et al., 2019; CASSOL et al., 2020).

Nevertheless, to advance knowledge regarding aboveground biomass estimation, it is crucial to address current limitations of remote sensing approaches. For example, SAR backscatter often saturates at intermediate-to-high biomass levels (>150–200 Mg/ha), reducing sensitivity in dense tropical forests (MITCHARD et al., 2011; YU; SAATCHI, 2016). Similarly, optical sensors are constrained by cloud cover and signal saturation, while LiDAR coverage is still spatially limited and costly at large scales. These challenges highlight the need for new sensors, such as GEDI and NISAR, and integrated methodological approaches that combine multi-sensor data, machine learning, and extensive field inventories to overcome individual limitations and improve AGB estimates across diverse forest types.

The future of spaceborne remote sensing with SAR is promising. One of the most recent developments in this regard is the European Space Agency's BIOMASS mission, launched in 2025 as part of the Earth Explorer program. BIOMASS aims to deliver global measurements of aboveground biomass at a spatial resolution of ~200 m, as well as canopy height at ~50 m, to support climate change mitigation strategies, including REDD+ initiatives (LE TOAN et al., 2011a; QUEGAN et al., 2019; THE EUROPEAN SPACE AGENCY, 2025). Operating at P-band (~435 MHz; wavelength ~70 cm), BIOMASS provides deeper canopy penetration than traditional L- and C-band systems, enabling the retrieval of structural information in dense, high-biomass forests where signal saturation is a known issue (QUEGAN et al., 2019). Complementing this effort, the NASA–ISRO Synthetic Aperture Radar (NISAR) mission, scheduled for launch in 2025, will operate in dual L- and S-bands with ~10–30 m resolution and a 12-day global revisit cycle. While not designed exclusively for biomass estimation, NISAR will generate consistent time-series data on forest structure and disturbance, providing critical information for monitoring forest dynamics at regional to global scales

BIOMASS is expected to produce consistent time series of AGB and forest disturbance at a near global scale, addressing major data gaps in Earth system science and climate modeling. Despite anticipated challenges such as radio-frequency interference and trade-offs in cloud penetration compared to optical sensors, the mission's design and data processing framework have been developed to mitigate these limitations. In future applications, BIOMASS data are expected to be fused with LiDAR datasets—such as those from the GEDI mission—and optical imagery to further enhance forest structure characterization and biomass estimation accuracy (QUEGAN et al., 2019).

2.3 Remote sensors

This section presents a brief review of key sensors used for estimating AGB, highlighting their main characteristics and relevance to forest structure monitoring.

2.3.1 Optical sensors

Optical sensors represent the majority of current spaceborne platforms and have undergone continuous technological advances over the past decades. Modern satellite constellations now provide images with increasingly fine spatial resolution (from sub-meter to tens of meters), diverse spectral coverage (from broad multispectral to narrow hyperspectral bands), and flexible temporal resolution (from daily to monthly revisit times), enabling a wide range of ecological and environmental applications. The selection of an appropriate optical sensor depends on the research objectives and the required scale of analysis—for example, high spatial resolution (<5 m) for detailed forest structure mapping, hyperspectral data for species or material discrimination, and high temporal resolution for monitoring disturbance dynamics or phenology. In practice, the choice among different optical missions (e.g., Landsat, Sentinel-2, Planet, WorldView) must balance sensor characteristics, data availability, and accessibility. With the increasing open access to optical datasets and the development of cloud-based processing platforms such as Google Earth Engine, the integration and analysis of large volumes of optical imagery have become more feasible for biomass and land-cover studies.

In recent years, the availability of medium- to high-resolution optical satellite imagery for public use has expanded significantly, with substantial improvements in both spatial and temporal resolution compared to earlier missions. The latest missions, Landsat 8 and Landsat 9, carry the Operational Land Imager (OLI) and Thermal Infrared Sensor (TIRS), providing 11 spectral bands and a 16-day revisit cycle and offering 30 m spatial. Due to its long temporal archive and consistent global coverage, Landsat is a critical tool for long-term forest monitoring and trend analysis, particularly when integrated with machine learning techniques and data from other sensor platforms (WULDER et al., 2019). Building upon this legacy, the Sentinel-2 mission (launched in 2015) provides free Multispectral Instrument (MSI) images at Level-2A, with 13 spectral bands covering visible, near-infrared, and short-wave infrared regions, a spatial resolution of up to 10 m, and a revisit time of 5 days when Sentinel-2A and 2B are combined (ESA, 2020a). These advances allow for more detailed and frequent monitoring of vegetation processes, particularly disturbances and successional dynamics, by capturing the interaction of electromagnetic radiation with different plant characteristics (PONZONI; SHIMABUKURO; KUPLICH, 2012).

Multispectral and hyperspectral sensors provide detailed spectral information that is fundamental for vegetation studies, particularly for image segmentation, classification, and biomass estimation. Recent advances demonstrate that, when combined with machine learning and deep learning techniques, these datasets can be scaled to regional applications, supporting forest monitoring and mapping with high accuracy (WAGNER et al., 2019). In parallel, more classical approaches such as the Linear Spectral Mixture Model (LSMM) remain relevant for deriving sub-pixel information. This method assumes that the reflectance of each pixel is a linear combination of the reflectance of its constituent elements (endmembers). By solving a system of linear equations for each pixel using the least squares method, LSMM produces fraction images that represent the proportional contribution of different components in the landscape (SHIMABUKURO; SMITH, 1991). Together, these approaches highlight the versatility of optical sensors for both traditional spectral unmixing and advanced data-driven modeling of forest attributes.

In addition, vegetation indices derived from optical data further enhance the ability to monitor forest condition and estimate aboveground biomass. Widely used indices such as the Normalized Difference Vegetation Index (NDVI), Enhanced Vegetation Index (EVI), and Soil-Adjusted Vegetation Index (SAVI) provide proxies of canopy greenness, density, and productivity. These indices improve land cover classification, support ecological modeling, and strengthen biomass estimation by linking spectral reflectance patterns to forest structure and physiological status. When combined with long time-series from Landsat and high-resolution observations from Sentinel-2, vegetation indices allow for detailed assessments of forest regrowth, degradation, and resilience across spatial and temporal scales. In summary, optical sensors remain essential instruments for AGB estimation by offering spectral information that supports both classification and predictive modeling, especially when used in conjunction with active sensors such as LiDAR or radar.

2.3.2 Synthetic Aperture Radar

SAR is an active remote sensing system that transmits microwave signals toward the Earth's surface and records the backscattered energy to generate high-resolution images. Unlike optical sensors, SAR operates independently of solar illumination and can penetrate clouds, haze, and smoke, making it particularly suitable for tropical forest monitoring (KNAPP et al., 2018). By measuring the amplitude and phase of the backscattered signal, SAR provides information about forest structure, including canopy height, density, and vertical complexity, which can be used to indirectly estimate aboveground biomass (AGB).

One of the most widely used platforms is the Sentinel-1 mission, which has provided freely available C-band (5.405 GHz) data with dual polarizations (VV and VH) and high temporal resolution since 2014 (ESA, 2020b). These characteristics enable systematic monitoring of forest cover dynamics and disturbance detection, although C-band penetration into dense canopies is limited compared to longer wavelengths. Consequently, the selection of radar frequency bands is critical (Table 2.1). In general, longer wavelengths provide greater penetration, enhancing sensitivity to woody biomass components, while

shorter wavelengths capture canopy-level properties. This wavelength-dependent behavior underscores the importance of frequency choice in tailoring SAR applications to biomass estimation.

Table 2.1 - Application of radar according to the frequency band.

Frequency Band	Frequency Range (MHz)	Wavelength (nm)	Application Example
Very High Frequency	300-300	$1x10^{9} – 1x10^{8}$	Foliage and ground penetration, biomass
P-band	250-500	$1.2x10^{8} – 6x10^{7}$	Biomass, soil moisture
L-band	1000-2000	$3x10^{7} – 1.5x10^{7}$	Agriculture, forestry, soil moisture
C-band	4000-8000	$7.5x10^{6} – 3.75x10^{6}$	Ocean, agriculture
X-band	8000-12000	$3.75x10^{6} – 2.5x10^{6}$	Agriculture, ocean, high resolution radar

Source: Podest et al., (2020).

Forest monitoring using SAR needs to take into consideration not only the characteristics of the radar instrument such as polarizations, incident angle and wavelength but also surface parameters such as structure and dielectric attributes. Radar signal is polarized, which means the signal transmitted and received has a different polarization (horizontal or vertical). With SAR techniques it is possible to identify the emitted and received polarization and its different combinations can determine physical properties of the targets. Additionally, the incident angle influences the brightness of the image, varying according to the angle of illumination and the earth's surface plane. One of the main constraints in biomass estimation is the saturation of the sensor response. According to the density of the forest and the radar band, at a certain point the pixel will saturate when reaching a threshold. In the Amazon, P-band backscattering saturates at about 100 t/ha (NEEFF et al., 2003). For broadleaf and coniferous forests L-band backscattering saturates at about 40 t/ha and 20 t/ha for C-band (IMHOFF, 1995). Indeed, moisture and water can affect the backscattering for estimating biomass, as an alternative for L-band, cross-image normalization can reduce these effects to less than 50% (HUANG et al., 2015).

Several studies have demonstrated the usefulness of SAR data for environmental monitoring of LULC dynamics, detecting forest change, and estimating AGB

(BOVOLO; BRUZZONE, 2005). In particular, Sentinel-1 C-band observations in VV and VH polarizations provide consistent backscatter signals that are sensitive to canopy density and structural degradation. VV polarization is more influenced by vertical structures such as stems and branches, while VH polarization is particularly responsive to horizontal and volumetric components of the canopy. Together, these responses enable the differentiation between intact, degraded, and secondary forests (KELLNDORFER, 2019). Although C-band backscatter tends to saturate in high-biomass environments, it remains valuable for detecting forest disturbance gradients and monitoring successional recovery.

One of the main satellites with SAR sensor in orbit now is Sentinel-1A (S1A), and its data is freely available on cloud computing platforms such as GEE. The dataset availability starts in October of 2014 up to now. S1A provides C-band dual-polarized SAR data with a spatial resolution of 10 meters and revisit time of 12 days (Table 2.2).

Table 2.2 - Sentinel 1A main characteristics.

SAR band	C-band (5.405 GHz, 5.625 cm)
Acquisition mode	Interferometric Wide Swath (IW)
Orbit mode	Descending
Image product	GRD, high resolution
Multilooking	4 x 1
Spatial resolution	10, 25, 40 meters
Revisit time	12 days
Polarization	VV, HH, VV+VH, HH+HV

Source: Adapted from Doblas et al., (2020)

The use of SAR for biomass estimation has been applied worldwide in complex and different regions (KUMAR et al., 2019; FORKUOR et al., 2020). In Brazil, most of the studies are concentrated in the Amazon but also in Cerrado and Atlantic Forest biomes. In the Central Brazilian Cerrado, woody AGB has been successfully mapped using a multi-sensor approach (SAR, LiDAR, and optical) combined with machine learning, showing significant improvements when integrating remote sensing data with field inventories (BISPO et al., 2020).

However, researchers have analyzed the effect of terrain on biomass estimation using SAR (SAATCHI et al., 2011a; MITCHARD et al., 2012b). In areas with variable topography, accurate terrain estimation is particularly important, whereas backscatter correction plays a comparatively smaller role in improving biomass estimation (SAATCHI et al., 2011a; BISPO et al., 2014).

In sum, SAR has a strong potential for mapping biomass in different biomes and forest structures. As remote sensing techniques advance and new sensor data become available. Recent literature highlights promising perspectives for SAR integration with emerging sensors such as the ESA BIOMASS mission (P-band) (LE TOAN et al., 2011b), NASA's GEDI LiDAR (DUBAYAH et al., 2020) and ICESat-2 (ATLAS LiDAR) (NEUENSCHWANDER; PITTS, 2019), the NISAR mission (dual-frequency L- and S-band SAR) (ROSEN et al., 2015), as well as upcoming hyperspectral missions like EnMAP and Surface Biology and Geology (SBG) (GUANTER et al., 2015). Nonetheless, challenges remain in integrating sensors with varying spatial and temporal resolutions, which must be overcome to improve results with advanced approaches (MARSELIS et al., 2020; SILVA et al., 2021).

2.3.3 Light Detection and Ranging (LiDAR)

LiDAR is an active remote sensing technology that uses laser pulses to measure distances between the sensor and the Earth's surface, generating high-resolution three-dimensional (3D) information about vegetation structure (DUBAYAH; DRAKE, 2000; GIONGO et al., 2010). LiDAR sensors can be deployed on terrestrial, airborne, or spaceborne platforms, and are particularly effective in capturing vertical forest attributes such as canopy height, vertical distribution of foliage, and understory density, key variables for accurate aboveground biomass estimation (HASSEBO, 2012).

ALS has been widely used in forest inventory and biomass studies, often providing accurate AGB models when combined with field plots and regression-based approaches (ASNER; MASCARO, 2014; LONGO et al., 2016a). ALS offers detailed structural information over relatively large areas, though logistical costs and limited temporal resolution remain challenges for broad-scale

applications (DUBAYAH; DRAKE, 2000; WULDER et al., 2008). Although LiDAR ALS metrics often present high correlation with AGB ($R^2 \geq 0.7$) (LONGO et al., 2016; ALMEIDA et al., 2019a), data acquisition is restricted by the cost and availability of airborne platforms, which makes it difficult to collect information at large spatial and temporal scales (DE ALMEIDA et al., 2020)

This three-dimensional data source is based on the time the laser pulse takes to reach the target and bounce back to the sensor. Then, according to the light speed it is calculated the distance from the target measuring its height (Equation 2.1)

$$Distance = \frac{3x10^8 \text{ m s}^{-1} \times \text{ signal time return}}{2} \quad (2.1)$$

At the orbital level, several spaceborne LiDAR missions have extended the capacity for global biomass monitoring. The Geoscience Laser Altimeter System aboard ICESat-1 (2003–2009) was the first mission to provide LiDAR data from space, enabling early global assessments of forest height and AGB (LEFSKY, 2010). Its successor, ICESat-2, launched in 2018, uses the Advanced Topographic Laser Altimeter System (ATLAS), which emits six laser beams at high temporal and spatial resolution. ICESat-2 focuses primarily on surface elevation, and also allows for vegetation height profiling in certain conditions, contributing to biomass and canopy structure analysis, particularly in open or sparse forests (NEUENSCHWANDER; PITTS, 2019).

More recently, NASA's GEDI LiDAR, deployed on the International Space Station in 2018, was specifically designed for forest structure measurements. GEDI captures full-waveform LiDAR data across tropical and temperate forests, providing metrics such as canopy height percentiles, plant area index, and vertical foliage distribution. These are crucial for large-scale AGB modeling and serve as reference data for calibrating optical or radar-based estimates (DUBAYAH et al., 2020).

While having the advantage of sampling height of forests on Earth, GEDI also has limitations with higher noise, atmospheric interference and geolocation error

when compared with ALS. Nevertheless, GEDI has progressively expanded its portfolio of derived products, such as canopy height, aboveground biomass density, and foliage height diversity, which increase its potential for integration with other datasets (DUBAYAH et al., 2020; DUNCANSON et al., 2020). Although noise and data-processing challenges remain, GEDI represents a strong source of global biomass information, especially when combined with ALS, SAR, or optical sensors.

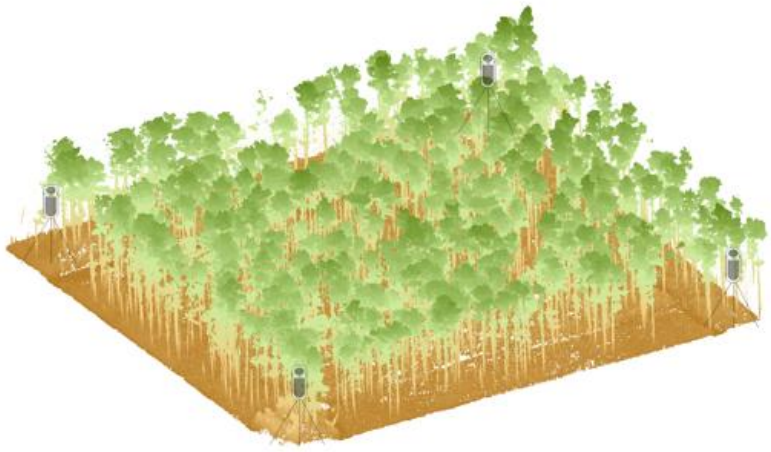
TLS, in turn, provides ground-based, high-resolution (millimeter level point spacing) structural information, capturing fine-scale understory complexity and individual tree architecture (WILKES et al., 2017; CALDERS et al., 2020; LOUDERMILK et al., 2023). TLS is particularly valuable in disturbed or regenerating forests where vertical heterogeneity is a key indicator of successional stage and carbon accumulation. Its precision enables detailed 3D reconstructions and has been shown to significantly improve biomass estimates when integrated with field inventories and machine learning approaches (WALLACE et al., 2022; TANEJA et al., 2023).

One of the key advantages of TLS is its ability to resolve the full vertical profile of vegetation, including the understory and complex mid-canopy layers, which are often poorly captured by airborne or spaceborne sensors. This makes TLS particularly effective in structurally complex or disturbed forests, such as those undergoing succession or recovering from fire (LOUDERMILK et al., 2012a, 2023; HUDAK et al., 2016a, 2016b). The ability to detect subtle differences in forest structure across small spatial gradients makes TLS a powerful tool for biomass modeling in heterogeneous landscapes.

Recent studies have demonstrated that TLS-based biomass estimates can approach the accuracy of destructive harvest methods, with errors often below 10% at the individual tree level (CALDERS et al., 2015; GONZALEZ DE TANAGO et al., 2018). Moreover, TLS facilitates the development of non-destructive allometric models, which can improve the reliability of inventory-based biomass estimates and provide a means to validate airborne and satellite-derived biomass products (CALDERS et al., 2020).

However, TLS also presents challenges. Occlusion effects from neighboring trees, the limited field of view in dense forests, and the need for multiple scan positions to reduce shadowing can complicate data acquisition and processing (Figure 2.1). Moreover, the scalability of TLS is limited due to the time-consuming nature of fieldwork and data processing, restricting its application to plot-level studies or model calibration (WILKES et al., 2017). Despite these limitations, TLS has become an indispensable tool for benchmarking remote sensing approaches, validating AGB models, and improving our understanding of structural drivers of biomass.

Figure 2.1 - Representation of TLS scanning positions and combined point cloud results.



The integration of TLS with machine learning methods, including Random Forests and Support Vector Machines, has further enhanced its utility for biomass prediction, enabling the selection of optimal structural predictors and improving model generalizability (GONZALEZ DE TANAGO et al., 2018). As TLS instruments become more compact, automated, and integrated with mobile platforms, the role of TLS in high-resolution forest monitoring is expected to expand significantly.

3 BIOMASS ACCUMULATION IN SECONDARY FORESTS: SPATIAL PATTERNS AND SUCCESSIONAL AGE EFFECTS IN THE BRAZILIAN AMAZON[1]

This chapter examines the first theme of AGB variation explored in this thesis: biomass accumulation along forest regeneration gradients. Specifically, it investigates the spatial distribution and age profile of secondary forests in the Brazilian Amazon and how these factors influence AGB levels. Using multitemporal land use and land cover data from the TerraClass project and airborne LiDAR-derived biomass estimates, the analysis focuses on two pilot regions in Pará state. The central aim is to understand how SF age affects carbon accumulation, and how historical land use patterns shape forest recovery. This chapter provides an important foundation for understanding the carbon dynamics of regenerating landscapes and complements the disturbance-focused analysis in the next chapter.

SF have expanded in recent decades worldwide, mainly in regions with a deforestation history (VIEIRA, 2019). However, in the BLA, there is a strong correlation between SF growth dynamics with agricultural and pastoral activities and much more related to illegal logging over the last decade (PERZ; SKOLE, 2003; CHAZDON et al., 2016; WANG et al., 2020b). Furthermore, this type of forest regenerates in previously deforested areas and is seen as a component of the landscape, potentially generating ecosystem services, especially for climate change mitigation (CHAZDON et al., 2016; POORTER et al., 2016b; ROZENDAAL et al., 2017b; HEINRICH et al., 2021). Within that context, the study sought to broaden the understanding of the role of SF regeneration in the current LULC change process in the BLA.

SF are understood as the natural vegetation in regeneration. It features tree species densification, which has already suffered total suppression of native

[1] This chapter is based on the published article: da Silva, G.M.; Adami, M.; Galbraith, D.; Nascimento, R.G.M.; Wang, Y.; Shimabukuro, Y.E.; Emmert, F. Spatial Distribution of Secondary Forests by Age Group and Biomass Accumulation in the Brazilian Amazon. Forests, 14(5), 924 (2023). https://doi.org/10.3390/f14050924

vegetation since deforestation monitoring began in the Amazon (COUTINHO et al., 2013; ALMEIDA et al., 2016b). In addition, it is meaningful to understand the dynamics of SF expansion and how they are spatially distributed according to the official Brazilian monitoring systems in the Amazon. For this reason, it is helpful to expand knowledge about the role of the dynamics of the gain, remanence and loss of SF in the current process of changing the land use and cover of the Brazilian Legal Amazon.

In BLA, old-growth forest losses have surpassed gains for three decades (INPE, 2021). However, according to data provided by the Brazilian national land use and land cover monitoring system (TerraClass), only in 2008, the SF area accounted for 150,800 km² in the BLA, which highlights the SF regeneration as a potential mitigation of deforestation (ALMEIDA et al., 2016b). As an ecological consequence, ombrophilous forests are replaced by savanna vegetation (LOVEJOY; NOBRE, 2018), causing large-scale loss of biodiversity and affecting part of the local people's livelihoods (MARENGO et al., 2009). However, these impacts can lead to lost opportunities for the sustainable use of forests and the production of traditional goods for timber forest management and sustainable non-timber products (FEARNSIDE, 2006).

In the current scenario, deforestation has been a major environmental problem in the Amazon. Until 2020, accumulated deforestation rates in the BLA corresponded to 457,237 km², with the state of Pará being the most significant contributor with 157,374 km² of deforestation (INPE, 2021). In 2001, Pará registered about 16,728 km² of old-growth forest deforestation rate (INPE, 2021), the highest in the last 20 years for this state. In this context, SF emerge from previously deforested areas with different land use.

Recent studies show that SF in the BLA may mitigate climate change by sequestering carbon up to 20 times faster than old-growth forests (HEINRICH et al., 2021). According to MapBiomas (MAPBIOMAS, 2021), in 2004, the state of Pará had 79.1% of its entire territory covered by forest, and in 2020 this reduced to 74.91%, representing a loss around 30,000 km² of the forest, including different types of forest formation. Given the importance of monitoring forest loss and gain,

this study selected a land use coverage dataset from TerraClass project in the state of Pará, in the BLA, to analyze a time series of 2004, 2008, 2012 and 2014.

Land coverage monitoring systems are important to understand the dynamics of forest changes and mapping the forest age. For example, in the Amazon, SF age is the primary driver to estimate aboveground carbon (HEINRICH et al., 2021). Within these spatial information policies, decision-makers can take actions to mitigate carbon emissions (SILVA JUNIOR et al., 2020), forest management planning and change environmental laws for sustainable use.

The biomass of tropical forests has been taking an important role in the global carbon cycle as a source of carbon stock and potential for carbon dioxide emissions in deforested areas. The SF aboveground biomass has been spotted as one of the main factors in the global carbon cycle as in the young ages it stocks high amounts of carbon to proceed with the forest successional processes (CHAZDON et al., 2007, 2009, 2016; POORTER et al., 2016b). The aboveground biomass in SF has been estimated using multiple sensors remote sensors (BACCINI et al., 2012b; POORTER et al., 2016b; CASSOL et al., 2021). Some studies have contributed to the great importance of the age factor to estimate aboveground biomass in SF (CHAZDON et al., 2007; REQUENA SUAREZ et al., 2019) but this needs to be more investigated for different regions.

In this context, the present study seeks to answer how the distribution of the SF and its deforestation occurs in Pará state according to the forest age estimation and the aboveground biomass estimation in two pilot areas in the Pará state. Based on the above, we tested the hypothesis that CRS drives the spatial distribution patterns of SF. For this, we used TerraClass dataset on a time series analysis to understand how SF distribution occurs in the state of Pará and the dynamics of land use and land cover changes in the region.

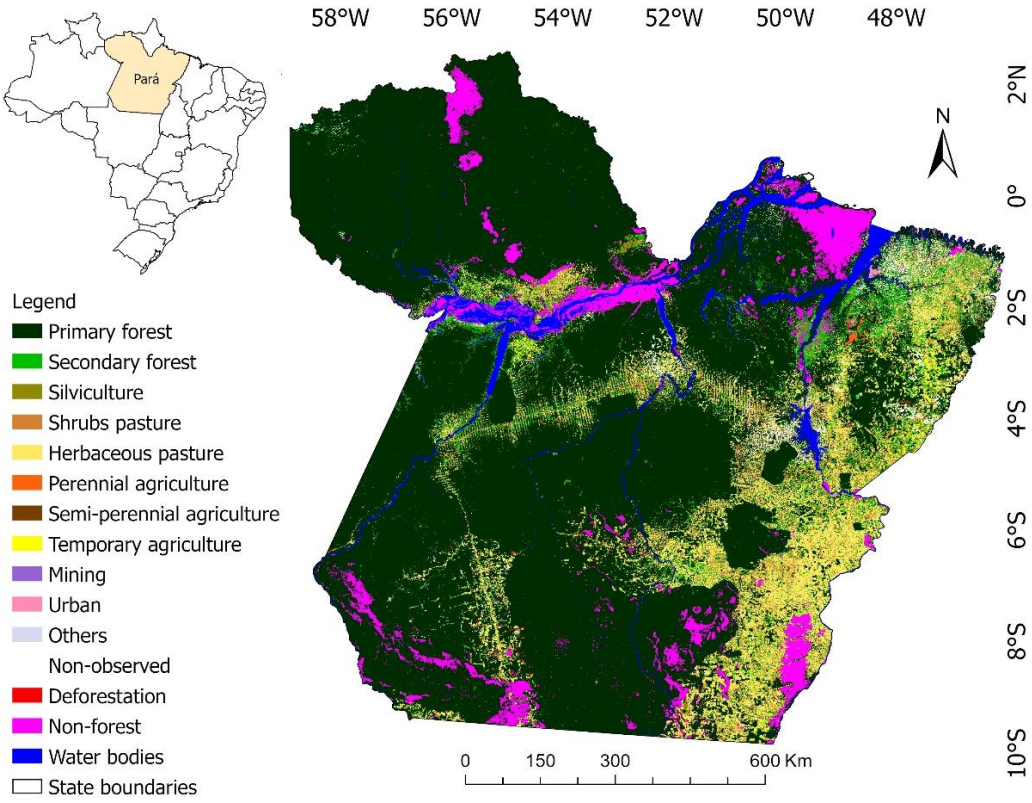
3.1 Materials and methods

3.1.1 Study area

The state of Pará is located in the north region of Brazil, with an approximate area of 1,248,000 km² (IBGE, 2021), located between the parallels 2°60’ North and

9°85’ South and the meridians 58°90’ and 46° West (Figure 3.1). The study region referring to the state of Pará was selected for this study because it presents a wide variety of vegetation cover and land use, especially SF, resulting in a formation with great complexity and spatial and temporal variability. In 2020, around 74.91% of the entire state was covered by forest, 3.3% by non-forest natural formation, 17.8% by farming, 0.001% of non-vegetated area, and 3.5% of water (MAPBIOMAS, 2021).

Figure 3.1 - Land use and land cover map of Pará state according to TerraClass for 2014.

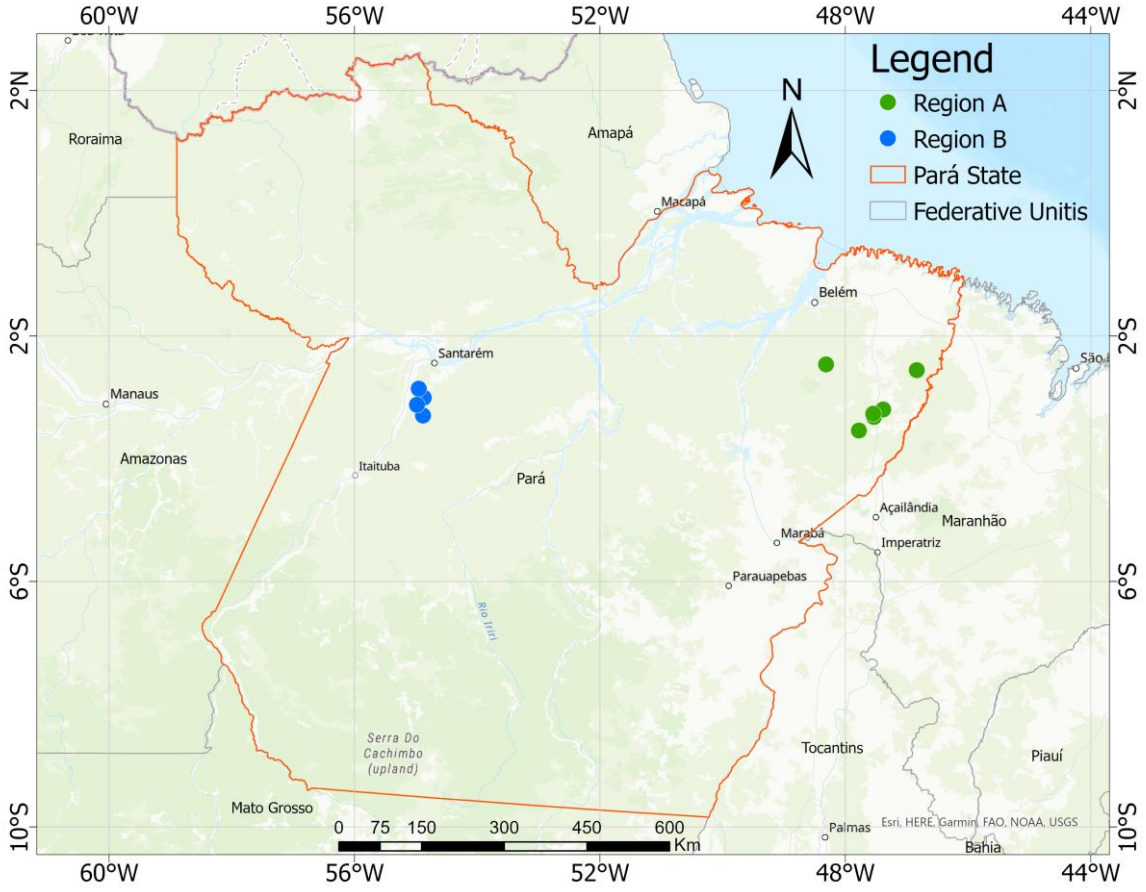


Two pilot areas were selected for aboveground biomass estimation, specifically, with SF land cover (Figure 3.2). The first one, named for this paper as region A, is mostly inserted within the municipality of Paragominas (3°15’ S and 47°30’ W). This municipality is known by the heavy logging activities from sustainable forest practices since 1960. With the decline of logging activity, the agricultural frontier expanded, mainly with monocultures such as soy and pasture areas. As of 2008, the municipality adopted policies to reduce the environmental impact of economic

activities, which led to a decline in deforestation for the first time in the history of Pará (GUIMARÃES et al., 2011). The second, named region B, is located in the municipality of Belterra (3°5’ S and 54°56’ W) near the Tapajós National Forest. Region B has a history of degradation, logging, anthropic occupation, pasture, and agriculture.

More details about the pilot areas are described on the Supporting Information for “Aboveground biomass variability across intact and degraded forests in the Brazilian Amazon” (LONGO et al., 2016b).

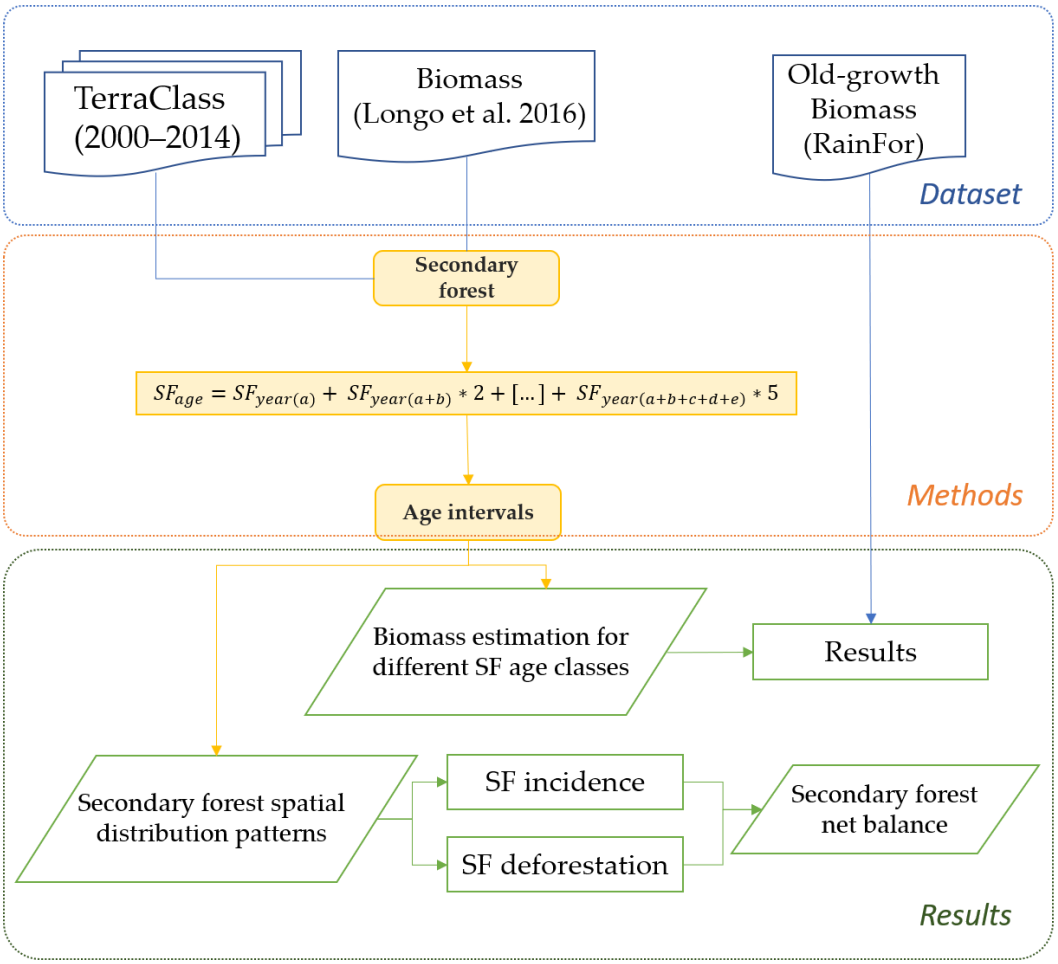
Figure 3.2 - Pilot study areas in Pará State.



3.1.2 Methodological approach

Figure 3.3 shows the general flowchart of the methodological approach developed for this work.

Figure 3.3 - Flowchart of the methodological approach.



3.1.3 Land use change and secondary forest

Land use and land cover maps were generated for every year under analysis, using the TerraClass thematic classes. The dataset is derived from medium-resolution Landsat-5 TM and MODIS images through supervised classification (COUTINHO et al., 2013; ALMEIDA et al., 2016b), and it is freely available on INPE's website. The global accuracy of TerraClass mapping is 76.64%, and 21.5% omission error and 20.2% of commission error for secondary vegetation class (ALMEIDA et al., 2016b). Then, we imported and preprocessed land use data from GEE platform into a raster format. After that, different rasters were generated for SF age classes based on previous land use.

3.1.4 Secondary forest age

Using cartographic modelling (TOMLIN, 1990), rasters with binary values for the absence or presence of SF in each year were used to classify the age interval per pixel of SF. The last year in our time series is 2014; before that, we have 2012 LULC mapped, meaning the minimum age interval of SF is 0 to 2 years old according to the previous LULC. The age classes were based on the difference in the age interval of each year studied, assigning a range from 1 to 5 to each interval, according to the Equation 3.1:

$$SF_{age} = SF_{year(a)} + SF_{year(a+b)} * 2 + [\dots] + SF_{year(a+b+c+d+e)} * 5 \quad (3.1)$$

where SF_{age} refers to the SF age class from 1 to 5 determining the age interval estimation, and SF_{year} refers to the mapped permanent year of SF multiplied by the age class.

An exploratory data analysis was performed about the age classes and the previous land use of each SF mapped (Table 3.1).

Table 3.1 - Classification of SF age in age interval.

Age interval (years)	Class	2004	2008	2010	2012	2014
0 to 2	1	Non SF	Non SF	Non SF	Non SF	SF
2 to 4	2	Non SF	Non SF	Non Secondary Forest	SF	SF
4 to 6	3	Non SF	Non SF	SF	SF	SF
6 to 10	4	Non SF	SF	SF	SF	SF
≥ 10	5	SF	SF	SF	SF	SF

For each year, every pixel classified as SF was looked up to the previous classification along the time to classify the age interval. According to the previous land use and land cover, the age range of SF was classified to fit the age range estimation of the forest.

3.1.5 Aboveground biomass estimation data

The AGBCD estimation data is provided by literature (LONGO et al., 2016b). The data was estimated using airborne LiDAR and calibrated using forest inventory measurements. For the chosen pilot areas, the estimated AGBCD selected LiDAR metrics were collected between 2012 and 2015 using parametric modelling (LONGO et al., 2016b). The uncertainty of the aboveground carbon density are described for each plot for the pilot areas on the published paper and in the Supporting Information for “Aboveground biomass variability across intact and degraded forests in the Brazilian Amazon” (LONGO et al., 2016b).The data were acquired by the Sustainable Landscapes Brazil project, supported by the Brazilian Agricultural Research Corporation (EMBRAPA), the US Forest Service, USAID and the US State Department, in areas nearby with similar characteristics as the pilot area. Also, the old-growth aboveground biomass data were acquired from plots provided by ForestPlot.net (LOPEZ-GONZALEZ et al., 2011).

3.1.6 Data analysis

3.1.6.1 Hot Spot analysis of SF spatial distribution

The geopolitical influence on the distribution of SF was analyzed from the variation of its spatial distribution mapped by TerraClass in the study area. The Optimized Hot Spot Analysis algorithm from ArcGIS Pro was performed for this context. This algorithm associates an attribute of each feature to the corresponding neighboring elements by mapping locations with statistically higher (hot spot) or lower (cold spot) values to the expected value of the attribute for the total area analyzed (MITCHELL, 2005).

The SF fragments of each age class in raster format with 30 meters of the spatial resolution were converted into points to enable the fragment area measurement based on the projected coordinate system South America Albers Equal Area Conic. Each point was assigned the area of its respective polygons given the municipal boundaries. This dataset was used as an input file in the first Hot Spot analysis, which considered the incidence (density of points) and forest fragments (ha) area with 90, 95, and 99% confidence levels by spatial location on the map.

Also, according to the SF fragments, descriptive statistic was taken considering the number and area of polygons within every age class.

3.1.6.2 Hot Spot analysis of deforestation of SF spatial distribution

To map the deforestation, we applied the difference along the time to detect the loss of SF. Then, we applied the Optimized Hot Spot Analysis algorithm using the area of secondary forest deforestation as input for each year of the time series. It was considered the area of SF deforestation (ha) with 90, 95, and 99% confidence levels by spatial location on the map, including areas where the deforestation occurred more than once.

3.1.6.3 SF net balance

We selected the SF incidence and deforestation areas to calculate the balance between the study period. Then, the data were analyzed in pairs to verify the cumulative SF (Accumulated SF mapped in the final year of analysis), the gain (new SF mapped), the remaining (permanent SF), the loss (Remain subtracted from the previous cumulative year) and the net balance (total SF mapped: Remain + Gain – Loss).

3.1.6.4 Aboveground biomass estimation for different SF age classes

To estimate the aboveground carbon density, we selected the SF fragments for each plot with the aboveground biomass estimation data provided by the literature. Then, we interpolated the aboveground biomass data after applying the method described to estimate the age interval for the time series after. After that, the old-growth aboveground biomass data for the nearby regions was considered to compare the aboveground biomass accumulation results. Also, according to the SF fragments, a descriptive statistic was taken considering the interpolation with the aboveground biomass data for every age class. Therefore, we applied the Kolmogorov-Smirnov test to check the normality of the data, then we computed the two-way analysis of variance (ANOVA) for unbalanced designs to test the null hypothesis that the mean aboveground biomass for different age intervals in the SF has no difference in the two pilot areas. Finally, we applied the

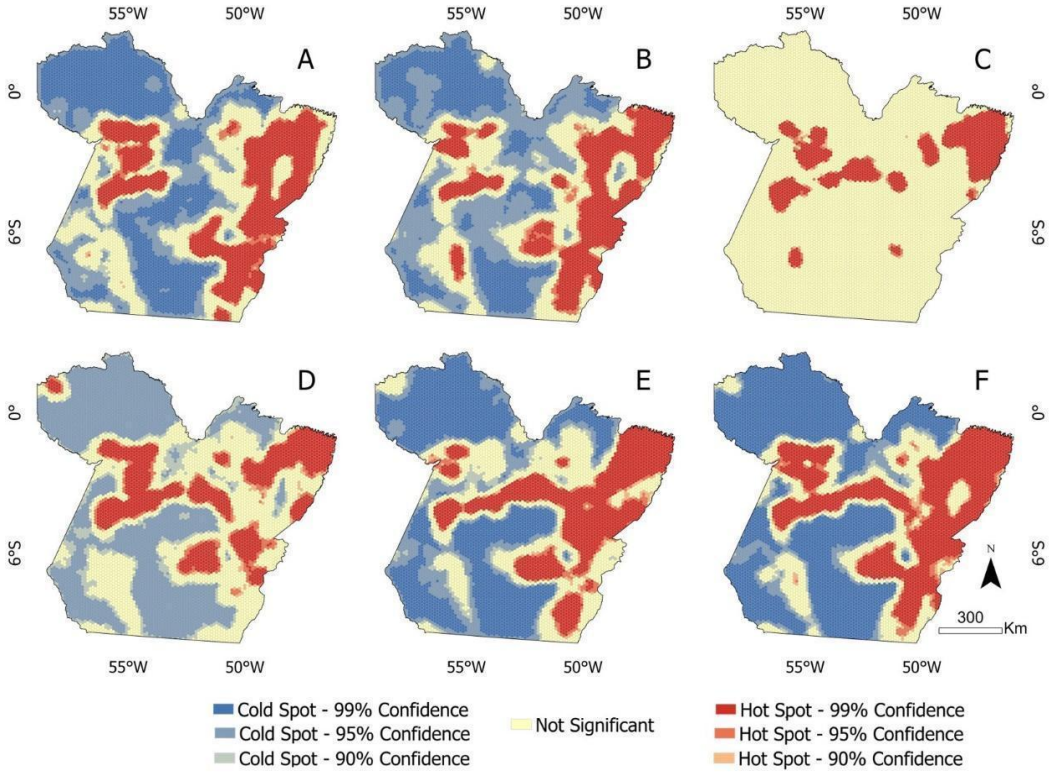
Tukey multiple comparisons test at a 95% family-wise confidence level to verify which classes differed in aboveground biomass accumulation.

3.2 Results

3.2.1 SF spatial distribution patterns

Using hot spot analysis, we detected the hot and cold spots for SF incidence in Pará state, according to the age class (Figure 3.4). In general, the spatial distribution of SF in Pará state presented a pattern of a hot spot in the northeast region of the State, also along the main highways and harbor areas of the State. The oldest mapped SF in Pará state (Figure 3.4A and Figure 3.4BB), presented similar patterns of cold and hot spots. These areas of hot spots are regions with long historic LULC changes. Compared with other age intervals, SF of 4 to 6 years old (Figure 3.4CC) had very defined locations across the State. On the other hand, the youngest mapped SF incidence connects the eastern side of the state with the Baixo Amazonas mesoregion (Figure 3.4D and E). To summarize the incidence of SF, Figure 3.4.F grouped the entire time series representing hot spot and cold spot areas.

Figure 3.4 - Hot spot analysis of SF incidence in Pará State by age class.

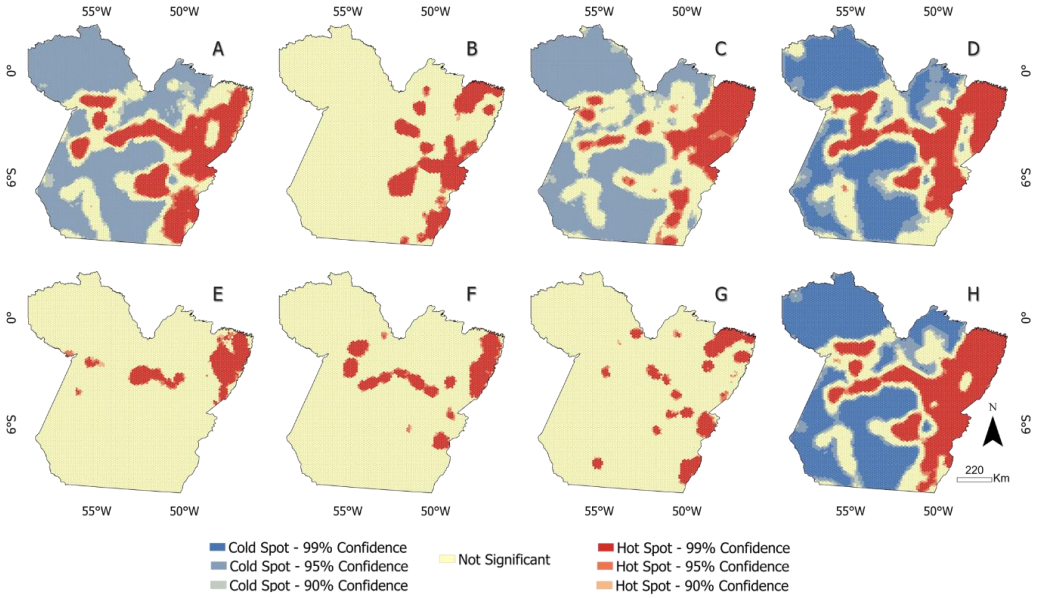


A) ≥ 10 years old; B) 6 to 10 years old; C) 4 to 6 years old; D) 2 to 4 years old; E) 0 to 2 years old; F) total incidence between 2004 and 2014.

The same analysis was performed for SF deforestation (Figure 3.5). A specific age interval could not define the pattern of deforestation determined. The regions with the most incidence of SF presented the hottest spot areas for deforestation. On the other hand, the map shows a few parts where deforestation occurred more than once in the time series. Further, the cold spot areas are primarily located in protected areas, highlighting the importance of environmental protection laws.

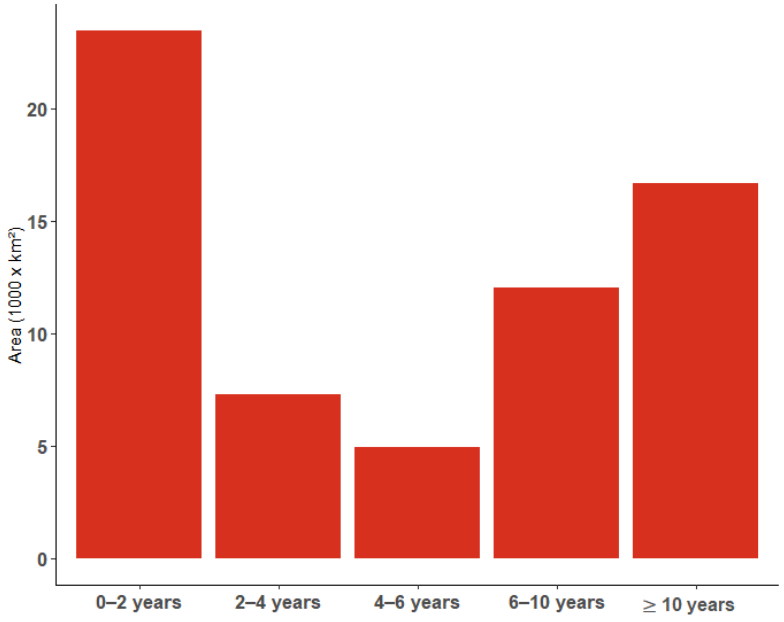
The total area of SF deforested in 2014 was 64,396.91 km² which represents around 5% of Pará's territory. The youngest age interval of 0–2 years old had the most deforested area with 23,465.4 km², that represents the fast land use and land cover changes in a short period. Then, the oldest SF (≥ 10 years old) had 16,653.2 km² deforested in 2014 (Figure 3.6).

Figure 3.5 - Hot spot analysis of SF deforestation on a time series.



A) Deforestation in 2008; B) Deforestation in 2010; C) Deforestation in 2012; D) Deforestation in 2014; E) Repeated deforestation in 2008 and 2012; F) Repeated deforestation in 2008 and 2014; G) Repeated deforestation in 2010 and 2014; H) Accumulated deforestation for the time series.

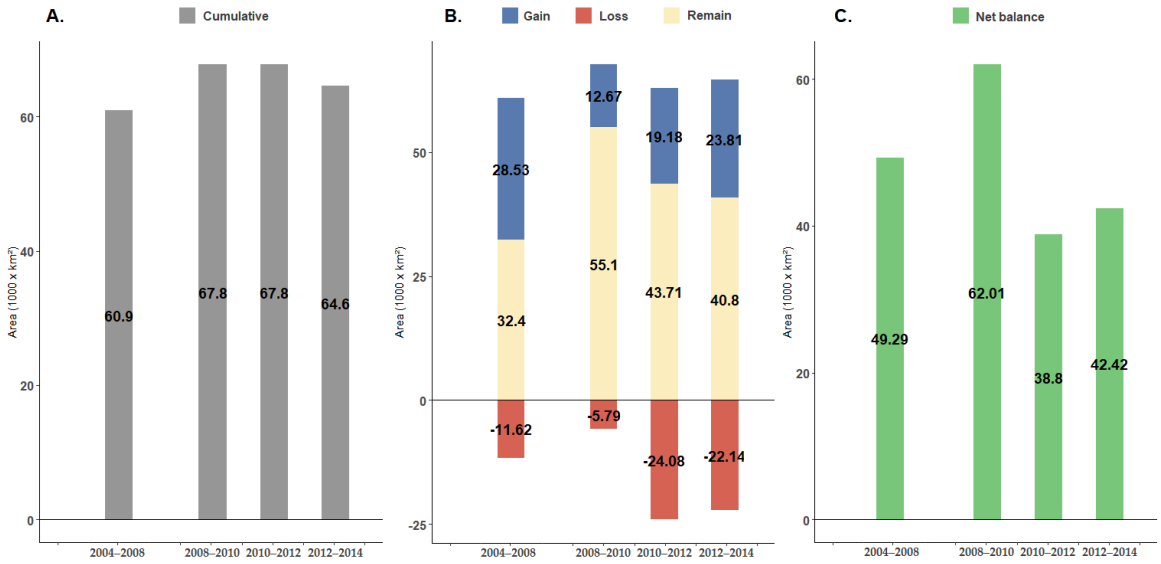
Figure 3.6 - Deforestation of SF in Pará State (2014).



We divided the temporal data into different intervals according to the available data to extract the area of SF balance mapped for the study period. The cumulative area did not vary much along the time series; the average for the time interval of analysis was 65,275.0 km² of SF (Figure 3.7A). As shown in the

balance (Figure 3.7B), a considered proportion of area remains growing along the time series, with some gains (new SF mapped) and losses. Therefore, the SF balance is still positive with the higher net balance is 2008–2010 (Figure 3.7C).

Figure 3.7. SF balance in Pará.

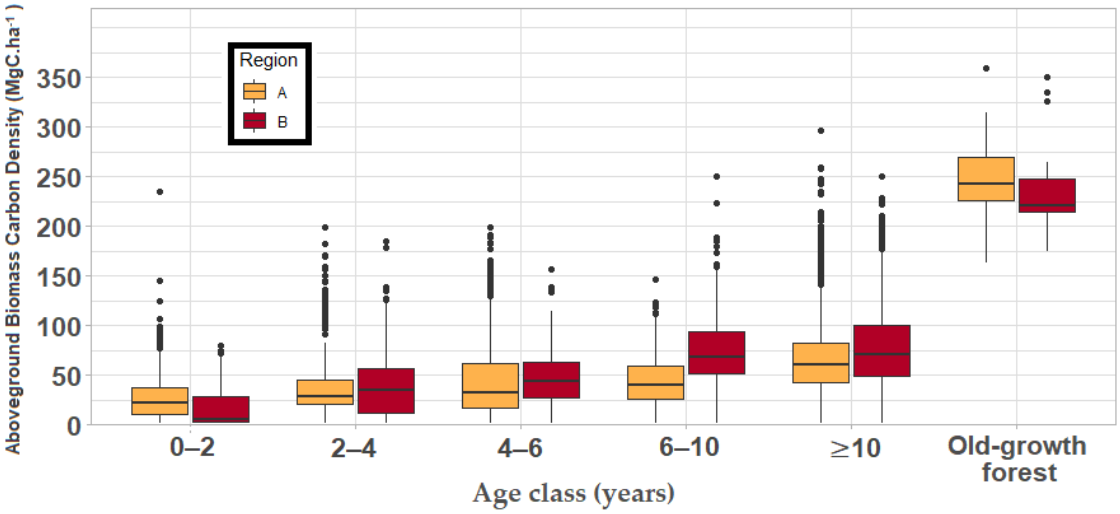


A. Cumulative = Accumulated SF mapped in the final year of analysis; B. Gain = New SF mapped, Remain = Permanent SF, Loss = Remain – previous cumulative year; C. Net balance = Total SF mapped (Remain + Gain – Loss).

3.2.2 Aboveground biomass estimation for different SF age classes

To point out the deforestation of SF, it is essential to understand how this has impacted aboveground biomass recovery over the years. We analyzed carbon density in aboveground biomass (MgC.ha-1) in two municipalities in the state of Pará (regions A and B), a similar behavior was observed about age classes, where the accumulation of aboveground biomass in the two municipalities is different over time. Over the years, SF store different amounts of carbon per hectare/year according to age classes. It was observed that SF ≥ 10 years old in pilot area A have an average of 23% of the aboveground biomass of an old-growth-forest in the same region. While for pilot area B, SF ≥ 10 years old have an average of 32.7% of the old-growth forest aboveground biomass (Figure 3.8).

Figure 3.8 - Distribution of aboveground biomass carbon density by SF age class group.



The lowest aboveground biomass estimates by age group found were in the 0–2 years old interval with the mean and standard deviation of 27.10 ± 20.98 and 17.18 ± 19.67 MgC.ha-1 for region A and region B, respectively. On the other hand, the age class that groups SF over ten years old had the highest mean aboveground biomass with 66 ± 37 and 77.01 ± 39.22 MgC.ha-1 (Table 3.2). Region A presents higher aboveground biomass in the early age groups (0–4 years old), meanwhile, the Region B presents a higher mean as the SF gets older (≥ 4 years old).

Table 3.2 - Descriptive statistics of aboveground biomass carbon density (MgC.ha-1).

Age interval (years)	Region A				Region B			
	$\bar{X}$	σ	σ^2	N	$\bar{X}$	σ	σ^2	N
0 to 2	27.11	20.98	439	2326	17.18	19.67	387	155
2 to 4	43.48	38.67	1,492	545	38.17	31.46	990	478
4 to 6	45.96	40.67	1,654	1,333	46.18	32.57	1,061	141
6 to 10	43.97	24.03	576	1,835	75.86	43.72	1,911	284
≥ 10	66.00	37.00	1,369	4,508	77.01	39.22	1,538	2,828
Old-growth forest	287.07	95.50	9,120	13	235.50	41.78	1745	29

$\bar{X}$ = mean; σ = standard deviation; σ^2 = variance; N= number of observations.

Using the two-way analysis of variance (Table 3.3), it was verified that there was a significant accumulation of aboveground biomass ($p<0.001$) over time in the age classes of SF. Also, it can be stated that there was a significant difference

(p<0.001) between the aboveground biomass comparing the two regions (A and B) when related to the accumulation of aboveground biomass in the period studied, denoting that regional variations (quality of the site) may influence the recovery of the aboveground biomass.

Table 3.3 - Analysis of variance test (ANOVA).

Source of variation	Df	Sum Sq	F_{value}	Pr(>F)
(Intercept)	1	1,709,123	1454.573	< 2.2e-16 ***
Age class	5	3,215,260	547.279	< 2.2e-16 ***
Region	1	14,319	12.187	0.0004828 ***
Age class + Region	5	282,406	48.069	< 2.2e-16 ***
Residuals	14,469	16,995,190		
Signif. codes: 0 '*' 0.001 '**' 0.01 '*' 0.05 '.' 0.1 ' ' 1**				

Then, we applied the Tukey test at a 95% family-wise confidence level and stated that for both regions in the same age interval, class 2 (2–4 years old), and 3 (4–6 years old) did not show a significant difference in the aboveground biomass accumulation (Table 3.4). The results show that in general, region B (western Pará) presents higher aboveground biomass accumulation as the SF get older when compared to region A, except for class 4 (4–6 years old) in region B which did not show the mean difference with class 3 (4–6 years old) in region A.

Table 3.4 - Tukey multiple comparisons of mean test at 95% family-wise confidence level.

Interaction	diff	lwr	upr	p adj
B – A	8.311	7.054	9.569	0.000
A – 1 – A – 2	16.374	11.042	21.706	0.000
A – 1 – A – 3	18.855	15.007	22.703	0.000
A – 1 – A – 4	16.862	13.364	20.360	0.000
A – 1 – A – 5	38.895	36.034	41.755	0.000
A – 1 – A – 7	259.966	228.805	291.127	0.000
B – 1 – A – 1	-9.927	-19.221	-0.632	0.024

continue

Table 3.5 - Continuation.

Interaction	diff	lwr	upr	p adj
B – 1 – A – 2	11.067	5.440	16.693	0.000
B – 1 – A – 3	19.071	9.354	28.789	0.000
B – 1 – A – 4	48.757	41.715	55.800	0.000
B – 1 – A – 5	49.899	46.763	53.035	0.000
B – 1 – A – 7	208.398	187.463	229.333	0.000
A – 2 – A – 3	2.481	-3.215	8.177	0.959
A – 2 – A – 4	0.488	-4.977	5.954	1.000
A – 2 – A – 5	22.521	17.440	27.602	0.000
A – 2 – A – 7	243.592	212.149	275.035	0.000
B – 2 – A – 1	-26.300	-36.499	-16.101	0.000
B – 2 – A – 2	-5.307	-12.328	1.714	0.359
B – 2 – A – 3	2.698	-7.888	13.284	1.000
B – 2 – A – 4	32.384	24.184	40.583	0.000
B – 2 – A – 5	33.525	28.284	38.767	0.000
B – 2 – A – 7	192.024	170.673	213.376	0.000
A – 3 – A – 4	-1.993	-6.024	2.039	0. 904
A – 3 – A – 5	20.040	16.548	23.532	0.000
A – 3 – A – 7	241.111	209.886	272.337	0.000
B – 3 – A – 1	-28.781	-38.289	-19.274	0.000
B – 3 – A – 2	-7.788	-13.761	-1.816	0.001
B – 3 – A – 3	0.217	-9.705	10.138	1.000
B – 3 – A – 4	29.903	22.581	37.225	0.000
B – 3 – A – 5	31.045	27.323	34.766	0.000
B – 3 – A – 7	189.543	168.513	210.574	0.000
A – 4 – A – 5	22.033	18.930	25.135	0.000
A – 4 – A – 7	243.104	211.920	274.288	0.000

continue

Table 3.6 – Continuation.

Interaction	diff	lwr	upr	p adj
B – 4 – A – 1	-26.789	-36.160	-17.417	0.000
B – 4 – A – 2	-5.795	-11.549	-0.042	0.046
B – 4 – A – 3	2.209	-7.582	12.001	1.000
B – 4 – A – 4	31.895	24.751	39.040	0.000
B – 4 – A – 5	33.037	29.679	36.396	0.000
B – 4 – A – 7	191.536	170.567	212.505	0.000
A – 5 – A – 7	221.071	189.952	252.190	0.000
B – 5 – A – 1	-48.821	-57.974	-39.669	0.000
B – 5 – A – 2	-27.828	-33.217	-22.439	0.000
B – 5 – A – 3	-19.823	-29.405	-10.241	0.000
B – 5 – A – 4	9.863	3.008	16.717	0.000
B – 5 – A – 5	11.005	8.317	13.692	0.000
B – 5 – A – 7	169.503	148.631	190.375	0.000
B – 7 – A – 1	-269.892	-302.244	-237.541	0.000
B – 7 – A – 2	-248.899	-280.393	-217.405	0.000
B – 7 – A – 3	-240.894	-273.370	-208.419	0.000
B – 7 – A – 4	-211.209	-242.986	-179.431	0.000
B – 7 – A – 5	-210.067	-241.212	-178.921	0.000
B – 7 – A – 7	-51.568	-88.964	-14.172	0.000
B – 1 – B – 2	20.993	10.637	31.349	0.000
B – 1 – B – 3	28.998	15.959	42.037	0.000
B – 1 – B – 4	58.684	47.495	69.873	0.000
B – 1 – B – 5	59.826	50.583	69.068	0.000
B – 1 – B – 7	218.325	195.656	240.993	0.000
B – 2 – B – 3	8.005	-2.733	18.742	0.381
B – 2 – B – 4	37.691	29.297	46.085	0.000

continue

Table 3.7 – Conclusion.

Interaction	diff	lwr	upr	p adj
B – 2 – B – 5	38.833	33.292	44.373	0.000
B – 2 – B – 7	197.331	175.904	218.759	0.000
B – 3 – B – 4	29.686	18.143	41.228	0.000
B – 3 – B – 5	30.828	21.160	40.496	0.000
B – 3 – B – 7	189.327	166.482	212.172	0.000
B – 4 – B – 5	1.142	-5.832	8.116	1.000
B – 4 – B – 7	159.641	137.799	181.482	0.000
B – 5 – B – 7	158.499	137.587	179.410	0.000

Region: A, B; Age classes: 1–5.

3.3 Discussion

This work proposed using the national land use and land cover system (TerraClass) to classify SF age and to estimate aboveground biomass accumulation in the Amazon region (Pará State). The result emphasizes the need of mapping and understanding the dynamics of SF in the regional carbon balance. The dynamics of LULC changes in tropical regions shift the carbon balance. Furthermore, the knowledge of aboveground biomass dynamics in SF in the context of changes in LULC has an essential role in the global carbon cycle (ARAGÃO et al., 2014b; POORTER et al., 2016b; ELIAS et al., 2020) and needs to be more investigated.

Pará's eastern region has had municipalities with great wood economic activity with forest management since the 1960s. With the decline of wood activity, the agricultural frontier expanded, mainly with monocultures such as soy and pasture areas. As of 2008, a few municipalities adopted policies to reduce the environmental impact of economic activities, which led to a decline in deforestation for the first time in the history of Pará state (GUIMARÃES et al., 2011).

According to the biennial report of the Green Municipalities Program 2013-2014 (WHATELY; CAMPANILI, 2013), the reasons for the reduction in deforestation were: (i) restriction on rural credit, (ii) list of embargoed areas, (iii) list of municipalities that more deforested in the Amazon due to the imposition of various administrative restrictions in these municipalities, (iv) accountability of the meat production chain; and, last but not least, (v) strengthening inspection operations. However, in 2008 about 45% of the municipality's natural vegetation area had already been deforested (PINTO et al., 2009).

We performed the hot spot analysis to test the CRS. The spatial distribution patterns of the SF did not present CRS, although the occurrence of SF is mostly along the main roads and harbors, regions where the old-growth forest has historically been deforested. The spatial distribution may have an influence of climate (ARAGÃO et al., 2014c; HEINRICH et al., 2021), the history of LULC (WANDELLI; FEARNSIDE, 2015; CASSOL et al., 2021), and other environmental factors (HOLL, 1999; WANG et al., 2019b).

The net balance of SF demonstrates the needs of forest management improvement. In Pará state, there are municipalities that had already deforested almost all of their old-growth forests; therefore, they sought resources from other LULC such as SF. The need to protect SF is something that has to be discussed in different spheres of society, and its loss can occur for several reasons, even due to the lack of official definition of when a forest begins to be considered SF (WANG et al., 2020b).

Moreover, the result obtained by the proposed method corroborates with what was found in the literature (ROZENDAAL et al., 2017b), where in SF in the neotropical region, different amounts of aboveground biomass accumulated distinct areas. SF have one of its ecological functions the sequester of carbon. Some studies states that in tropical regions, SF can sequester carbon up to 20 times faster than old-growth forest, the drives that influence the absolve carbon varies within sites, age, environmental conditions, and regrowth rates (BAKER et al., 2004; HEINRICH et al., 2021; ROZENDAAL et al., 2022). That shows the importance of monitoring SF sites in the Amazon region. However, the old-growth

forest stills have the most important driver on the Brazilian Amazon carbon balance (SAATCHI et al., 2007; SMITH et al., 2020).

In general, region B, located in western Pará, accumulated more aboveground biomass compared to region A (eastern Pará). A recent study found that young SF (<20 years old) from western Amazon regions absorb ~60% higher rates when compared to eastern regions (HEINRICH et al., 2021). The drivers of aboveground biomass changes are usually explained by previous land use (WANDELLI; FEARNSIDE, 2015; CASSOL et al., 2021), age (CHAZDON et al., 2009; SILVA JUNIOR et al., 2020; WANG et al., 2020b) environmental factors (HOLL, 1999; BECKNELL; KISSING KUCEK; POWERS, 2012; HEINRICH et al., 2021), and mainly the climate which can influence the occurrence and the quality sites of SF, which impacts the aboveground biomass accumulation (HEINRICH et al., 2021).

In the Amazon, previous land use and land cover may have a negative impact on the SF aboveground biomass if the area has suffered repeated burning events, also the growth rate can be affected according to the LULC history (WANDELLI; FEARNSIDE, 2015). The history of LULC also has an impact on the aboveground biomass estimates. A study conducted in the Amazon using L-band SAR found that the LULC history information may explain 71% of the AGB using this information in the input model (CASSOL et al., 2021). Then, the LULC information is crucial to determine the SF age using cartographic modeling, and also to consider in the discussion the aboveground biomass accumulation in different sites.

The SF age has been considered one of the most important variables influencing aboveground carbon in the BLA (WANG et al., 2020b; HEINRICH et al., 2021). The age effect may affect the rates that SF in tropical regions can accumulate carbon. Younger SF have higher aboveground biomass rate variation (POORTER et al., 2016b; REQUENA SUAREZ et al., 2019), but as the forest succession process occurs these rates are downgraded (CHAZDON et al., 2007). For this, mapping the SF age allows more investigation into the accumulation of aboveground biomass. In our study, the is a data limitation that does not allow us

to investigate greater time series and estimate aboveground biomass for a higher range of SF age. Therefore, improving LULC mapping is an important tool to estimate SF age in longer time series and explore more information about it. Further, as the SF is not officially protected by any specific Brazilian environmental legislation, national monitoring systems such as TerraClass and MapBiomas are crucial to survey the data and begin new discussions on the environmental panel. This would also benefit the Brazilian Amazon from reducing emissions from deforestation and forest enhancements (REDD+) programs improving forest carbon stocks, following the Intergovernmental Panel on Climate Change (IPCC) (IPCC 2006, 2008; CARVALHO et al., 2019; IPCC 2019, 2019b).

3.4 Conclusion

The land use and land cover monitoring system revealed cold and hot spots in the distribution of SF in Pará state. Although the balance of SF is positive, gains and losses varied over the period studied. Also, aboveground biomass accumulation differs according to the SF ages along the study period as evaluated in two pilot areas. As the old-growth forest is cleared in the Brazilian Amazon, new LULC changes are mostly used for agriculture and pasture, then after years of exploring these LULC, new SF regenerate from those are-as. For this reason, new environmental legislation and official monitoring systems are crucial to develop strategies to protect SF in the Brazilian Amazon.

3.5 Framing the analysis of biomass in fire-affected forests

The findings from the analysis of SF dynamics highlight how historical land use and successional stages influence aboveground biomass accumulation in regenerating landscapes. However, in many tropical forest regions, particularly in fire-prone ecosystems, biomass patterns are also shaped by recurrent disturbances that alter forest structure, composition, and fuel availability. Understanding these processes requires high-resolution structural measurements capable of capturing fine-scale heterogeneity in both overstory and understory layers. Importantly, many tropical ecosystems are not naturally fire-prone; rather, fire occurrence is strongly associated with anthropogenic drivers such as deforestation, agricultural expansion, and land-use change,

which increase fuel continuity and ignition sources (COCHRANE, 2003; ARAGÃO et al., 2018).

This context sets the stage for the next chapter, which examines biomass loss and fuel consumption in landscapes subjected to different fire return intervals, using TLS combined with field data and machine learning models. By linking successional recovery patterns with disturbance-driven biomass loss, the two studies together provide a comprehensive perspective on carbon dynamics under contrasting ecological pathways.

4 BIOMASS LOSS IN FIRE-PRONE LANDSCAPES: TLS-BASED ANALYSIS OF FUEL LOAD AND CONSUMPTION ACROSS FIRE REGIMES IN PINE ECOSYSTEMS

Fire plays a critical role in shaping and maintaining the structure and function of fire-prone ecosystems worldwide. Research focused on the frequency of burning in southeastern USA pine forests underscores the profound impact of fire on litter accumulation (LOUDERMILK et al., 2012b; JONES; VUKOMANOVIC, 2023; SÁNCHEZ-LÓPEZ et al., 2023), forest composition, and ecological resilience. Key determinants influencing fire spread and fuel consumption in this frequently burned ecosystem include surface biomass accumulation and fuel layers (LOUDERMILK et al., 2012b, 2023; SÁNCHEZ-LÓPEZ et al., 2023). The dynamics of fire behavior are intricately tied to factors such as surface fuel availability (LOUDERMILK et al., 2012b), weather conditions (JENSEN et al., 2025), and wind patterns (DUPUY et al., 2011). However, fuel characteristics that are important to understanding fire behavior can vary at very fine scales (e.g., ~1 m), making measurement and prediction difficult (BLAYDES; CANNON; AUBREY, 2023; GONÇALVES LAZZARO et al., 2024). Understanding the interconnections between fuel availability at fine scales with resulting fire effects is pivotal for comprehending the broader implications of fire within ecosystems.

Currently, the emphasis on characterizing fuels for wildland fire management has grown significantly, with a notable focus on leveraging remote sensing techniques (ROCHA et al., 2023; SÁNCHEZ-LÓPEZ et al., 2023; TANEJA et al., 2023). Despite the ability of airborne platforms to capture canopy-scale biomass patterns, they often lack the spatial resolution necessary to resolve fine-scale surface fuel and understory structural variability that are critical for modeling fire behavior (WILKES et al., 2017; ROWELL et al., 2020).

In this context, TLS emerges as a robust alternative, offering a comprehensive means of mapping not only forest canopy structure but also surface litter and understory vegetation (GARCÍA et al., 2011; VIERLING et al., 2013; ROWELL et al., 2016; WILKES et al., 2017; WALLACE et al., 2022). TLS enables sub-meter three-dimensional characterization of vegetation and surface fuels, making it an

invaluable tool for fine-scale fuel characterization. TLS has increasingly expanded from traditional forestry applications to broader forest ecological studies, providing detailed structural information critical for AGB estimation, fuel load assessment, and habitat characterization (CALDERS et al., 2020). Nevertheless, it is important to recognize that TLS, despite its strengths, can exhibit limitations in detecting very fine fuels such as compacted litter layers near the ground surface (GARCÍA et al., 2011; WILKES et al., 2017).

Recent studies have demonstrated the operational potential of TLS for mapping fuels at fine scales, facilitating fire management planning and hazard reduction strategies (GARCÍA et al., 2011; WALLACE et al., 2022). Optimized scan configurations and multi-angle acquisitions have been proposed to mitigate occlusion and enhance the detectability of surface fuels (VIERLING et al., 2013; WILKES et al., 2017; ROWELL et al., 2020). Furthermore, coupling TLS-derived structural metrics with machine learning models, particularly Random Forest algorithms, has shown promise for predicting biomass and fuel loads with high accuracy (SILVA et al., 2017a; XU et al., 2020; D'ESTE et al., 2021). Machine learning approaches also enable the upscaling of plot-level TLS information to landscape scales, addressing challenges associated with spatial extrapolation (SILVA et al., 2017a; LEITE et al., 2022). The integration of TLS-based approaches to characterize fuels provides new opportunities to explore fire–vegetation interactions not possible before.

This work contributes to a better understanding of surface fuel consumption in the north-central Florida pine ecosystem. Slash pine (*Pinus elliottii* Engelm. var. *elliottii*) is one of the main species found in Florida, commonly associated with saw palmetto (*Serenoa repens* (Bartr.) Small) (HUDAK et al., 2016b). Saw palmetto is a common dominant understory species in pine ecosystems in Florida, and is often considered a management problem for timber production. Mapping and quantifying vegetation in this type of ecosystem is key to understanding how frequent forest fires impact biomass accumulation and consumption dynamics.

However, despite its potential, only a limited number of studies have integrated TLS with machine learning for fuel estimation, and these efforts have often been restricted to aggregated biomass pools or single fuel types (ROWELL et al., 2016; SULLIVAN et al., 2018). In contrast, this study provides a more detailed characterization by producing spatially explicit, component-level fuel estimates across multiple surface fuel categories in frequently burned forests, thereby directly addressing ecological questions related to fire recurrence and fuel dynamics.

This study addresses this gap by combining TLS-derived structural metrics with Random Forest modeling to predict and map multiple components of TSAGB before and after prescribed fire events in a frequently burned pine ecosystem in north-central Florida. This research assesses biomass consumption using TLS at the plot level across a replicated fire return interval experiment. We aim to evaluate model performance across different fuel classes and demonstrate the potential of TLS-based approaches for operational fire management and ecological monitoring by leveraging a rigorous variable selection strategy and robust modeling framework. Our approach combines TLS-derived height-based variables with Random Forest to estimate fuel load in degraded areas. Additionally, we consider structural complexity in low-stature systems by incorporating best practices to demonstrate the utility of TLS in capturing fine-scale heterogeneity (MUUMBE et al., 2021).

Our specific objectives were to: (1) assess the predictive performance of TLS-derived metrics for estimating pre- and post-fire biomass components using Random Forest models, (2) evaluate fuel consumption by comparing spatial predictions across time, and (3) identify key structural drivers of biomass variability across burn intervals. This study contributes to advancing the use of TLS in fire ecology by providing a scalable, high-resolution method for monitoring surface biomass and informing prescribed burning strategies.

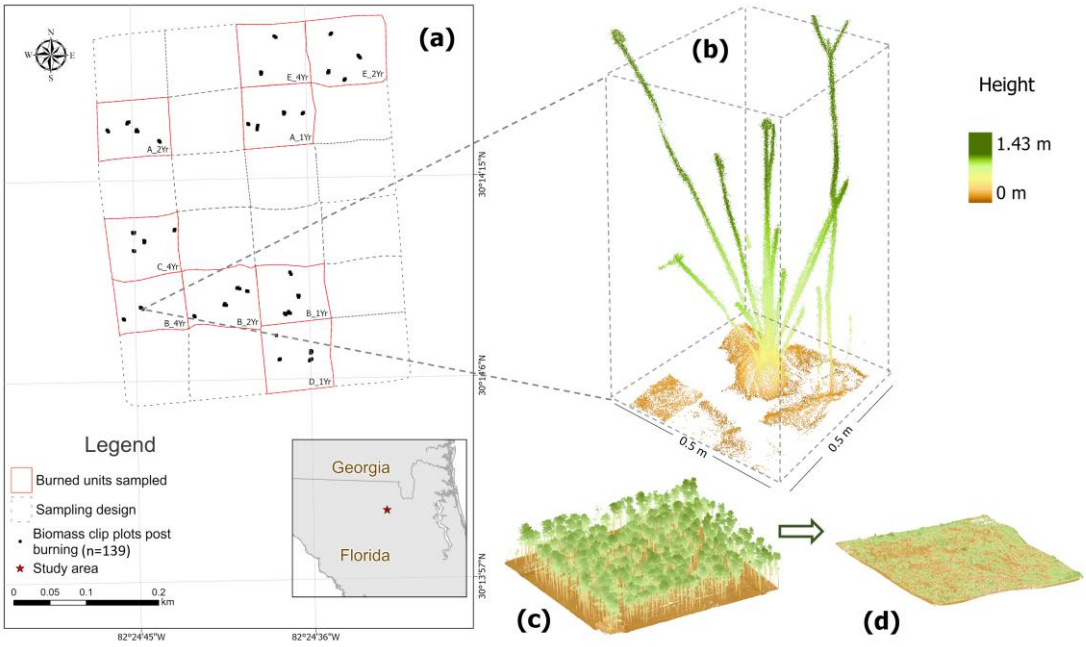
4.1 Materials and methods

4.1.1 Study site

Osceola National Forest (ONF) (30° 17′ 26″ N 82° 19′ 18″ W) is in northeast Florida, west of Jacksonville, located in Sanderson, Lake City, and North Columbia counties, USA (Figure 4.1). The climate of ONF is classified as humid subtropical, although this region may present distinct wet and dry seasons. The combination of warm temperatures and high precipitation promotes the growth of specific species, including natural stands of P. *elliottii* Engelm. and P. *palustris* Mill., characteristic of the Flatwoods Forest type (HUDAK et al., 2016b). Additionally, plantations of P. *elliottii* Engelm. thrive in these favorable climatic conditions (OUTCALT; WADE, 2004; KROFCHECK et al., 2019). ONF also encompasses wetland areas that were not included in this study due to their frequent inundation; these areas typically do not ignite or contribute to the spread of forest fires (LOUDERMILK et al., 2023; ROSS et al., 2024).

The ONF has a historic of periodic prescribed burning since 1958 using dormant season burns and growing season burning (MCKEE, 1982; OUTCALT; WADE, 2004), and it has been used as a study site for many studies (OUTCALT; WADE, 2004; LOUDERMILK et al., 2012b, 2023; SÁNCHEZ-LÓPEZ et al., 2023). This site was originally established in a randomized block design to evaluate different fire recurrence intervals in six replicates of four treatments, with prescribed burning regularly every 1, 2, or 4 years (Figure 4.1), and no-burn treatment (control).

Figure 4.1 - Study area and sampling distribution of TLS scans and vegetation and fuel biomass samples (n = 139).



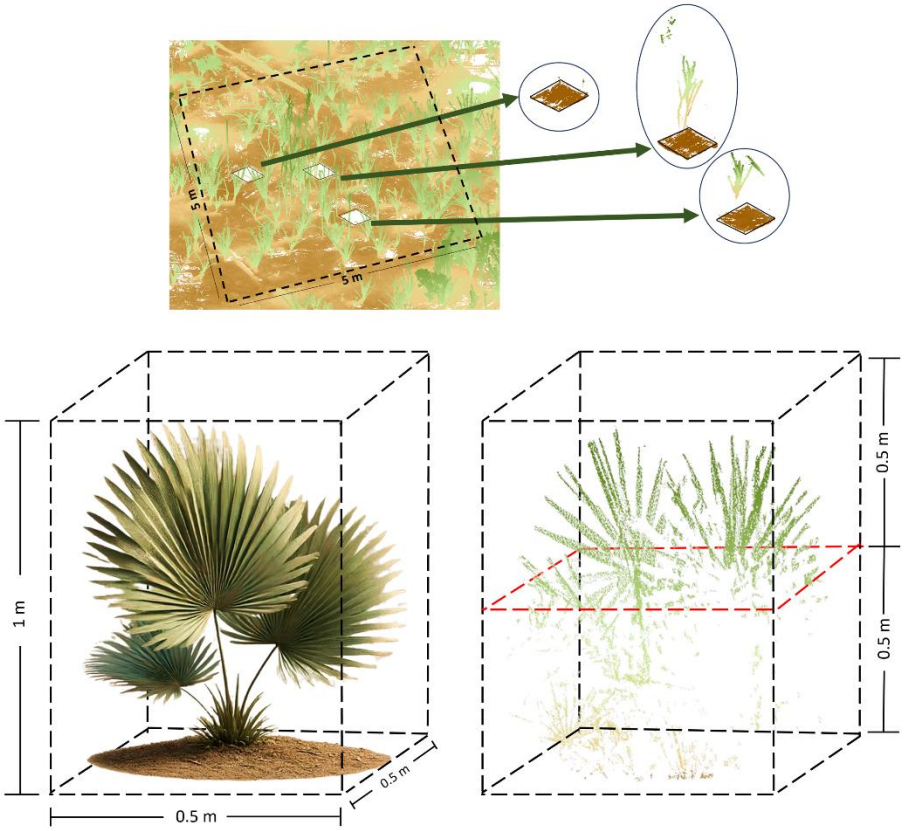
4.1.2 Sampling design and in situ fuel load collection

Terrestrial surface aboveground biomass (TSAGB, g/m²) was measured in both pre- and post-burn conditions during two field campaigns conducted in 2020 and 2022, respectively, across 18 prescribed burn units located in Osceola National Forest, Florida. These units were stratified by fire return interval, with six units assigned to each of the 1-, 2-, and 4-year burning treatments. For this study, we selected nine units—three per fire return interval—for detailed sampling (Figure 4.1a).

Within each selected burn unit, two linear transects were established: one along the edge of the unit and one in the interior. Edge transects were oriented parallel to the burn unit perimeter, while interior transects were placed perpendicular to it. The cardinal direction for each transect was randomly assigned. Each transect supported two 5 × 5 m plots, positioned using randomly selected distances. For edge transects, plots were located between 5 and 10 meters from the unit boundary; for interior transects, plots were positioned at a minimum distance of 15 meters from the edge.

Each 5 × 5 m plot was permanently monumented using 1.27 cm diameter electrical metallic tubing (EMT) conduits (~1.5 m tall), marked with reflective tape. Of the two plots along each transect, one was designated for pre-burn sampling and the other for post-burn sampling. Within each plot, a 0.5 × 0.5 × 1.0 m clip plot was placed at the center (Figure 4.2), with an additional clip plot randomly located within the plot area. In total, 74 pre-burn and 65 post-burn clip plots were sampled across the nine selected units.

Figure 4.2 - Representation of the 3D fuel clip plot.



Geographic coordinates were recorded for each plot, prioritizing the northwest corner as a georeferencing anchor. Prior to the prescribed burns, each 5 × 5 m plot was scanned with TLS and photographed. The 3D fuel clip plots were voxelized and destructively sampled for biomass determination (HAWLEY et al., 2018). Following the prescribed burns conducted on February 3–4, 2022, post-burn TLS scans, photographs, and destructive sampling of the 3D clip plots were

conducted between February 5–7, 2022. Hemispherical canopy photographs were also collected at the plot centers under both pre- and post-burn conditions.

Each clip plot was configured as a vertical rectangular prism (0.5 m × 0.5 m × 1.0 m) and subdivided into 250 voxels, arranged into 10 horizontal strata of 10 cm height each, totaling 25 voxels per stratum. A total of 75 pre-burn and 65 post-burn 3D fuel clip plots were sampled and evenly distributed among the nine study units. Biomass data collected from each voxel provided fine-scale inputs for both pre- and post-fire fuel load characterization.

4.1.3 Terrestrial laser scan collection and processing

TLS data were collected within each 5 × 5 meter plot using Riegl VZ 400i coupled with a NIKON D850 45.7 MegaPixel digital camera and a differential GNSS RTK Receiver (KLAUBERG et al., 2023). TLS acquisitions were conducted both before and after prescribed burns, during campaigns in 2020 (pre-fire) and 2022 (pre- and post-fire), and for the entire fire unit in 2022 (pre and post-fire). We used a boom lift to scan all the fire units' perimeter at two heights (mid and top canopy), and on top of a truck at the fire breaks.

We positioned and scanned the area from i) each unit corner for the pre-fire data and ii) each corner of the burned units for the post-fire data. The scans were done at ~18 m and ~9 m from the ground by elevating the TLS with a boom lift using full and half-length of its arm, respectively. For units’ corners that were not accessible with the boom lift, the TLS tripod was mounted on the back of a truck and the scans were performed at ~3 m from the ground. It was possible to collect all the outermost unit corners (i.e., those that intersect the study area outer perimeter) with the boom lift. For all scans, the TLS configuration was set to panorama 20 with a laser frequency of 1200kHz.

The point clouds from the TLS scans were first filtered to remove noise and stray points with reflectance below -15 dB, above 50 dB and with a deviation >14 (REICH; KUNZ; VON OHEIMB, 2021). Next, the points were registered using the automatic registration and multi-station adjustment tools of the software RiSCAN Pro® Version 2.9.0 (RIEGL LASER MEASUREMENT SYSTEMS GMBH., 2024).

Finally, the point clouds were clipped to each unit and exported to .laz format, using CloudCompare® Version 2.12 (CLOUDCOMPARE., 2024).

Also, for the selected burn units, 1 scan in each corner was conducted and combined using RiSCAN Pro® Version 2.9.0 to obtain one point cloud for each burn unit, pre and post fire. From each burn unit, the trees were removed manually using CloudCompare® Version 2.12 (Figure 4.3). Then, we calculated a total of 46 TLS-derived cloud metrics for each clip plot and burn units (Table 4.1), following methods described in Loudermilk et al. (2023).

Figure 4.3 - Tree extraction representation on the point cloud.

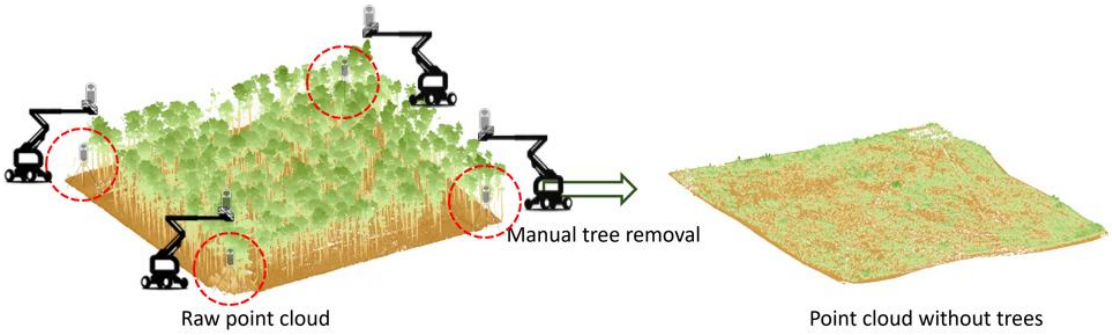


Table 4.1- TLS-Derived Predictor metrics used in the Random Forest model (n=46).

N°	Definition	Metric	Category
1	Minimum height	H_min	Height and Structural
2	Maximum height	H_max	
3	Mean height	H_mean	
4	Median height	H_median	
5	Standard deviation of height distribution	H_sd	
6	Skewness of height distribution	H_skew	
7	Coefficient of variation of height $cv = \frac{sd\ height}{mean\ height}$	H_CV	
8	Kurtosis of height distribution	H_kurt	
9	$D1 = \frac{\text{n° returns} > 0.5\text{m}}{\text{n° total returns}}$	D1	
10	$D2 = \frac{n°\ returns < 0.5m}{n°\ total\ returns}$	D2	

continue

Table 4.2- Conclusion.

N°	Definition	Metric	Category
11	Height 5th percentile	H_5th	Quantile Metrics (Height Percentiles)
12	Height 10th percentile	H_10th	
13	Height 15th percentile	H_15th	
14	Height 20th percentile	H_20th	
15	Height 25th percentile	H_25th	
16	Height 30th percentile	H_30th	
17	Height 35th percentile	H_35th	
18	Height 40th percentile	H_40th	
19	Height 45th percentile	H_45th	
20	Height 50th percentile	H_50th	
21	Height 55th percentile	H_55th	
22	Height 60th percentile	H_60th	
23	Height 65th percentile	H_65th	
24	Height 70th percentile	H_70th	
25	Height 75th percentile	H_75th	
26	Height 80th percentile	H_80th	
27	Height 85th percentile	H_85th	
28	Height 90th percentile	H_90th	
29	Height 95th percentile	H_95th	
30	Height 96th percentile	H_96th	
31	Height 97th percentile	H_97th	
32	Height 98th percentile	H_98th	
33	Height 99th percentile	H_99th	
34	Cumulative percentage of 1st return	H_pcum1	Cumulative Proportion
35	Cumulative percentage of 2nd return	H_pcum2	
36	Cumulative percentage of 3rd return	H_pcum3	
37	Cumulative percentage of 4th return	H_pcum4	
38	Cumulative percentage of 5th return	H_pcum5	
39	Cumulative percentage of 6th return	H_pcum6	
40	Cumulative percentage of 7th return	H_pcum7	
41	Cumulative percentage of 8th return	H_pcum8	
42	Cumulative percentage of 9th return	H_pcum9	
43	Proportion of points below 1st height	p1th	Threshold-Based Proportion
44	Proportion of points below 2nd height	p2th	
45	Proportion of points below 3rd height	p3th	
46	Percentage of returns above mean	pHabovezmean	

4.1.4 Reference fuel classes

A total of fifteen response variables were derived from the field measurements (Table 4.3) and fuel load data and converted to biomass density (g/m²) based on the sample plot area (0.25 m²). These variables represent different components of surface and near-surface forest fuels. However, due to data limitations (e.g., missing values or low-quality returns) and redundancy among correlated variables, only eight components were retained for modeling using TLS-derived metrics. The fuel classes used as response variables included total bio-mass, total fine fuels, fine woody debris (FWD), total biomass excluding FWD, 1-hour fuels, 10-hour fuels, pine needle litter, and woody live biomass.

Table 4.3- Table of fuel categories collected in the field and their descriptions.

Fuel category	Description
Woody live (Wlive)	Dry weight (grams) of live material from evergreen and deciduous broadleaf shrubs or trees except saw palmetto. This material is defined as all living aboveground material – stems, leaves, flowers, buds, etc. NOTE: This does not include live saw palmetto petiole or leaves. See LSP and LSL.
LSP	Dry weight (grams) of live saw palmetto petioles that were standing live and manually removed from the source.
LSL	Dry weight (grams) of live saw palmetto leaves that were standing live and manually removed from the petiole
Woody Litter (Wlit)	Dry weight (grams) of downed leaf and litter material from evergreen and deciduous broadleaf shrubs or trees except saw palmetto. This material is defined as material detached from its source, such as leaves, flowers, buds, etc. NOTE: This does not include dead saw palmetto petiole or leaf material. See DSP and DSL.
Pinecones (PC)	Dry weight (grams) of intact female cones (aka megastrobilus, seed cone, or ovulate cone) from Pinus species
Pine Needle (PN)	Dry weight (grams) of downed pine needles from Pinus species with long or short needles. This material is defined as live or dead detached foliage from long needle species such as Pinus palustris, Pinus *taeda*, and Pinus *elliottii* or short needle species such as Pinus *echinata*.
Conifer Litter (CL)	Dry weight (grams) of downed woody material from conifer species that is too small to fit into the 1-hour fuel category. Examples of this material include flashy fuels such as paper-thin pieces of bark, male pollen cones (aka microstrobilus), and pinecone fragments.

continue

Table 4.4- Conclusion.

Fuel category	Description
1hr	Dry weight (grams) of 1-hour fuel. This material is defined as downed dead branches, twigs, and other small woody pieces that are severed from their original source of growth and dead woody species that is still standing and attached to the ground. A 1-hour fuel is less than 0.25 inch (0.64 cm) in diameter. NOTE: This fuel category does not include foliage such as pine needles. See PN.
10hr	Dry weight (grams) of 10-hour fuel. This material is defined as downed, dead branches, twigs, and other small woody pieces that are severed from their original source of growth, female cones (aka megastrobilus, seed cone, or ovulate cone) from non-Pinus species, and dead woody species that is still standing and attached to the ground. A 10-hour fuel is 0.25 inch to 1.0 inch (0.64 to 2.54 cm) in diameter.
ETE	Dry weight (grams) of bunchgrass species, wiregrass species, other graminoids, forbs, vines, and conifer seedlings. ETE is short for “everything else” and is fine material that does not fit in any other category.
FL	Dry weight (grams) of fragmented litter that is not decayed but too small (less than 0.5 centimeters) to be identified or realistically sorted into a fuel type.
Fine fuels	Included all grass, forb, and vine material (live and dead), dead leaves (pine and cypress needles, and broadleaves), other fine tree organs: (bark flakes, reproductive organs: catkins, etc.), and 1h fuels.
FWD	Fine vegetation and fuels only.
Total no FWD	Total biomass minus the fine woody debris (10hr and 100hr) and pinecones.
Total Biomass	Total mass of all living and dead vegetation.

4.1.5 Fuel load modeling and assessment

4.1.5.1 Variable selection

To accurately estimate the fuels using TLS data, it is essential to select the most significant LiDAR-derived metrics within a parsimonious statistical model framework. Given the potentially large number of TLS-derived metrics at the clip plot scale, our study employed a two-step variable selection procedure to optimize predictor inclusion in our Random Forest models for AGB estimation.

Although Random Forest is relatively robust to collinearity (BREIMAN, 2001) we applied a correlation filter to reduce redundancy and improve interpretability. Following common practice in ecological and remote sensing studies, we excluded variables with Pearson's r > 0.7 (CUTLER et al., 2007; DORMANN et al., 2013). In cases where two or more variables were highly correlated, we retained the metric with the strongest theoretical or empirical relevance and excluded the others to avoid redundancy and reduce dimensionality.

Then, we applied the Model Improvement Ratio (MIR) approach (MURPHY; EVANS; STORFER, 2010) for variable selection following the methodology described by Silva et al. (2017a). The MIR provides a standardized measure of variable importance by dividing each variable's raw importance score (as generated by the RF algorithm) by the maximum importance score observed within the same model. This normalization scales importance values between 0 and 1, allowing for consistent interpretation across models. Importantly, MIR was computed separately for each biomass component model, enabling comparison of variable contributions tailored to specific fuel types.

The final set of variables retained for each model is presented in Table 4.5. From the initial 46 TLS-derived metrics, this process reduced the predictor set to 11 variables, ensuring that only the most informative and least redundant metrics were used to model fuel loads across different biomass pools, thereby improving both model accuracy and interpretability.

Table 4.5 - Selected metrics used in the Random Forest model.

Biomass/Fuel Component	Selected Variables (MIR > 0.25)
Total biomass	p2th, p3th, H_CV, H_sd, H_pcum1, pHabovemean
Total fine fuels	p2th, p3th, H_pcum1, pHabovemean, H_CV
Fine woody debris (FWD)	p2th, p3th, H_min, H_sd, H_CV
Total no FWD	p2th, p3th, pHabovemean, H_sd, H_CV, H_pcum1
1hr fuels	p2th, H_99th, H_pcum1, H_CV, H_min
10hr fuels	p2th, H_CV, H_pcum9, H_sd, H_kurt, H_min
Pine needle	p2th, p3th, H_skew, H_pcum1
Woody live	p2th, p3th, H_pcum1, H_CV

4.1.5.2 Random Forest modeling and bootstrapping

Random Forest models were implemented using the randomForest package in R (BREIMAN, 2001) to predict biomass and fuel load components from TLS-derived structural metrics (BRIGHT et al., 2022). For each of the eight response variables, an individual RF model was trained using the final set of predictor variables selected through the correlation filter and MIR analysis.

Each Random Forest model was configured with 1,000 decision trees to ensure stable predictions and reduce variance. The number of variables randomly selected at each node split (the mtry parameter) was set to 2. This value was determined based on preliminary testing and aligned with commonly recommended settings for regression problems involving relatively small numbers of predictor variables. The use of a fixed mtry value across models ensured comparability of model structure and complexity.

To evaluate the robustness and internal consistency of the models, we applied a bootstrapping procedure with 500 iterations, following the methodology of Silva et al (2017a). This approach provides a measure of model stability but does not represent true generalization performance, which would require independent data for validation. In each iteration, the dataset was resampled with replacement

to form a training subset equal in size to the original dataset (n). Due to the nature of bootstrap resampling, approximately 70% of the observations were selected for training, while the remaining 30% (not included in the resample) were used as an internal test set (out-of-bag). This resampling procedure allowed the models to be trained and validated repeatedly under varying data conditions, capturing variability in model performance due to sampling fluctuations.

During each bootstrap iteration, a Random Forest model was trained on the resampled training data using the same parameter settings. Predictions were then generated for both the training and testing datasets. Model performance was evaluated for each iteration by calculating a series of statistical metrics, including RMSE, Bias or MAE, RMSE%, Bias%, Adjusted R^2, and PMRE.

The results from all 500 iterations were aggregated to compute mean performance metrics, standard deviations, and percentiles, allowing the estimation of model uncertainty and predictive reliability. The bootstrapping framework also enabled the visualization of model performance through scatterplots of observed versus predicted values, residual distributions, and variable importance profiles averaged across iterations.

In addition to standard performance metrics, we applied the Wilcoxon signed-rank test within each bootstrap iteration to evaluate whether the differences between observed and predicted values were statistically significant. The Wilcoxon signed-rank test is a non-parametric paired test that does not assume normality of the differences, making it appropriate for residual distributions that deviate from Gaussian assumptions. Prior to this, the Shapiro–Wilk test was used to verify the normality of the residuals, which confirmed the use of a non-parametric approach. This procedure was repeated across all 500 bootstrap iterations, allowing us to assess whether systematic biases were present in model predictions.

4.1.5.3 Model assessment

The predictive performance of the models was quantified using several statistical metrics that compare observed values y_i to predicted values $\hat{y}_i$ across n observations. The following evaluation metrics were used:

RMSE

$$RMSE = \sqrt{\frac{1}{n}\sum_{i=1}^{n}(y_i - \hat{y}_i)^2} \quad (4.1)$$

where: n is the number of clip plot samples, y_i and $\hat{y}_i$ are the observed and predicted values for clip plot *i*; y and $\hat{y}$ are the observed and predicted mean values for clip plot *i*;

RMSE%

Expresses RMSE as a percentage of the mean observed value, facilitating scale-independent comparisons:

$$RMSE\% = \left(\frac{RMSE}{\bar{y}}\right) \times 100 \quad (4.2)$$

Bias

Indicates the average error of the mean observed value:

$$Bias = \frac{1}{n}\sum_{i=1}^{n}(\hat{y}_i - y_i) \quad (4.3)$$

Bias%

Indicates the average error as a percentage of the mean observed value:

$$\text{Bias}\% = \left(\frac{Bias}{\bar{y}}\right) \times 100 \quad (4.4)$$

MAE

Calculates the average of the absolute prediction errors:

$$MAE = \frac{1}{n}\sum_{i=1}^{n}|y_i - \hat{y}_i| \quad (4.5)$$

PMRE

Provides a scale-independent accuracy metric by expressing the relative error as a percentage:

$$PMRE = \frac{1}{n}\sum_{i=1}^{n}\left(\frac{|y_i - \hat{y}_i|}{y_i}\right) \times 100 \quad (4.6)$$

R^2

R^2 describes the proportion of variance in the observed values that is explained by the model predictions. It is calculated as:

$$R^2 = 1 - \frac{\sum_{i=1}^{n}(y_i - \hat{y}_i)^2}{\sum_{i=1}^{n}(y_i - \bar{y})^2} \quad (4.7)$$

Adjusted R^2 was calculated to account for the number of predictors used in the Random Forest models. Unlike the standard R^2, which can increase with the inclusion of additional variables regardless of their relevance, the Adjusted R^2 penalizes the inclusion of non-informative predictors by adjusting for model complexity. It provides a more reliable metric for comparing models with different numbers of input variables, particularly in high-dimensional datasets.

$$\text{Adjusted } R^2 = 1 - \left(\frac{(1 - R^2)(n - 1)}{n - k - 1}\right) \quad (4.8)$$

Where:

R^2= coefficient of determination (proportion of variance explained by the model).

n = sample size (number of observations).

k = number of predictor variables included in the model.

Thus, while R^2 can only increase or remain constant as more predictors are added, Adjusted R^2 increases only if the new predictor improves the model more than would be expected by chance, otherwise it decreases. This makes it a more conservative and informative measure of model explanatory power.

In addition to performance metrics, a Wilcoxon signed-rank test was used to test for systematic differences between observed and predicted values. This non-parametric test evaluated the null hypothesis that the median difference between observed and predicted values is zero, at a significance level of α = 0.05.

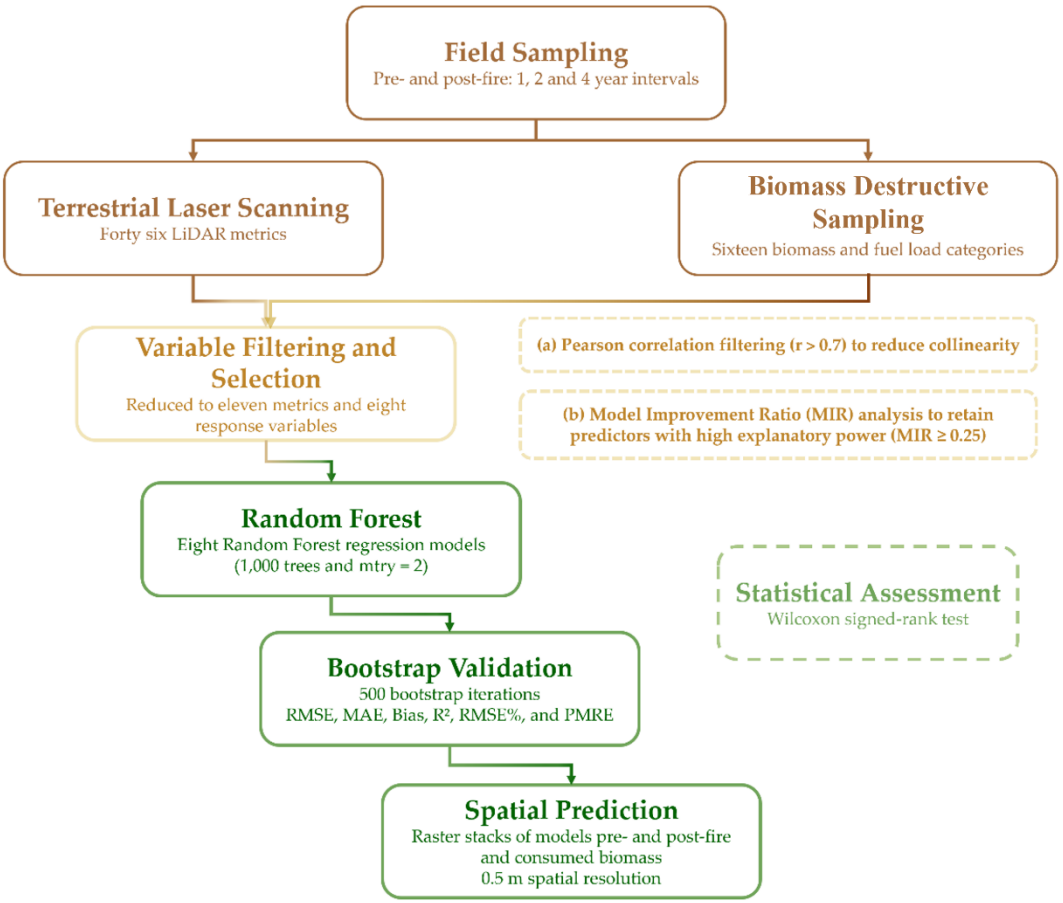
4.1.5.4 Spatial prediction of biomass components and biomass consumption estimation

Final Random Forest models were applied to raster stacks of TLS-derived metrics across the study area to produce spatially explicit predictions of each biomass component. Raster inputs matched the variable structure of the training dataset, using only the MIR-selected predictors. Predictions were generated at a 0.5 m resolution across each burn unit and saved as multiband GeoTIFF files, with one layer per biomass component for both pre- and post-fire conditions. Spatial biomass consumption was calculated as the difference between pre- and post-fire layers.

4.1.5.5 Methodological workflow

The workflow applied in this study is summarized in Figure 4.4. Field sampling provided both TLS-derived metrics and destructive biomass data. After variable filtering (Pearson correlation and MIR analysis), Random Forest regression models were fitted using eight AGB components as response variables. Model robustness was evaluated through 500 bootstrap iterations, from which performance metrics (RMSE, MAE, Bias, R^2, RMSE%, and PMRE) were derived. The bootstrapping approach allowed the internal division of data into training and test subsets at each iteration, avoiding the need for a fixed dataset split. Final models were then used for spatial prediction, generating high-resolution biomass maps pre- and post-fire.

Figure 4.4 - Workflow of biomass and fuel load modeling using TLS-derived metrics and Random Forest regression.



4.2 Results

Random Forest model performance, evaluated through 500 bootstrap iterations, demonstrated varying levels of predictive accuracy across biomass and fuel components. The most consistent and accurate predictions were observed for total biomass, total fine fuels, and total biomass excluding fine woody debris, with RMSE values ranging from 26.57 to 54.83 g/m² and adjusted R^2 values of 0.86. These models showed low relative bias, suggesting minimal systematic over- or underestimation across bootstrap samples. In contrast, models targeting smaller or sparser fuel classes, such as 1-hour fuels, 10-hour fuels, and FWD—exhibited higher RMSE% values (typically >90%) and undefined Percent Mean Relative Error (PMRE), indicating difficulty in predicting low-density or discontinuous biomass types (Table 4.6).

Among the individual fuel categories, the pine needle model achieved relatively good performance compared to other fine-scale classes. It yielded an RMSE of 18.02 g/m² (35.1% relative error) and an adjusted R^2 of 0.89, indicating a strong relationship between observed and predicted values. Despite this accuracy, the model showed a slight negative bias (−1.01 g/m²; −1.97%), suggesting a tendency toward underestimation. These results highlight that TLS-derived metrics are particularly effective at capturing continuous and homogeneous surface fuel layers, such as pine needle cover, which are less spatially discontinuous than woody debris or coarser fuel categories

Table 4.6 - Model Performance Metrics (bootstrap).

Model	RMSE	RMSE%	Bias	Bias%	MAE	PMRE	R^2
Total Biomass	54.83	27.72	-1.51	-0.76	3,006.74	32.54	0.86
Fine Fuels	26.57	24	-1.16	-1.05	706.06	26.42	0.86
FWD	16.92	88.57	-0.31	-1.64	286.15	-	0.77
Total no FWD	51.44	28.78	-1.04	-0.58	2,645.83	33.67	0.86
1H Fuel	4.07	102.65	-0.12	-2.93	16.53	-	0.77
10H Fuel	13.39	90.97	-0.32	-2.17	103.9	-	0.8
Pine needle	18.02	35.1	-1.01	-1.97	324.64		0.89
Woody live	26.85	85.22	-0.86	-2.73	721.11	-	0.79

Statistical tests further supported the performance assessment. The Wilcoxon signed-rank test, applied across 500 bootstrap iterations, indicated that for models predicting total biomass, fine fuels, and total biomass excluding FWD, the differences between observed and predicted values were not statistically significant ($p > 0.05$ in the majority of bootstrap runs), confirming the absence of systematic bias. Similarly, Kolmogorov–Smirnov and equivalence tests showed no significant deviations between observed and predicted TSAGB distributions ($p > 0.05$). In contrast, models targeting highly variable or sparse fuel classes (1-hour fuels, 10-hour fuels, and FWD) frequently exhibited significant differences ($p < 0.05$), in line with their higher RMSE% values.

Despite this variability, most models remained relatively unbiased, presented bias% < -0.58 and performance was visually consistent with strong clustering near the 1:1 line in plots of predicted versus observed values for higher biomass

classes, as illustrated in Figure 4.5. For sparse or variable fuels, more scattered residuals were observed, indicating reduced model precision.

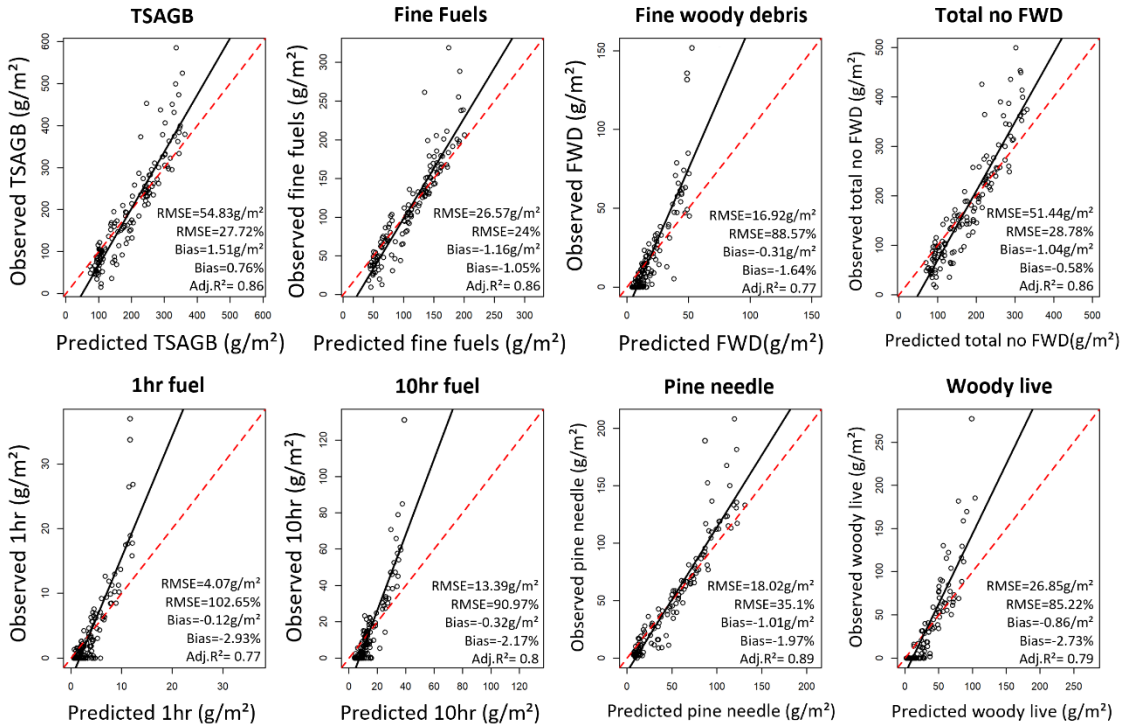
The coefficient of variation in height (H_CV) and the standard deviation of height (H_sd) also emerged as key structural metrics, contributing to the predictive power of models for both total biomass and individual fuel components such as fine woody debris and 10-hour fuels. These findings suggest that vertical heterogeneity, not just the presence of vegetation but its distribution along the vertical profile, is a critical factor in determining fuel mass and availability.

Moreover, cumulative proportion metrics (e.g., H_pcum1, H_pcum9) and the proportion of points above mean height (pHabovemean) played important roles in models for fine fuels and pine needle litter. These features likely reflect variations in vegetation openness and vertical layering, which influence both fuel deposition and consumption potential.

Across burning intervals, plots with longer fire recurrence periods (2- and 4-year treatments) exhibited greater values for these structural indicators, aligning with higher pre-fire biomass levels and more pronounced consumption. This reinforces the idea that structural complexity increases with time since fire, which in turn affects both the amount and distribution of surface fuels. Therefore, the metrics most frequently selected by the Random Forest models not only serve as strong predictors but also offer interpretable ecological insights into how structural traits drive biomass accumulation and fire-related dynamics over time.

The observed and the average of the predicted TSAGB from the 500 bootstrap runs were also compared and according to the KS and equivalence tests those values did not differ significantly (p-values > 0.05) too.

Figure 4.5 - Predicted vs observed surface fuel at the clip plot scale.



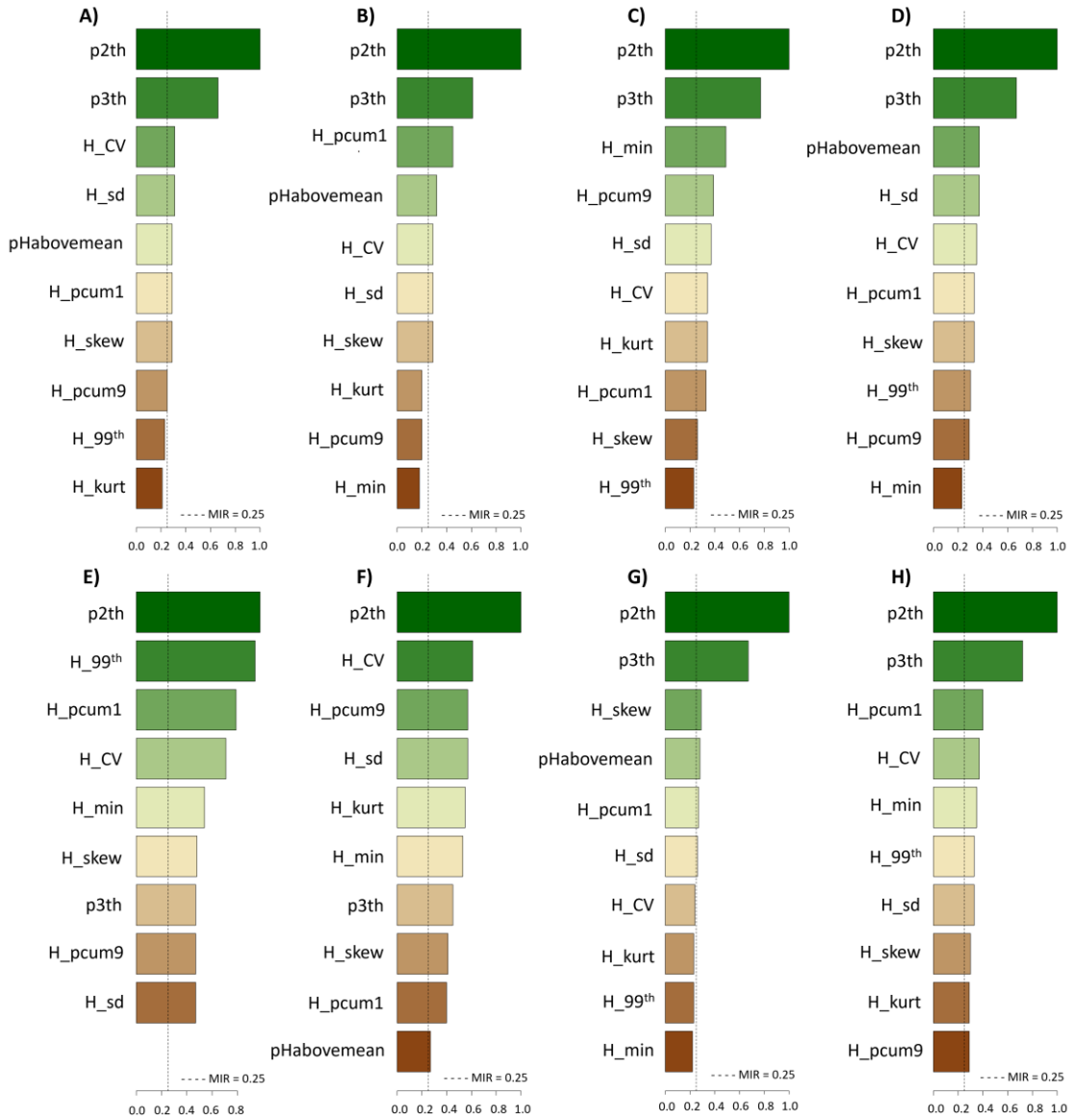
A) Total biomass; B) Total fine fuels; C) Fine wood debris (FWD); D) Total no FWD; E) Total 1hr fuel; F) Total 10hr Fuel, G) Total pine needle; H) Total woody live.

The Random Forest models showed variable predictive performance across biomass and fuel components, emphasizing limitations in modeling fine-scale variability in smaller fuel categories. Despite this, most models remained unbiased, as evidenced by low bias% values. Collectively, these findings suggest that TLS-derived metrics are particularly effective for estimating well-distributed biomass pools but are more limited for classes characterized by low density or high spatial heterogeneity.

Figure 4.5 and Figure 4.6 visually reinforce these trends, with strong clustering near the 1:1 line for high biomass classes and more scattered distributions for fuels with high temporal or spatial variability. Figure 4.6 illustrates the relative importance of predictor variables for each biomass and fuel component model, derived using the Model Improvement Ratio (MIR) within a Random Forest framework. Each panel (A–H) corresponds to a specific model, matching the components evaluated in the previous model performance figure. Higher MIR

values indicate a greater contribution of that variable to the predictive accuracy of the model.

Figure 4.6 - Variable importance for eight Random Forest models predicting different biomass and fuel components.



Each panel (A–H) corresponds to a separate model: (A) total biomass, (B) total fine fuels, (C) fine woody debris (FWD), (D) total no FWD, (E) total 1hr, (F) total 10hr fuel, (G) total pine needle, and (H) total woody live.

Across all models, percentile-based metrics (notably p2th and p3th) consistently ranked among the most influential variables (Figure 4.6). These metrics, which describe lower height percentiles, were especially important for predicting total

biomass (Figure 4.6A), fine fuels (Figure 4.6B), and fine woody debris (Figure 4.6C), suggesting that the vertical structure of the lower vegetation plays a key role in determining fuel availability and composition.

Variables related to height variability, such as H_CV (coefficient of variation of height) and H_sd (standard deviation of height), also exhibited high MIR values in multiple models, particularly for woody live fuels (H), pine needles (G), and 10-hour fuels (F). This highlights the relevance of vertical heterogeneity in forest structure to explaining differences in fuel loads.

Other structure-related variables, such as H_pcum1 and H_pcum9 (percent of cumulative height at given thresholds), were moderately important across models, particularly for pine needles (G) and total no FWD (D). pHabovemean (proportion of points above mean height) was moderately significant in some models, like fine fuels and no FWD, but had limited influence elsewhere.

In contrast, variables like H_skew, H_kurt, and H_99th (skewness, kurtosis, and 99th percentile of height distribution) generally showed lower MIR values, indicating a more limited role in enhancing model performance across most components. A dashed line at MIR = 0.25 is included as a reference threshold; variables exceeding this value are considered relatively more important. Overall, these results emphasize the predictive strength of lower height percentiles and measures of vertical structure variation, and provide insight into the structural drivers of fuel distribution in frequently burned forests.

Boxplot comparisons of various fuel components across different fire return intervals (1-year, 2-year, and 4-year) illustrate clear patterns in pre-fire biomass, post-fire residuals, and total consumption (Figure 4.7). Statistical tests confirmed these patterns, with significant differences among fire intervals for most fuel categories (Wilcoxon rank-sum, $p < 0.05$). Overall, longer fire intervals were associated with increased fuel accumulation and greater absolute consumption during fire events.

Total biomass and fine fuels exhibited a tendency to accumulate as fire recurrence intervals increased. Plots subjected to 4-year intervals showed the highest median pre-fire biomass values, whereas 1-year intervals maintained

consistently lower fuel loads. Post-fire biomass followed similar trends, though with reduced magnitude, indicating partial fuel consumption in all treatments. Notably, consumption was greatest in the 4-year treatment, reflecting higher pre-fire fuel availability.

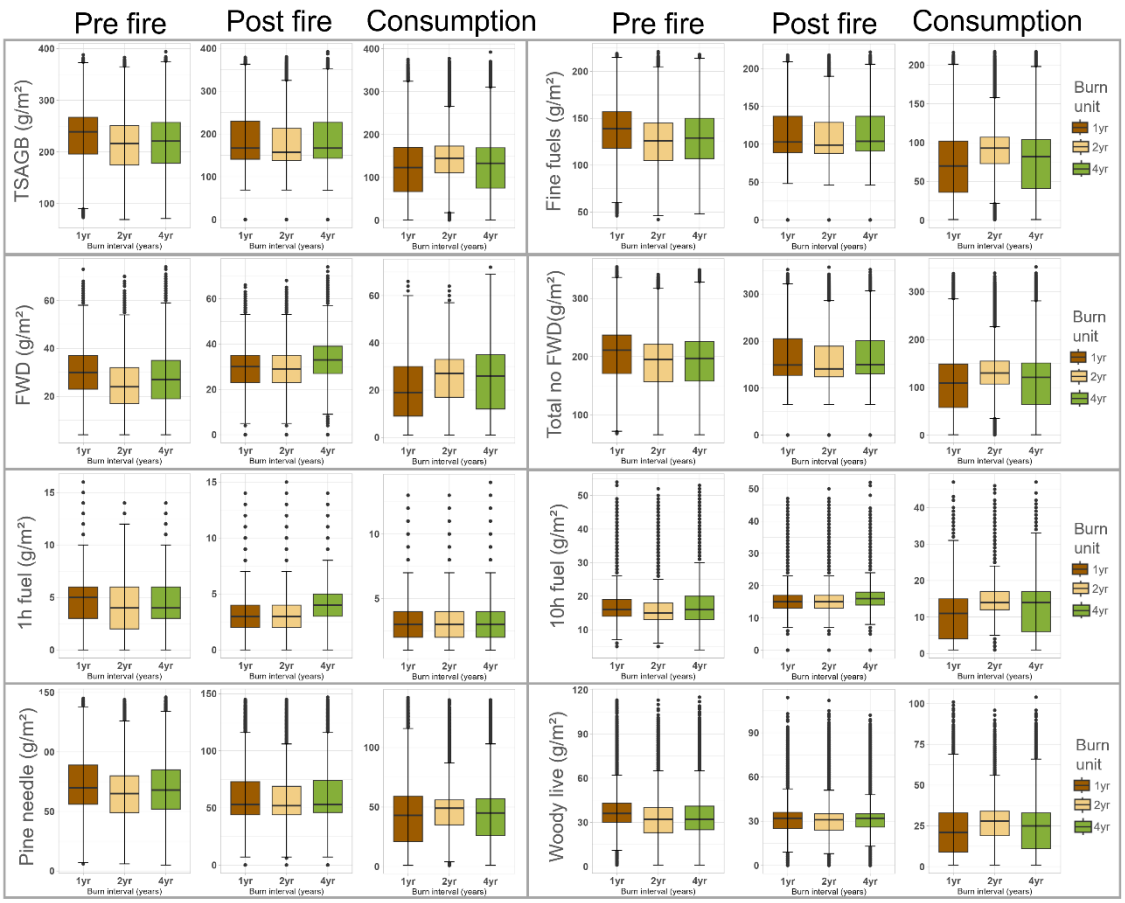
Fine woody debris and total 1-hour fuels also increased with longer intervals, with significantly higher pre-fire values in the 4-year treatment. The post-fire reduction in FWD was more pronounced in longer intervals, resulting in higher overall consumption. This pattern suggests that accumulated woody fuels in less frequently burned areas contribute substantially to fire intensity.

The 1-hour and 10-hour fuel classes demonstrated distinct responses based on combustion dynamics and moisture sensitivity. One-hour fuels were most efficiently consumed in annually burned plots, with lower post-fire residuals indicating effective combustion of fine materials. In contrast, 10-hour fuels were more abundant in 4-year treatments, both pre- and post-fire, leading to higher absolute consumption in these less frequently burned areas.

Pine needle litter and woody litter followed similar accumulation-consumption trends, with higher values observed in the 4-year treatment. These fuel types are particularly responsive to fire return interval, with greater buildup in the absence of regular burning and increased consumption once ignited.

Collectively, these results underscore the influence of fire frequency on fuel dynamics. Frequent burning (1-year interval) limits fuel accumulation and promotes consistent consumption of fine materials, potentially reducing fire severity. In contrast, longer intervals allow for substantial fuel buildup, increasing the amount of biomass available to burn and potentially elevating fire intensity and ecological impact. These findings highlight the importance of fire regime management in maintaining ecosystem resilience and mitigating severe fire behavior.

Figure 4.7 - Boxplots of pre-fire, post-fire, and consumed biomass and fuel components across three fire return intervals (1-year, 2-year, and 4-year).



Fuel categories include total biomass, fine fuels, fine woody debris (FWD), 1-hour fuels, 10-hour fuels, pine needles, and woody live.

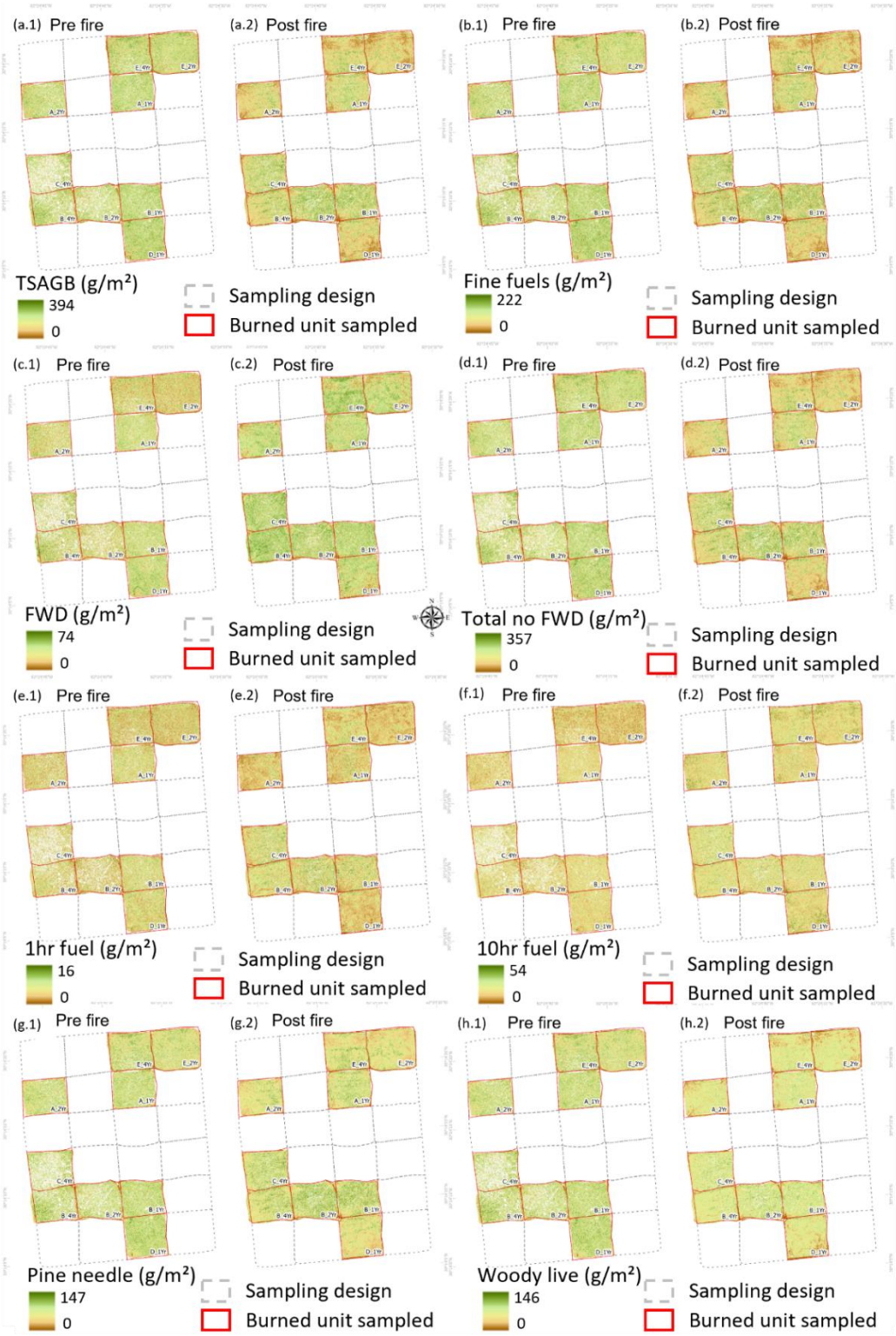
Figure 4.8 presents spatial predictions of biomass and fuel components under pre-fire and post-fire conditions, generated using Random Forest models. Each subplot corresponds to one of eight fuel components, displayed across a gridded landscape following the sampling design. For each component, subpanel ".1" shows pre-fire biomass estimates, while subpanel ".2" shows post-fire values. The components include (a) total biomass, (b) fine fuels, (c) fine woody debris (FWD), (d) total no FWD, (e) 1-hour fuels, (f) 10-hour fuels, (g) pine needle litter, and (h) woody live biomass.

Predictions are shown using a brown-to-green color gradient, where orange-brown shades represent lower fuel loads and darker greens indicate higher biomass density. Red outlines delineate burned units, while dashed lines represent the sampling design applied across the landscape.

Visual comparison between pre- and post-fire panels reveals a general decrease in biomass and fuel loads following fire, particularly in fine fuels and 1-hour fuel classes. This pattern aligns with the observed consumption data presented earlier. Spatial variability is evident within and among burn units, with some areas showing substantial fuel loss and others retaining higher post-fire biomass, likely reflecting differences in fire intensity, fuel moisture, or vegetation structure.

These maps demonstrate the capacity of the Random Forest models to capture spatial heterogeneity in fuel distribution and fire effects across the landscape, reinforcing their utility for ecological assessment and fire management planning.

Figure 4.8 - Spatial distribution of predicted biomass (g/m²) for eight fuel components under pre-fire (.1) and post-fire (.2) conditions using Random Forest models.



Panels show: (a) total biomass, (b) fine fuels, (c) fine woody debris (FWD), (d) total no FWD, (e) 1-hour fuels, (f) 10-hour fuels, (g) pine needle litter, and (h) woody live biomass. Burned units are outlined in red, and the sampling design is shown in dashed black.

Figure 4.9 illustrates spatial predictions of fuel consumption (g/m²) for eight biomass and fuel components across a fire-managed landscape. Estimates were derived from Random Forest model predictions of pre-fire and post-fire biomass, allowing the calculation of consumption as the difference between these two states. Each panel (A–H) represents a specific biomass component, with predictions shown over a gridded sampling design where burned units are outlined in red.

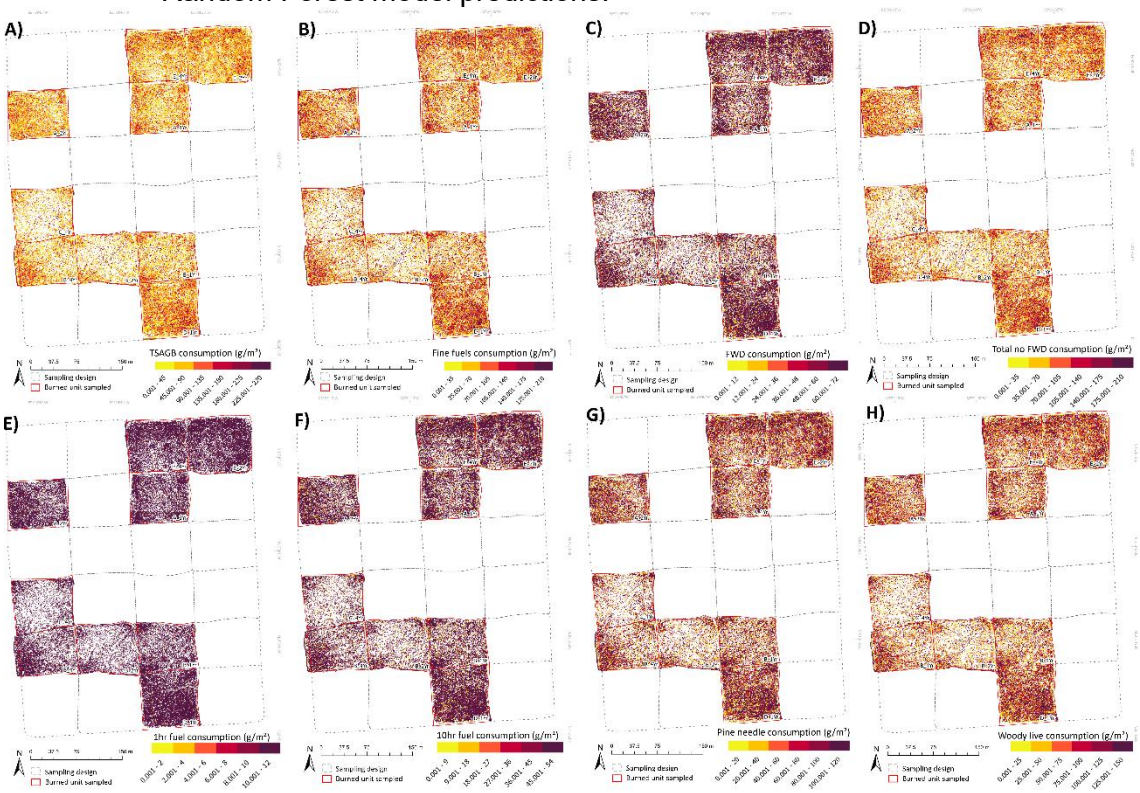
Panel A shows total biomass consumption, panel B displays fine fuels consumption, and panels C and D represent fine woody debris (FWD) and total FWD consumption, respectively. Panels E and F correspond to 1-hour and 10-hour fuels, while panels G and H depict consumption of pine needle litter and woody live biomass.

The maps use a yellow-to-purple color gradient, where lighter tones represent lower levels of fuel consumption and darker purple shades indicate higher consumption. This visual representation highlights substantial spatial heterogeneity in fire effects, with varying consumption intensities both within and across burn units.

Fine fuels and pine needles (Panels B and G) exhibit broad and intense consumption patterns, consistent with their high flammability and rapid combustion during fire. Conversely, components such as 1-hour fuels (Panel E) and woody live biomass (Panel H) show more spatially variable and generally lower levels of consumption, likely due to fuel moisture, structural resistance to burning, or lower fire residence time in certain areas.

These spatial patterns reinforce prior findings from model evaluation and boxplot analyses, confirming that Random Forest models can effectively capture localized fuel consumption dynamics. This figure supports the utility of integrating remote sensing and machine learning for fire ecology research and management planning.

Figure 4.9 - Spatial distribution of predicted fuel consumption (g/m²) for eight biomass components, calculated as the difference between pre-fire and post-fire Random Forest model predictions.



Panels represent (A) total biomass, (B) fine fuels, (C) fine woody debris (FWD), (D) total FWD, (E) 1-hour fuels, (F) 10-hour fuels, (G) pine needle litter, and (H) woody live biomass.

4.3 Discussion

Integrating plot-derived fuel metrics with ancillary predictor variables constitutes a critical step in developing landscape-scale fuel hazard predictions (D'ESTE et al., 2021; LEITE et al., 2022; TANEJA et al., 2023). Machine learning models, particularly Random Forest, have become invaluable for performing this integration due to their robustness and capability to handle complex ecological data (SILVA et al., 2017a; XU et al., 2020; D'ESTE et al., 2021). Our analysis consistently identified lower height percentiles and vertical structure variability among the most influential metric predictors across biomass components and fuels, aligning with prior studies that emphasized the importance of fine-scale vertical variability for accurate biomass estimation (LOUDERMILK et al., 2012b; HUDAK et al., 2016a; ROWELL et al., 2016).

4.3.1 Structural predictors of biomass and fuels

Our study demonstrated that TLS-derived structural metrics, particularly those related to low-height percentiles and vertical variability, were the most consistent predictors of surface fuel loads across fire return intervals. These findings highlight that the majority of biomass and fine fuels are concentrated near the ground level, making them both critical for fire spread and accessible to TLS measurements. This result underscores the value of TLS for capturing fine-scale heterogeneity in surface fuels that directly influences fire behavior.

These patterns are consistent with previous research. Rowell et al., (2016) also reported that fine-scale vertical structure measured by TLS correlates strongly with fuel mass distribution, while (HUDAK et al., 2016a) emphasized the importance of low-height returns for estimating surface fuels in fire-prone ecosystems. (LOUDERMILK et al., 2012b) further highlighted the role of litter and grasses as drivers of fire dynamics, supporting our observation that homogenous fuel layers such as pine needle litter were predicted with relatively high accuracy. These results are consistent with findings from (XU et al., 2020), who found that TLS-derived structural metrics related to height variability and canopy density were robust predictors of AGB when coupled with Random Forest, aligning with our results and reinforcing the broader applicability of TLS-based modeling in fire-affected systems. Their study showed that even under sparse sampling conditions, TLS-based features significantly enhanced prediction accuracy across various vegetation types.

Consistent with these findings, our variable importance analysis identified lower height percentiles and vertical structure variability as consistently among the most influential predictors across all biomass components and fuels, underscoring the necessity of capturing detailed vertical structural attributes for accurate landscape-scale biomass modeling. In particular, the proportion of laser returns below threshold heights (p2th and p3th) emerged as dominant predictors across most biomass component models, suggesting a close association between biomass accumulation and the density of low-lying vegetation. This observation aligns well with the findings of Greaves et al. (2015) (GREAVES et

al., 2015), who reported the significance of vertical heterogeneity derived from TLS in biomass estimation for structurally comparable low-stature vegetation systems.

Additionally, metrics such as the coefficient of variation in height (H_CV) and the standard deviation of height (H_sd) significantly enhanced model predictive accuracy, particularly for fine woody debris and 10-hour fuels. Such structural variability metrics have been recognized in other TLS-based studies as pivotal for quantifying fuel loads and predicting fire behavior (WALLACE et al., 2022; LOUDERMILK et al., 2023). While our study focused on a fire-prone pine ecosystem, other studies demonstrated that TLS is also effective in capturing complex fuel structures in savanna environments, where mixed woody and herbaceous layers contribute to surface fuel dynamics (MUUMBE et al., 2021). TLS-derived metrics in these heterogeneous systems outperformed airborne LiDAR in resolving vertical vegetation structure, underscoring the potential for broader biome-level applications. Our models relied on area-based biomass predictions, whereas recent studies suggest that object-based and voxel-based approaches can enhance tree-level estimates (BLACKBURN; BUSCAGLIA; SÁNCHEZ MEADOR, 2021; WHELAN et al., 2023), and may further refine assessments of understory biomass.

Across all biomass components, variable importance analysis revealed that lower height percentiles and vertical structure variability were consistently among the most influential predictors. In particular, the proportion of laser returns below threshold heights (p2th and p3th) appeared as dominant drivers in nearly all models, indicating that biomass accumulation and fuel loading are strongly associated with the density of low-lying vegetation, emphasizing limitations in modeling fine-scale variability in smaller fuel categories. These metrics are especially sensitive to fine fuels, litter, and short understory growth, which tend to dominate the surface fuel layer in frequently burned systems.

Despite the potential limitations imposed by occlusion in densely vegetated plots, particularly in longer fire return intervals, TLS-derived metrics such as p2th, H_CV, and H_sd consistently emerged as key predictors of shrub biomass,

especially in systems dominated by low-stature vegetation such as saw palmetto. Given that most vegetation in the understory layer was less than one meter in height, occlusion effects primarily arise from horizontal and intra-canopy complexity rather than from overstory obstruction. This suggests that TLS, even when partially occluded, can capture meaningful variation in low-stature biomass structure. Nonetheless, occlusion may still contribute to underestimation of denser lower layers, emphasizing the value of scan design optimization (e.g., multi-angle or multi-scan setups) and the continued assessment of occlusion-sensitive metrics in dense shrub-dominated fuels.

4.3.2 Fire regime effects and ecological interpretation

The cumulative proportion metrics (e.g., H_pcum1, H_pcum9) and the proportion of points above mean height (pHabovemean) played important roles in models for fine fuels and pine needle litter. These features likely reflect variations in canopy openness and vertical layering, which influence both fuel deposition and consumption potential. Previous research has consistently shown that these factors significantly affect fuel deposition and combustion potential (LOUDERMILK et al., 2012b, 2023; WALLACE et al., 2022).

Across recurrent burning intervals, plots with longer fire recurrence periods (2- and 4-year treatments) exhibited greater values for these structural indicators, aligning with higher pre-fire biomass levels and more pronounced consumption. These findings corroborate earlier studies highlighting structural complexity as a key driver of biomass accumulation and fire dynamics over time (LOUDERMILK et al., 2012b; KROFCHECK et al., 2019; SÁNCHEZ-LÓPEZ et al., 2023). These findings suggest that vertical heterogeneity, not just the presence of vegetation but its distribution along the vertical profile, is a critical factor in determining fuel mass and availability.

4.3.3 Advances, applications and limitations

Moreover, although our primary objective was biomass estimation, advances in TLS-based structural heterogeneity indices may support fire behavior modeling and ecological classification. In this context, (REICH; KUNZ; VON OHEIMB,

2021) introduced a Structural Heterogeneity Index (SHITLS) capable of distinguishing canopy and crown structure variations across forest types, even when traditional structure indices showed limited sensitivity. While not directly applied to fuel mapping in our study, such approaches illustrate how TLS-derived 3D structure could complement biomass and fuel modeling, providing additional insights for fire behavior modeling and multi-scale ecological classification.

Despite the potential limitations imposed by occlusion in densely vegetated plots—particularly in longer fire recurrence intervals—TLS-derived metrics such as p2th, H_CV, and H_sd consistently emerged as key predictors of shrub biomass, especially in systems dominated by low-stature vegetation such as saw palmetto. These results support previous studies (OLSOY et al., 2014), which demonstrated that TLS can reliably characterize shrub biomass even under conditions of moderate occlusion. Given that most vegetation in the understory layer was less than one meter in height, occlusion effects primarily arise from horizontal and intra-canopy complexity rather than from overstory obstruction. This suggests that TLS, even when partially occluded, can capture meaningful variation in low-stature biomass structure.

Our findings regarding the strong predictive power of lower height percentiles and structural variability align with those of Bright et al. (2022) (BRIGHT et al., 2022), who demonstrated that understory density and low canopy height metrics derived from airborne LiDAR were key indicators of surface fuel loads. Their application of multitemporal LiDAR to quantify pre- and post-fire biomass and fuel consumption highlights the value of repeat lidar acquisitions for landscape-scale fire monitoring and fuel dynamics assessment. Nonetheless, occlusion may still contribute to underestimation of denser lower layers, emphasizing the value of scan design optimization (e.g., multi-angle or multi-scan setups) and the continued assessment of occlusion-sensitive metrics in dense shrub-dominated fuels (VIERLING et al., 2013; OLSOY et al., 2014; WALLACE et al., 2022).

4.4 Conclusions

This study presents the novel integration of high-resolution TLS with a machine learning framework to accurately estimate and map TSAGB and fuel

consumption across multiple biomass components in a frequently burned pine ecosystem. Unlike most previous approaches that rely on coarser airborne data or limited field sampling, our method captures fine-scale structural variability through 3D TLS metrics and leverages a robust variable selection procedure to optimize Random Forest performance. The models performed particularly well for total biomass and fine fuels, achieving high accuracy and minimal bias, while performance was more variable for fuel types characterized by low density or discontinuous spatial distribution. These results align with findings from recent TLS-based studies in longleaf pine and other fire-prone systems, yet our approach advances the field by enabling spatial prediction of pre- and post-fire biomass at sub-meter resolution.

From an applied perspective, this methodology offers forest managers a scalable and non-destructive tool for quantifying biomass dynamics, improving prescribed fire planning, and evaluating fire effects with greater spatial precision than traditional methods. Furthermore, the model outputs can be directly integrated into fire behavior models or carbon accounting frameworks. Nonetheless, limitations remain in accurately modeling sparse fuel classes, particularly when zero-inflated or highly variable, as reflected in the performance of FWD and 1-hour fuels. Future work should explore hybrid approaches that combine TLS with multispectral or hyperspectral data to improve classification of fine fuel types, as well as assess transferability of models across broad-er landscapes and forest conditions. Continued refinement of variable selection, resolution trade-offs, and integration with operational fire management tools will further enhance the utility of TLS in fire ecology and forest monitoring.

5 GENERAL CONCLUSION: INTEGRATING BIOMASS DYNAMICS FROM REGENERATION TO DISTURBANCE

This thesis investigated aboveground biomass (AGB) estimation in forest ecosystems by integrating structural metrics derived from LiDAR, field inventories, and machine learning algorithms, while accounting for key ecological drivers such as land-use history and fire recurrence. The central hypothesis was that AGB estimation accuracy could be significantly improved by combining fine-scale forest structure data with spatiotemporal information reflecting ecological trajectories and disturbance regimes.

Chapter 3 addressed AGB accumulation during forest regeneration, focusing on the spatial distribution and age dynamics of SF in Pará state, Brazil. Using TerraClass multitemporal land-use data and ALS-derived AGB estimates, the study revealed that SF are not randomly distributed but rather concentrated in areas historically affected by deforestation and road expansion. Biomass accumulation increased with forest age; however, even mature SF (≥10 years) stored only 23–33% of the biomass of adjacent old-growth forests. Regional differences in accumulation patterns highlighted the influence of local ecological and socioeconomic conditions on forest recovery.

Chapter 4 examined AGB loss under fire disturbance, evaluating how repeated prescribed burns affect TSAGB using TLS-derived structural metrics. The study demonstrated that fire recurrence significantly reduces AGB, especially in early successional stages. TLS enabled detailed detection of structural changes, particularly in understory and mid-canopy layers-zones typically underrepresented in satellite and airborne LiDAR data. Random Forest models trained on TLS metrics achieved high predictive performance (R^2 up to 0.82), confirming the effectiveness of TLS for modeling biomass and surface fuel loads in degraded or fire-affected forests.

Together, the findings validate the initial hypothesis and demonstrate that integrating TLS with ecological history, specifically, land-use trajectories and fire recurrence, enhances the accuracy and ecological relevance of AGB modeling. This hybrid approach bridges plot-scale precision with landscape-scale

applicability, offering a robust framework for quantifying carbon stocks in structurally complex and dynamic tropical environments.

The methodological advances presented here have practical implications for forest monitoring, restoration planning, and climate policy mechanisms such as REDD+. By improving our understanding of how biomass responds to different ecological pathways, whether through regeneration or disturbance, this research supports more effective, evidence-based conservation strategies, particularly in regions facing high rates of deforestation and degradation.

Nevertheless, limitations remain, including the spatial scaling of TLS-based estimates and the integration of multi-source remote sensing data with varying resolutions and temporal coverage. Future work should explore the automation of TLS acquisition, fusion with satellite LiDAR missions such as GEDI, and ICESat-2, and expanded applications in landscape-level restoration monitoring.

Ultimately, recognizing the ecological memory embedded in land-use and fire history, and capturing it through advanced remote sensing, is essential for refining our understanding of forest carbon dynamics and informing science-based environmental governance in the Amazon and beyond.

REFERENCES

AGUIAR, D. R.; GAMA, J. R. V.; BELDINI, T. P. Estoque de carbono por grupo ecológico na Floresta Nacional do Tapajós. **Espacios**, v. 38, n. 32, p. 21, 2017.

ALMEIDA, D. R. A. et al. The effectiveness of lidar remote sensing for monitoring forest cover attributes and landscape restoration. **Forest Ecology and Management**, v. 438, p. 34–43, 2019.

ALMEIDA, C. A. et al. High spatial resolution land use and land cover mapping of the Brazilian Legal Amazon in 2008 using Landsat-5/TM and MODIS data. **Acta Amazonica**, v. 46, n. 3, p. 291–302, 2016.

ARAGÃO, L. E. O. C. et al. 21st Century drought-related fires counteract the decline of Amazon deforestation carbon emissions. **Nature Communications**, v. 9, n. 1, p. 536, 2018.

ARAGÃO, L. E. O. C. et al. Environmental change and the carbon balance of Amazonian forests. **Biological Reviews**, v. 89, n. 4, p. 913–931, 2014.

ASNER, G. P. et al. High-resolution mapping of forest carbon stocks in the Colombian Amazon. **Biogeosciences**, v. 9, n. 7, p. 2683–2696, 2012.

ASNER, G. P.; MASCARO, J. Mapping tropical forest carbon: calibrating plot estimates to a simple LiDAR metric. **Remote Sensing of Environment**, v. 140, p. 614–624, 2014.

BACCINI, A. et al. Estimated carbon dioxide emissions from tropical deforestation improved by carbon-density maps. **Nature Climate Change**, v. 2, n. 3, p. 182–185, 2012.

BAKER, T. R. et al. Variation in wood density determines spatial patterns inAmazonian forest biomass. **Global Change Biology**, v. 10, n. 5, p. 545–562, 2004.

BARLOW, J.; LAGAN, B. O.; PERES, C. A. Morphological correlates of fire-induced tree mortality in a central Amazonian forest. **Journal of Tropical Ecology**, v. 19, n. 3, p. 291–299, 2003.

BECKNELL, J. M.; KISSING KUCEK, L.; POWERS, J. S. Aboveground biomass in mature and secondary seasonally dry tropical forests: a literature review and global synthesis. **Forest Ecology and Management**, v. 276, p. 88–95, 2012.

BISPO, P. C. et al. Integration of polarimetric PALSAR attributes and local geomorphometric variables derived from SRTM for forest biomass modeling in central Amazonia. **Canadian Journal of Remote Sensing**, v. 40, n. 1, p. 26–42, 2014.

BISPO, P. D. C. et al. Mapping forest successional stages in the Brazilian Amazon using forest heights derived from TanDEM-X SAR interferometry. **Remote Sensing of Environment**, v. 232, e111194, 2019.

BISPO, P. C. et al. Woody aboveground biomass mapping of the Brazilian Savanna with a multi-sensor and machine learning approach. **Remote Sensing**, v. 12, n. 17, e2685, 2020.

BLACKBURN, R. C.; BUSCAGLIA, R.; SÁNCHEZ MEADOR, A. J. Mixtures of airborne lidar-based approaches improve predictions of forest structure. **Canadian Journal of Forest Research**, v. 51, n. 8, p. 1106–1116, 2021.

BLAYDES, S. H.; CANNON, J. B.; AUBREY, D. P. Modeling spatial patterns of longleaf pine needle dispersal using long-term data. **Fire Ecology**, v. 19, n. 1, 2023.

BOURGOIN, C. et al. The potential of multisource remote sensing for mapping the biomass of a degraded Amazonian forest. **Forests**, v. 9, n. 6, p. 303, 2018.

BOVOLO, F.; BRUZZONE, L. An adaptive multiscale approach to unsupervised change detection in multitemporal SAR images. In: IEEE INTERNATIONAL CONFERENCE ON IMAGE PROCESSING, 2005, Genova, Italy. **Proceedings...** IEEE, 2005

BRANDO, P. M. et al. Abrupt increases in Amazonian tree mortality due to drought–fire interactions. **Proceedings of the National Academy of Sciences**, v. 111, n. 17, p. 6347–6352, 2014.

BREIMAN, L. Random Forests. **Machine Learning**, v. 45, p. 5–32, 2001.

BRIGHT, B. C. et al. Multitemporal lidar captures heterogeneity in fuel loads and consumption on the Kaibab Plateau. **Fire Ecology**, v. 18, n. 1, p. 18, 2022.

BROWN, S.; LUGO, A. E. Tropical secondary forests. **Journal of Tropical Ecology**, v. 6, n. 1, p. 1–32, 1990.

CALDERS, K. et al. Terrestrial laser scanning in forest ecology: expanding the horizon. **Remote Sensing of Environment**, v. 251, e112102, 2020.

CALDERS, K. et al. Nondestructive estimates of above-ground biomass using terrestrial laser scanning. **Methods in Ecology and Evolution**, v. 6, n. 2, p. 198–208, 2015.

CARVALHO, R. et al. Changes in secondary vegetation dynamics in a context of decreasing deforestation rates in Pará, Brazilian Amazon. **Applied Geography**, v. 106, p. 40–49, 2019.

CASSOL, H. L. G. et al. Maximum fraction images derived from year-based Project for On-Board Autonomy-Vegetation (PROBA-V) data for the rapid assessment of land use and land cover areas in Mato Grosso State, Brazil. **Land**, v. 9, n. 5, e139, 2020.

CASSOL, H. L. G. et al. Quad-pol advanced land observing satellite/phased array L-band synthetic aperture radar-2 (ALOS/PALSAR-2) data for modelling secondary forest above-ground biomass in the central Brazilian Amazon. **International Journal of Remote Sensing**, v. 42, n. 13, p. 4985–5009, 2021.

CHATURVEDI, R. K.; RAGHUBANSHI, A. S.; SINGH, J. S. Effect of grazing and harvesting on diversity, recruitment and carbon accumulation of juvenile trees in tropical dry forests. **Forest Ecology and Management**, v. 284, p. 152–162, 2012.

CHAVE, J. et al. Improved allometric models to estimate the aboveground biomass of tropical trees. **Global Change Biology**, v. 20, n. 10, p. 3177–3190, 2014.

CHAZDON, R. L. et al. Carbon sequestration potential of second-growth forest regeneration in the Latin American tropics. **Science Advances**, v. 2, n. 5, e1501639, 2016.

CHAZDON, R. L. et al. Rates of change in tree communities of secondary Neotropical forests following major disturbances. **Philosophical Transactions of the Royal Society B: Biological Sciences**, v. 362, n. 1478, p. 273–289, 2007.

CHAZDON, R. L. et al. The potential for species conservation in tropical secondary forests. **Conservation Biology**, v. 23, n. 6, p. 1406–1417, 2009.

CLOUDCOMPARE. **CloudCompare®.** 2024.

COCHRANE, M. A. Fire science for rainforests. **Nature**, v. 421, n. 6926, p. 913–919, 2003.

COCHRANE, M. A.; SCHULZE, M. D. Fire as a recurrent event in tropical forests of the eastern Amazon: effects on forest structure, biomass, and species composition. **Biotropica**, v. 31, n. 1, p. 2–16, 1999.

COUTINHO, A. C. et al. **Uso e cobertura da terra nas áreas desflorestadas da Amazônia Legal: TerraClass 2008**. Brasília, DF: Embrapa, 2009. 107 p.

CUTLER, D. R. et al. Random forests for classification in ecology. **Ecology**, v. 88, n. 11, p. 2783–2792, 2007.

DA SILVA, G. M. et al. Spatial distribution of secondary forests by age group and biomass accumulation in the Brazilian Amazon. **Forests**, v. 14, n. 5, p. 924, 2023.

DALAL, R. C.; ALLEN, D. E. Greenhouse gas fluxes from natural ecosystems. **Australian Journal of Botany**, v. 56, n. 5, p. 369, 2008.

DEBASTIANI, A. B. et al. Evaluating SAR-optical sensor fusion for aboveground biomass estimation in a Brazilian tropical forest. **Annals of Forest Research**, v. 62, n. 1, p. 109–122, 2019.

D'ESTE, M. et al. Machine learning techniques for fine dead fuel load estimation using multi-source remote sensing data. **Remote Sensing**, v. 13, n. 9, e1658, 2021.

DOBLAS, J. et al. Optimizing near real-time detection of deforestation on tropical rainforests using Sentinel-1 data. **Remote Sensing**, v. 12, n. 23, e3922, 2020.

DORMANN, C. F. et al. Collinearity: a review of methods to deal with it and a simulation study evaluating their performance. **Ecography**, v. 36, n. 1, p. 27–46, 2013.

DUBAYAH, R. et al. The global ecosystem dynamics investigation: high-resolution laser ranging of the Earth's forests and topography. **Science of Remote Sensing**, v. 1, e100002, 2020.

DUBAYAH, R. O.; DRAKE, J. B. Lidar remote sensing for forestry. **Jornal of Forestry**, v. 98, n. 6, p. 44–46, 2000.

DUNCANSON, L. et al. Aboveground woody biomass product validation good practices protocol. In: DUNCANSON, L. et al. (Ed.). **Good practices for satellite derived land product validation**. [S.l: s.n.], 2024. p.236.

DUNCANSON, L. et al. Remote sensing of environment biomass estimation from simulated GEDI , ICESat-2 and NISAR across environmental gradients in Sonoma County, California. **Remote Sensing of Environment**, v. 242, e111779, 2020.

DUPUY, J. L. et al. Exploring three-dimensional coupled fireatmosphere interactions downwind of wind-driven surface fires and their influence on backfires using the HIGRAD-FIRETEC model. **International Journal of Wildland Fire**, v. 20, n. 6, p. 734–750, 2011.

ELIAS, F. et al. Assessing the growth and climate sensitivity of secondary forests in highly deforested Amazonian landscapes. **Ecology**, v. 101, n. 3, 2020.

ELMQVIST, T. et al. **Urbanization, biodiversity and ecosystem services: challenges and opportunities**. Dordrecht: Springer, 2013. 755p.

EUROPEAN SPACE AGENCY (ESA). **Sentinel-2 MSI introduction**. Available from: https://sentinels.copernicus.eu/web/sentinel/user-guides/sentinel-2-msi. Access on: 16 Nov. 2020a.

EUROPEAN SPACE AGENCY (ESA). **Sentinel-1 SAR user guide introduction**. Available from: https://sentinels.copernicus.eu/web/sentinel/user-guides/sentinel-1-sar. Access on: 22 Oct. 2020b.

FEARNSIDE, P. M. Desmatamento na Amazônia: dinâmica, impactos e controle. **Acta Amazonica**, v. 36, n. 3, p. 395–400, 2006.

FENG, Y. et al. Examining effective use of data sources and modeling algorithms for improving biomass estimation in a moist tropical forest of the Brazilian Amazon. **International Journal of Digital Earth**, v. 10, n. 10, p. 996–1016, 2017.

FORKUOR, G. et al. Above-ground biomass mapping in West African dryland forest using Sentinel-1 and 2 datasets: a case study. **Remote Sensing of Environment**, v. 236, e111496, 2020.

GARCÍA, M. et al. Terrestrial laser scanning to estimate plot-level forest canopy fuel properties. **International Journal of Applied Earth Observation and Geoinformation**, v. 13, n. 4, p. 636–645, 2011.

GIONGO, M. et al. LiDAR: princípios e aplicações florestais. **Pesquisa Florestal Brasileira**, v. 30, n. 63, p. 231–244, 2010.

GONÇALVES LAZZARO, L. et al. Overstory and fuel traits drive moisture dynamics of mesophytic and pyrophytic leaf litter and 10-h woody debris fuels in a mixed longleaf pine-hardwood woodland. **Fire Ecology**, v. 20, n. 1, 2024.

GONZALEZ DE TANAGO, J. et al. Estimation of above-ground biomass of large tropical trees with terrestrial LiDAR. **Methods in Ecology and Evolution**, v. 9, n. 2, p. 223–234, 2018.

GREAVES, H. E. et al. Estimating aboveground biomass and leaf area of low-stature Arctic shrubs with terrestrial LiDAR. **Remote Sensing of Environment**, v. 164, p. 26–35, 2015.

GUANTER, L. et al. The EnMAP spaceborne imaging spectroscopy mission for Earth observation. **Remote Sensing**, v. 7, n. 7, p. 8830–8857, 2015.

GUIMARÃES, J. et al. **Municipios verdes: caminhos para a sustentabilidade**. Belém: Imazon, 2011.

HASSEBO, Y. Active remote sensing: Lidar SNR improvements. In: ESCALANTE, B. (Ed.). **Remote sensing: advanced techniques and platforms**. [S.l.]: InTech, 2012. p. 313–340.

HAWLEY, C. M. et al. A novel approach to fuel biomass sampling for 3D fuel characterization. **MethodsX**, v. 5, p. 1597–1604, 2018.

HEINRICH, V. H. A. et al. Large carbon sink potential of secondary forests in the Brazilian Amazon to mitigate climate change. **Nature Communications**, v. 12, n. 1, e1785, 2021.

HOLL, K. D. Factors limiting tropical rain forest regeneration in abandoned pasture: seed rain, seed germination, microclimate, and soil. **Biotropica**, v. 31, n. 2, p. 229–242, 1999.

HUANG, W. et al. Sensitivity of multi-source SAR backscatter to changes in forest aboveground biomass. **Remote Sensing**, v. 7, n. 8, p. 9587–9609, 2015.

HUDAK, A. T. et al. Mapping forest structure and composition from low-density LiDAR for Informed forest, fuel, and fire management at Eglin Air Force Base, Florida, USA. **Canadian Journal of Remote Sensing**, v. 42, n. 5, p. 411–427, 2016a.

HUDAK, A. T. et al. Measurements relating fire radiative energy density and surface fuel consumption – RxCADRE 2011 and 2012. **International Journal of Wildland Fire**, v. 25, n. 1, p. 25, 2016b.

IMHOFF, M. L. Radar backscatter and biomass saturation: ramifications for global biomass inventory. In: IEEE TRANSACTIONS ON GEOSCIENCE AND REMOTE SENSING, 1995. **Proceedings...** IEEE, 1995

INSTITUTO BRASILEIRO DE GEOGRAFIA E ESTATÍSTICA (IBGE). **Área territorial brasileira 2020**. Rio de Janeiro: IBGE, 2021.

INSTITUTO NACIONAL DE PESQUISAS ESPACIAIS (INPE). **PRODES - Monitoramento de floresta Amazônica brasileira por satelite**. Available from: http://www.obt.inpe.br/OBT/assuntos/programas/amazonia/prodes. Access on: 26 Apr. 2021.

INTERGOVERNMENTAL PANEL ON CLIMATE CHANGE (IPCC). **2006 IPCC guidelines for national greenhouse gas inventories**. Hayama, JAPAN: IPCC, 2008.

INTERGOVERNMENTAL PANEL ON CLIMATE CHANGE (IPCC). **Refinement to the 2006 IPCC guidelines for national greenhouse gas inventories: agriculture, forestry and other land use**. Japan: IGES, 2019.

JENSEN, G. L. et al. Vegetation–fuel–fire feedbacks in patches of longleaf pine (Pinus palustris Mill.) regeneration. **Fire Ecology**, v. 21, n. 1, 2025.

JONES, K.; VUKOMANOVIC, J. Mapping South Florida daily fire risk for decision support using fuel type, water levels, and burn history. **Fire**, v. 6, n. 6, 2023.

JUCKER, T. et al. Allometric equations for integrating remote sensing imagery into forest monitoring programmes. **Global Change Biology**, v. 23, n. 1, p. 177–190, 2017.

KELLNDORFER, J. Using SAR data for mapping deforestation and forest degradation. In: FLORES, A. et al. (Ed.). **The SAR handbook: comprehensive methodologies for forest monitoring and biomass estimation**. [S.l.]: NASA, 2019. p. 65–81.

KELLNDORFER, J. M. et al. Statistical fusion of lidar, InSAR, and optical remote sensing data for forest stand height characterization: a regional-scale method based on LVIS, SRTM, Landsat ETM+, and ancillary data sets. **Journal of Geophysical Research: Biogeosciences**, v. 115, n. G2, 2010.

KLAUBERG, C. et al. Post-hurricane damage severity classification at the individual tree level using terrestrial laser scanning and deep learning. **Remote Sensing**, v. 15, n. 4, p. 1165, 2023.

KNAPP, N. et al. Model-assisted estimation of tropical forest biomass change: a comparison of approaches. **Remote Sensing**, v. 10, n. 5, p. 731, 2018.

KROFCHECK, D. J. et al. The effects of management on long-term carbon stability in a southeastern U.S. forest matrix under extreme fire weather. **Ecosphere**, v. 10, n. 3, 2019.

KUMAR, A. et al. Tree diversity assessment and above ground forests biomass estimation using SAR remote sensing: a case study of higher altitude vegetation of North-East Himalayas, India. **Physics and Chemistry of the Earth, Parts A/B/C**, v. 111, p. 53–64, 2019.

LAURANCE, W. F. Biomass collapse in Amazonian forest fragments. **Science**, v. 278, n. 5340, p. 1117–1118, 1997.

LE TOAN, T. et al. The BIOMASS mission: mapping global forest biomass to better understand the terrestrial carbon cycle. **Remote Sensing of Environment**, v. 115, n. 11, p. 2850–2860, 2011.

LEFSKY, M. A. A global forest canopy height map from the Moderate Resolution Imaging Spectroradiometer and the Geoscience Laser Altimeter System. **Geophysical Research Letters**, v. 37, n. 15, 2010.

LEITE, R. V. et al. Large scale multi-layer fuel load characterization in tropical savanna using GEDI spaceborne lidar data. **Remote Sensing of Environment**, v. 268, e112764, 2022.

LONGO, M. et al. Aboveground biomass variability across intact and degraded forests in the Brazilian Amazon. **Global Biogeochemical Cycles**, v. 30, n. 11, p. 1639–1660, 2016.

LOPEZ-GONZALEZ, G. et al. ForestPlots.net: a web application and research tool to manage and analyse tropical forest plot data. **Journal of Vegetation Science**, v. 22, n. 4, p. 610–613, 2011.

LOUDERMILK, E. L. et al. Linking complex forest fuel structure and fire behaviour at fine scales. **International Journal of Wildland Fire**, v. 21, n. 7, p. 882, 2012.

LOUDERMILK, E. L. et al. Terrestrial laser scan metrics predict surface vegetation biomass and consumption in a frequently burned southeastern U.S. ecosystem. **Fire**, v. 6, n. 4, p. 151, 2023.

LOVEJOY, T. E.; NOBRE, C. Amazon tipping point. **Science Advances**, v. 4, n. 2, 2018.

MAPBIOMAS. **Projeto MapBiomas – Coleção 6 da série anual de mapas de cobertura e uso de solo do Brasil**. Available from: https://plataforma.mapbiomas.org/. Access on: 10 Oct. 2021.

MARENGO, J. et al. Global warming and climate change in Amazonia: Climate-vegetation feedback and impacts on water resources. In: KELLER, M. et al. (Ed.). **Amazonia and global change**. [S.l.]: AGU, 2009. p. 273–292.

MARSELIS, S. M. et al. Evaluating the potential of full-waveform lidar for mapping pan-tropical tree species richness. **Global Ecology and Biogeography**, v. 29, n. 10, p. 1799–1816, 2020.

MCKEE, W. H. **Changes in soil fertility following prescribed burning on coastal plain pine sites**. [S.l.]: U.S. Department of Agriculture, Southeastern Forest Experiment Station, Forest Service, 1982. v. 234

MITCHARD, E. T. A. et al. Measuring biomass changes due to woody encroachment and deforestation/degradation in a forest–savanna boundary region of central Africa using multi-temporal L-band radar backscatter. **Remote Sensing of Environment**, v. 115, n. 11, p. 2861–2873, 2011.

MITCHARD, E. T. A. et al. Mapping tropical forest biomass with radar and spaceborne LiDAR in Lopé National Park, Gabon: overcoming problems of high biomass and persistent cloud. **Biogeosciences**, v. 9, n. 1, p. 179–191, 2012.

MITCHELL, A. **The ESRI guide to GIS analysis 2: spatial measurements and statistics**. Redlands: ESRI, 2005. 252 p.

MURPHY, M. A.; EVANS, J. S.; STORFER, A. Quantifying Bufo boreas connectivity in Yellowstone National Park with landscape genetics. **Ecology**, v. 91, n. 1, p. 252–261, 2010.

MUUMBE, T. P. et al. Terrestrial laser scanning for vegetation analyses with a special focus on savannas. **Remote Sensing,** 2021.

NEEFF, T. et al. Tropical forest biomass measurement by backscatter and DEM information as derived from airborne SAR. In: INTERNATIONAL GEOSCIENCE AND REMOTE SENSING SYMPOSIUM (IGARSS), 2003, Toulouse, France. **Proceedings...** IEEE, 2003. Available from: http://ieeexplore.ieee.org/document/1294512/.

NELSON, B. W. et al. Allometric regressions for improved estimate of secondary forest biomass in the central Amazon. **Forest Ecology and Management**, v. 117, n. 1/3, p. 149–167, 1999.

NEUENSCHWANDER, A.; PITTS, K. The ATL08 land and vegetation product for the ICESat-2 Mission. **Remote Sensing of Environment**, v. 221, p. 247–259, 2019.

OLSOY, P. J. et al. Aboveground total and green biomass of dryland shrub derived from terrestrial laser scanning. **ISPRS Journal of Photogrammetry and Remote Sensing**, v. 88, p. 166–173, 2014.

OUTCALT, K. W.; WADE, D. D. Fuels management reduces tree mortality from wildfires in southeastern United States. **Southern Journal of Applied Forestry**, v. 28, n. 1, p. 28–34, 2004.

PAN, Y. et al. A large and persistent carbon sink in the world's forests. **Science**, v. 333, n. 6045, p. 988–993, 2011.

PAN, Y. et al. The structure, distribution, and biomass of the world's forests. **Annual Review of Ecology, Evolution, and Systematics**, v. 44, n. 1, p. 593–622, 2013.

PEREIRA, C. A. et al. Recurrent wildfires alter forest structure and community composition of *terra firme* Amazonian forests. **Environmental Research Letters**, v. 19, n. 11, e114051, 2024.

PERZ, S. G.; SKOLE, D. L. Secondary forest expansion in the brazilian Amazon and the refinement of forest transition theory. **Society and Natural Resources**, v. 16, n. 4, p. 277–294, 2003.

PINTO, A. et al. **Diagnostico Socioeconômico e Florestal do município de Paragominas**. Belém, PA: [s.n.], 2009.

PODEST, E. et al. **Forest mapping and monitoring with SAR Data**. Available from: https://appliedsciences.nasa.gov/join-mission/training/english/arset-forest-mapping-and-monitoring-sar-data. Access on: 9 Aug. 2021.

PONZONI, F. J.; SHIMABUKURO, Y. E.; KUPLICH, T. M. **Sensoriamento remoto da vegetação**. 2.ed. São Paulo: Oficina de Textos, 2012. 168 p.

POORTER, L. et al. Biomass resilience of Neotropical secondary forests. **Nature**, v. 530, n. 7589, p. 211–214, 2016.

QUEGAN, S. et al. The European Space Agency BIOMASS mission: measuring forest above-ground biomass from space. **Remote Sensing of Environment**, v. 227, p. 44–60, 2019.

REICH, K. F.; KUNZ, M.; VON OHEIMB, G. A new index of forest structural heterogeneity using tree architectural attributes measured by terrestrial laser scanning. **Ecological Indicators**, v. 133, 2021.

REQUENA SUAREZ, D. et al. Estimating aboveground net biomass change for tropical and subtropical forests: Refinement of IPCC default rates using forest plot data. **Global Change Biology**, v. 25, n. 11, p. 3609–3624, 2019.

RIBEIRO, M. C. et al. The Brazilian Atlantic Forest: how much is left, and how is the remaining forest distributed? Implications for conservation. **Biological Conservation**, v. 142, n. 6, p. 1141–1153, 2009.

RIEGL LASER MEASUREMENT SYSTEMS GMBH. **RiSCAN Pro®.** Horn: RIEGL Laser Measurement Systems GmbH, 2024.

ROCHA, K. D. et al. Crown-level structure and fuel load characterization from airborne and terrestrial laser scanning in a longleaf pine (Pinus palustris Mill.) Forest Ecosystem. **Remote Sensing**, v. 15, n. 4, 2023.

RODRIGUES, R. R. et al. Large-scale ecological restoration of high-diversity tropical forests in SE Brazil. **Forest Ecology and Management**, v. 261, n. 10, p. 1605–1613, 2011.

ROSEN, P. A. et al. The NASA-ISRO SAR mission: an international space partnership for science and societal benefit. In: RADAR CONFERENCE (RadarCon), 2015. **Proceedings…** IEEE, 2015.

ROSS, C. W. et al. Lidar-derived estimates of forest structure in response to fire frequency. **Fire Ecology**, v. 20, n. 1, 2024.

ROWELL, E. et al. Coupling terrestrial laser scanning with 3D fuel biomass sampling for advancing wildland fuels characterization. **Forest Ecology and Management**, v. 462, 2020.

ROWELL, E. et al. Using simulated 3D surface fuelbeds and terrestrial laser scan data to develop inputs to fire behavior models. **Canadian Journal of Remote Sensing**, v. 42, n. 5, p. 443–459, 2016.

ROZENDAAL, D. M. A. et al. Demographic drivers of aboveground biomass dynamics during secondary succession in neotropical dry and wet forests. **Ecosystems**, v. 20, n. 2, p. 340–353, 2017.

ROZENDAAL, D. M. A. et al. Aboveground forest biomass varies across continents, ecological zones and successional stages: refined IPCC default values for tropical and subtropical forests. **Environmental Research Letters**, v. 17, n. 1, 2022.

SAATCHI, S. et al. Impact of spatial variability of tropical forest structure on radar estimation of aboveground biomass. **Remote Sensing of Environment**, v. 115, n. 11, p. 2836–2849, 2011a.

SAATCHI, S. S. et al. Benchmark map of forest carbon stocks in tropical regions across three continents. **Proceedings of the National Academy of Sciences**, v. 108, n. 24, p. 9899–9904, 2011b.

SAATCHI, S. S. et al. Distribution of aboveground live biomass in the Amazon basin. **Global Change Biology**, v. 13, n. 4, p. 816–837, 2007.

SÁNCHEZ-LÓPEZ, N. et al. A spatially explicit model of tree leaf litter accumulation in fire maintained longleaf pine forests of the southeastern US. **Ecological Modelling**, v. 481, 2023.

SANTORO, M.; CARTUS, O. Research pathways of forest above-ground biomass estimation based on SAR backscatter and interferometric SAR observations. **Remote Sensing**, v. 10, n. 4, p. 608, 2018.

SANTOS, E. G. et al. Multi-scale approach to estimating aboveground biomass in the Brazilian Amazon using Landsat and LiDAR data. **International Journal of Remote Sensing**, v. 40, n. 22, p. 8635–8645, 2019.

SHIMABUKURO, Y. E. et al. Mapping degraded forest areas caused by fires during the year 2010 in Mato Grosso state, Brazilian Legal Amazon using Landsat-5 TM fraction images. **Revista Brasileira de Cartografia**, v. 69, n. 1, 2017.

SHIMABUKURO, Y. E. et al. Monitoring annual Landsat-based deforestation using LSMM and MODIS-burned area product in Rondônia, Brazilian Amazon. **Discover Conservation**, v. 2, n. 1, p. 21, 2025.

SHIMABUKURO, Y. E. et al. Fraction images derived from Terra Modis data for mapping burnt areas in Brazilian Amazonia. **International Journal of Remote Sensing**, v. 30, n. 6, p. 1537–1546, 2009.

SHIMABUKURO, Y. E.; SMITH, J. A. The least-squares mixing models to generate fraction images derived from remote sensing multispectral data. **IEEE Transactions on Geoscience and Remote Sensing**, v. 29, n. 1, p. 16–20, 1991.

SILVA, C. A. et al. Fusing simulated GEDI, ICESat-2 and NISAR data for regional aboveground biomass mapping. **Remote Sensing of Environment**, v. 253, e112234, 2021.

SILVA, C. A. et al. Predicting stem total and assortment volumes in an industrial Pinus taeda L. forest plantation using airborne laser scanning data and random forest. **Forests**, v. 8, n. 7, 2017a.

SILVA, C. et al. Impacts of airborne lidar pulse density on estimating biomass stocks and changes in a selectively logged tropical forest. **Remote Sensing**, v. 9, n. 10, p. 1068, 2017b.

SILVA JUNIOR, C. H. L. et al. Benchmark maps of 33 years of secondary forest age for Brazil. **Scientific Data**, v. 7, n. 1, p. 269, 2020.

SILVEIRA, E. M. O. et al. Modelling aboveground biomass in forest remnants of the Brazilian Atlantic Forest using remote sensing, environmental and terrain-related data. **Geocarto International**, v. 36, n. 3, p. 281–298, 2021.

SINHA, S. et al. A review of radar remote sensing for biomass estimation. **International Journal of Environmental Science and Technology**, v. 12, n. 5, p. 1779–1792, 2015.

SMITH, C. C. et al. Secondary forests offset less than 10% of deforestation-mediated carbon emissions in the Brazilian Amazon. **Global Change Biology**, v. 26, n. 12, p. 7006–7020, 2020.

SRINIVAS, K.; SUNDARAPANDIAN, S. Biomass and carbon stocks of trees in tropical dry forest of East Godavari region, Andhra Pradesh, India. **Geology, Ecology, and Landscapes**, v. 3, n. 2, p. 114–122, 2019.

SULLIVAN, M. J. P. et al. Long-term thermal sensitivity of Earth's tropical forests. **Science**, v. 368, n. 6493, p. 869–874, 2020.

SULLIVAN, M. J. P. et al. Field methods for sampling tree height for tropical forest biomass estimation. **Methods in Ecology and Evolution**, v. 9, n. 5, p. 1179–1189, 2018.

TANEJA, R. et al. Up-scaling fuel hazard metrics derived from terrestrial laser scanning using a machine learning model. **Remote Sensing**, v. 15, n. 5, 2023.

THE EUROPEAN SPACE AGENCY. **Biomass - ESA's forest mission**. ESA, 2024.

TOMLIN, C. D. **Geographic information systems and cartographic modeling**. Englewood Cliffs: Prentice Hall, 1990. 249p.

VIEIRA, I. C. G. Land use drives change in amazonian tree species. **Anais da Academia Brasileira de Ciências**, v. 91, Suppl 3, 2019.

VIERLING, L. A. et al. Shrub characterization using terrestrial laser scanning and implications for airborne LiDAR assessment. **Canadian Journal of Remote Sensing**, v. 38, n. 6, p. 709–722, 2013.

WAGNER, F. H. et al. Using the U-net convolutional network to map forest types and disturbance in the Atlantic rainforest with very high resolution images. **Remote Sensing in Ecology and Conservation**, v. 5, n. 4, p. 360–375, 2019.

WALLACE, L. et al. Terrestrial laser scanning: an operational tool for fuel hazard mapping? **Fire**, v. 5, n. 4, 2022.

WANDELLI, E. V.; FEARNSIDE, P. M. Secondary vegetation in central Amazonia: Land-use history effects on aboveground biomass. **Forest Ecology and Management**, v. 347, p. 140–148, 2015.

WANG, Y. et al. Upturn in secondary forest clearing buffers primary forest loss in the Brazilian Amazon. **Nature Sustainability**, v. 3, n. 4, p. 290–295, 2020.

WANG, Y. et al. Mapping tropical disturbed forests using multi-decadal 30 m optical satellite imagery. **Remote Sensing of Environment**, v. 221, p. 474–488, 2019.

WHATELY, M.; CAMPANILI, M. **Programa municípios verdes: lições aprendidas e desafios para 2013/2014**. Belém, PA: Governo do Estado, 2013. 96 p.

WHELAN, A. W. et al. Improving generalized models of forest structure in complex forest types using area- and voxel-based approaches from lidar. **Remote Sensing of Environment**, v. 284, e113362, 2023.

WIEDERKEHR, N. C. et al. Discriminating forest successional stages, forest degradation, and land use in central Amazon using ALOS/PALSAR-2 full-polarimetric data. **Remote Sensing**, v. 12, n. 21, p. 3512, 2020.

WILKES, P. et al. Data acquisition considerations for terrestrial laser scanning of forest plots. **Remote Sensing of Environment**, v. 196, p. 140–153, 2017.

WULDER, M. A. et al. The role of LiDAR in sustainable forest management. **The Forestry Chronicle**, v. 84, n. 6, p. 807–826, 2008.

WULDER, M. A. et al. Current status of Landsat program, science, and applications. **Remote Sensing of Environment**, v. 225, p. 127–147, 2019.

XU, K. et al. Estimation of degraded grassland aboveground biomass using machine learning methods from terrestrial laser scanning data. **Ecological Indicators**, v. 108, 2020.

YU, Y.; SAATCHI, S. Sensitivity of L-Band SAR backscatter to aboveground biomass of global forests. **Remote Sensing**, v. 8, n. 6, p. 522, 2016.